2-12-2012

Proceedings of International Conference on Advanced Research in Mechanical Engineering

Prof.Srikanta Patnaik Mentor
IRNet India, patnaik_srikanta@yahoo.co.in

Proceedings of International Conference on

ADVANCED RESEARCH IN MECHANICAL ENGINEERING

(ICARME-2012)
12th February, 2012
AHMEDABAD, India

Interscience Research Network (IRNet)
Bhubaneswar, India

Editorial

In the Race of Scientific Civilization and Engineering Development Mechanical Engineering appears to be the oldest and broadest discipline. Till date it has accomplished many efficient mechanical systems using advanced practices of material science and Structural Analysis. As a matured academic discipline it has become an integrated component of Industrial Revolution. It has surpassed an odyssey of two centuries since its emergency in Europe. The basic philosophy although integrates two highlighting disciplines like Physics and Material Sciences but over the years it has developed its linkage with other domains like Composites, Mechatronics and Nanotechnology. Today's Mechanical Engineers uses the core principles with some sophisticated tools like Computer Aided Designing, and Product Life Cycle Management. These tools are also employed in Aerospace Engineering, Civil Engineering, Petroleum Engineering and Chemical Engineering, Aircraft, Watercraft, Robotics and Medical Devices.

In the advent of modern research there is a significant growth in Mechanical Engineering as Computer Aided Design has become instrumental in many industrialized nations like USA, European Countries, Scotland and GermOther CAE programs commonly used by mechanical engineers include product lifecycle management (PLM) tools and analysis tools used to perform complex simulations. Analysis tools may be used to predict product response to expected loads, including fatigue life and manufacturability. These tools include Finite Element Analysis (FEA), Computational Fluid Dynamics (CFD), and Computer-Aided Manufacturing (CAM). Using CAE programs, a mechanical design team can quickly and cheaply iterates the design process to develop a product that better meets cost, performance, and other constraints. No physical prototype need be created until the design nears completion, allowing hundreds or thousands of designs to be evaluated, instead of a relative few. In addition, CAE analysis programs can model complicated physical phenomena which cannot be solved by hand, such as viscoelasticity, complex contact between mating parts, or non-Newtonian flows.

As mechanical engineering begins to merge with other disciplines, as seen in mechatronics, multidisciplinary design optimization (MDO) is being used with other CAE programs to automate and improve the iterative design process. MDO tools wrap around existing CAE processes, allowing product evaluation to continue even after the analyst goes home for the day. They also

utilize sophisticated optimization algorithms to more intelligently explore possible designs, often finding better, innovative solutions to difficult multidisciplinary design problems.

Apart from Industrial Development there is also an hourly need for creation of an influential professional body which can cater to the need of research and academic community. The current scenario says there existsd a handfull of bodies like American Society of Mechanical Engineers (ASME). Hence we must strive towards formation of a harmonious professional research forum committed towards discipline of Mechanical Engineering.

The conference is designed to stimulate the young minds including Research Scholars, Academicians, and Practitioners to contribute their ideas, thoughts and nobility in these two integrated disciplines. Even a fraction of active participation deeply influences the magnanimity of this international event. I must acknowledge your response to this conference. I ought to convey that this conference is only a little step towards knowledge, network and relationship.

I congratulate the participants for getting selected at this conference. I extend heart full thanks to members of faculty from different institutions, research scholars, delegates, IRNet Family members, members of the technical and organizing committee. Above all I note the salutation towards the almighty.

Editor-in-Chief

DR. CH R. VIKRAM KUMAR
Dept. of Mechanical Engineering
N.B.K.R.I.S.T, Vidyanagar
Nellore(dt) Andhra pradesh
India – 524 413

Exprimental Investigation on Effect of Process Parameters In Cold Backward Extrusion

P. J. Pawar & D. D. Patil

Department of Production Engineering, K.K.W.I.E.E & R, Nashik, India.

Abstract - Cold backward extrusion is one of the youngest forming processes. It shows numerous qualitative advantages like high production rate, short piece production time, better surface quality and good static and dynamic quality's of formed component. Having such enormous application, some of biggest hindrances are power requirement of process to form the product at cold state and non- homogeneous distribution of strain, as result dimensional instability occurs. Aim of study is to find the effect of process parameters in cold backward extrusion process used to manufacture aluminum collapsible tubes. Extrusion force, stroke length, slug diameter and back pressure are treated as process variables while response of power, extrusion length, thickness of diaphragm and thickness of nozzle is recorded. Experimental trials with subsequent data collection are performed and empirical relation amongst the process variable and performance measures were determined by means of response surface methodology (RSM). Results reveals some stimulating fact about cold backward extrusion process, it is observe that all process parameters has influence the response.

Keywords - *cold backward extrusion, response surface methodology.*

I. INTRODUCTION

Extrusion, though one of the most important manufacturing processes today, is a relatively young metalworking process. Some of the latest developments within the manufacturing industry have revealed how emerging extrusion technologies can be used to reduce production lead time and manufacture mass range of product [1,2]. The main benefits cold backward extrusion process offer as compared to other manufacturing process are optimal usage of material, high production rate with short piece-production time and forms coupled with a good surface quality, good static and dynamic properties of the components due to the favorable fiber structure and work hardening [1,2,3]. With these merits cold backward extrusion processes is capable to produce complex part design for special purpose use and serve for many industries like pharmaceutical, aerospace, automobile, consumer goods etc.

Having such enormous advantages some of the biggest hindrance in the full scale application of cold backward extrusion technology are requirement of huge amount of power to form product in to cold state [1], which substantially increased the manufacturing cost of the product. The distribution of the comparative strain for cold backward extrusion is clearly non-homogeneous, which means cold backward extrusion process deals with a non-stationary process behavior which produced dimensional instability [1,4].

Many researchers contributed to predict effects of various process parameters. A. H. Elkholy [5] introduced analytical model for studying hydrostatic extrusion. The model is use to investigate various parameters affecting extrusion, these parameters being: die cone angle, reduction ratio and frictional coefficient die shape. Model is extended to optimize power requirement and frictional losses.

Effect of reduction ratio on power requirement of process is significant while improvement in the process can be possible [4, 6]. M. Gierzynska-dolna [7] performed attempt to optimum selection of extrusion condition for determined range of process parameter, Minimization of crack with in product was established as main criterion. K. Kuzman [6] discus the influence of tool geometry, friction and lubrication as well as work-piece properties on balanced material flow in combined extrusion process. J. Mstowski [4] worked on optimization of cold backward extrusion; aim of the study was constant thickness of internal anti-frictional cladding on a plain bearing in one operation. Study suggested theoretical model of velocity field permit the approach of geometrical optimization.

J. Danckert [8] elaborated effect of punch land on cold backward extrusion. The results show that a slight tilt of the punch land changes the contact conditions between punch land and can wall causing on the punch a net force, which will deflect the punch off Centre leading to variations in wall thickness. S.O Onuh [9] expressed relation of die geometry and extrusion speed of cold backward extrusion. An experimental investigation is made on the effects of die reduction in area, die angle, loading rate on the quality of the extrusion products, extrusion pressures and flow pattern of cold extruded aluminium and lead alloys shapes of inner circular sections with four symmetrical

projections. The radii of curvature for both extruded lead and aluminium alloys and the average hardness values of the extruded products along the projections and along the circumferential solid positions are found to increase with increase in die reduction in area, and slightly with increase of the loading rates [9,10]. M. Bakhshi-Jooybari [10] studied optimum die design and illustrated that the extrusion load for optimum curved die is reduced by 11%, compared to that in the optimum conical die.

Cold backward extrusion processes in engineering industries need to be cost and quality efficient for industries to sustain and excel in current competitive scenario. A significant improvement in process efficiency may be obtain if effect of process parameters on power requirement and dimensional variation are identifies and determines the regions of critical process control factors leading to desired outputs or responses with acceptable variations ensuring a lower cost of manufacturing. So work is carried out with aim to find effect of process parameters on power requirement and dimensional variation of final product.

In this study response surface methodology is used to elaborate relationship between cold backward extrusion process parameters and response of the process. Response surface methodology is very useful and modern technique for the prediction and optimization of machining performances. Response surface methodology (RSM) is a collection of statistical and mathematical techniques useful for developing, improving, and optimizing processes. The most extensive applications of RSM are in the particular situation where several input variables potentially influence some performance measures or quality characteristics of the process [11, 12].

II. SELECTION OF PROCESS PARAMETERS AND PERFORMANCE MEASURES

Mathematical model is developed by using response surface methodology. Process parameters and responses selected for the study are as follows.

Process Variables :

The process variables chosen for the optimization of the process are as follows:

- Extrusion force : F_e (kN),
- Stroke length : S_l (mm)
- Diameter of slug : d_s (mm),
- Back pressure : P_b (N/mm^2)

Performance measures:

- Power requirement of process : P_w (watt)
- Extrusion length : L_e (mm)
- Thickness of diaphragm : T_d (mm)
- Thickness of nozzle : T_n (mm)

Here thickness of diaphragm (T_d) and thickness of nozzle (T_n) are critical dimensions of specimen and aim to be controlled with in specified limit. Maximum possible range of each process variable is defined below.

Variable bounds:

$$380 \le F_e \le 770(kN)$$

$$341 \le S_l \le 344(mm)$$

$$19 \le d_s \le 22(mm)$$

$$50 \le P_b \le 125(N/mm^2)$$

III. EXPERIMENTATION

An extrusion press of 100 ton is utilized to manufacture aluminum collapsible tube part i.e. benthovate-c, the experimental setup is as shown in Fig. 1. Benthovate-c made of 96% pure aluminum is used for experimental trials product design of the part is as shown in Fig. 2.

Fig. 1 : Extrusion press utilized for experimentation

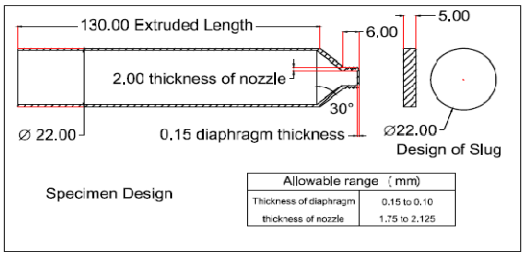

Fig. 2 : Specieman test sample design

Pri-experimental trials are performed to record initial condition of the process utilized by industry. In pri-experimental trial, overall shift production is taken in to account and two parts per sample are randomly selected from the batch of twenty pieces. Three samples are taken at starting, middle and end of the shift. Data collected is given in Table 1.

TABLE I. PRE-EXPERIMENTAL DATA COLLECTION

No.	F_e	S_l	d_s	P_b	P_w (watt)	L_e (mm)	T_d (mm)	T_n (mm)
1	614	343	22	75	5780.22	162.29	0.144	1.325
2	614	343	22	75	5815.39	162.96	0.139	1.356
3	614	343	22	75	5808.22	161.33	0.141	1.386

In order to build empirical relation for power requirement, extruded length, diaphragm thickness and nozzle thickness experiments are conducted based on central composite design (CCD). The CCD is capable for fitting second order polynomial and preferable if curvature is assumed to be present in the system. Central composite design consists of factorial points (n_f), central points (n_c) and axial points (n_a). Number of center point (n_c) and distance of axial runs from design Centre (a) are two parameter in CCD design. Value's of a and n_c can be chosen so that the composite Centre design is not to be block.

If the precision of the estimated response surface at some points depend only on the distance of point from origin and not on direction, then the design is said to be rotatable. When rotatable design rotates about center, variance of response remains same. Since the reason for using response surface is to locate the unknown optimization, it makes sense to use a rotatable design [11]. Choice of "a" make central composite design rotatable by using

$$a = 2^{q/4} = 2. \quad (1)$$

Where q is numbers of input variables

While factorial points use in experimental design having "q" number of variable can calculate by.

$$n_f = 2^q = 16 \quad (2)$$

And axial points are calculated by.

$$n_a = 2q = 8 \quad (3)$$

Total numbers of experimental trials are as follows.

$$N = n_f + n_a + n_c = 16 + 8 + 4 = 28 \quad (4)$$

Table 2 shows variables and levels selected for study. Central composite design of 28 run is chosen to account for factors and their levels (Table 3).

TABLE II. LIST OF PROCESS VARIABLES AND THEIR LEVELS.

Factor	Level				
	(-2)	(-1)	(0)	(1)	(2)
Extrusion force (kN)	380	477.5	575	672.5	770
Stroke Length (mm)	341	341.75	342.5	343.25	344
Diameter Of slug (mm)	19	19.75	20.50	21.25	22
Back pressure (N/mm^2)	50	67.75	87.5	106.25	125

from the experimentation trials various values of performance measures like power, extruded length, diaphragm thickness and nozzle thickness are calculated as show in Table 4 by using instruments i.e. Clamp meter, digital varnier and digital micrometer.

IV. MODELING USING RSM

Analysis of the experimental data obtained from CCD design runs is done on Microsoft Excel software using full quadratic response surface model as given by[9,10].

$$y = \beta + \sum_{j=1}^{q} \beta_j x_j + \sum_{i=1}^{q} \beta_{jj} x_j^2 + \sum \sum_{i<j} \beta_{ij} x_i x_j + \varepsilon \quad (5)$$

Where y is the predicted response, x_i and x_j are input variables which influence the response variable y. β_0 is the offset term, β_j is the j^{th} linear coefficient, β_{jj} is jj^{th} quadratic coefficient and β_{ij} is the ij^{th} interaction coefficient.

TABLE III. DESIGN MATRIX USED IN EXPERIMENTS

Trial	Extrusion force	Stroke length	Slug diameter	Back pressure
1	-1	-1	-1	-1
2	1	-1	-1	-1
3	-1	1	-1	-1
4	1	1	-1	-1
5	-1	-1	1	-1

6	1	-1	1	-1
7	-1	1	1	-1
8	1	1	1	-1
9	-1	-1	-1	1
10	1	-1	-1	1
11	-1	1	-1	1
12	1	1	-1	1
13	-1	-1	1	1
14	1	-1	1	1
15	-1	1	1	1
16	1	1	1	1
17	-2	0	0	0
18	2	0	0	0
19	0	-2	0	0
20	0	2	0	0
21	0	0	-2	0
22	0	0	2	0
23	0	0	0	-2
24	0	0	0	2
25	0	0	0	0
26	0	0	0	0
27	0	0	0	0
28	0	0	0	0

TABLE IV. EXPERIMENTAL DATA COLLECTED FROM CCD MATRIX

Trials	P_w (watt)	L_e(mm)	T_d(mm)	T_n (mm)
1	4117.84	143.78	0.174	1.3662
2	4894.256	155.52	0.147	1.3336
3	4627.513	157.71	0.156	1.3463
4	5103.188	161.42	0.1256	1.23
5	4490.618	140.74	0.179	1.5396
6	4967.325	148.83	0.1556	1.4196
7	4864.835	148.57	0.1583	1.2393
8	5498.863	159.93	0.143	1.3363
9	4574.045	140.11	0.1146	1.336
10	5209.307	146.48	0.095	1.239
11	4914.082	149.9	0.1016	1.208
12	5768.091	156.52	0.069	1.0153
13	4957.027	141.9	0.1266	1.3896
14	5647.879	146.7	0.0946	0.946
15	5543.543	142.57	0.1156	1.267
16	5982.594	146.8	0.0616	1.055
17	4483.468	148.49	0.0933	1.4226
18	5349.148	163.81	0.0456	1.216
19	4466.842	146.38	0.082	1.173
20	5300.034	166.22	0.0463	1.35
21	4664.581	157.11	0.0586	1.316
22	5393.984	147.26	0.076	1.2663
23	4798.097	153.33	0.0697	1.3346
24	5839.419	144.79	0.0596	1.1213
25	5157.407	151.34	0.136	1.2753
26	5175.785	151.35	0.1353	1.2636
27	5162.706	151.39	0.1356	1.3036
28	5169.874	151.42	0.1373	1.2933

With help of response relation model , empirical equation for power, extruded length, Diaphragm thickness and Nozzle thickness are developed.

For power

$$P_w = 5166443 + 279.723x_1 + 212949x_2 + 175.132x_3 + 254782x_4 - 56.597x_1^2 - 64.815x_2^2 - 28.354x_3^2 + 44.014x_4^2 - 11.029x_1x_2 - 31.295x_1x_3 + 16.021x_1x_4 + 13.097x_2x_3 + 12.230x_2x_4 + 36.667x_3x_4 \quad (6)$$

For extrusion length

$$L_e = 151375 + 3.648x_1 + 4.126x_2 - 2.2958x_3 - 2.6083x_4 + 0.4927x_1^2 + 0.5302x_2^2 - 0.4985x_3^2 - 1.2797x_4^2 - 0.3175x_1x_2 + 0.0025x_1x_3 - 0.805x_1x_4 - 1.2475x_2x_3 - 1.135x_2x_4 + 0.3325x_3x_4 \quad (7)$$

For diaphragm thickness

$$T_d = 0.13605 - .013737x_1 - 0.009462x_2 + 0.0035958x_3 - 0.020004x_4 - 0.006703x_1^2 - 0.008028x_2^2 - 0.0072406x_3^2 - 0.0079031x_4^2 - 0.0018937x_1x_2 - 0.000943x_1x_3 - 0.00263125x_1x_4 + 0.0000687x_2x_3 - 0.0006437x_2x_4 - 0.00094375x_3x_4 \quad (8)$$

For nozzle thickness

$$T_n = 1.28395 - 0.0637666x_1 - 0.0216x_2 + 0.000775x_3 - 0.0742333x_4 + 0.0074541x_1^2 - 0.0069958x_2^2 + 0.00041666x_3^2 - 0.01538333x_4^2 + 0.16825x_1x_2 - 0.015x_1x_3 - 0.483375x_1x_4 + 0.004875x_2x_3 + 0.088625x_2x_4 - 0.0249625x_3x_4 \quad (9)$$

A. ANOVA analysis

The statistical significance of second order model is check by F-test (ANOVA). computations are carried and listed in Table 5, 6, 7 and 8. Variable processing the maximum values of variance is said to have most significant effect on process under consideration.

For power model value of F-ratio is 44.826, which is greater than significance-F value. It can predict that operating variable of model is highly significant. For length model F-ratio (7.227) is far greater than and significance-F value is (0.0005) so model shows significant variable. Thickness of diaphragm and thickness of nozzle models are also shows significance as shown in table. 6,7. For both models F-ratio is 0.802 and 2.295 respectively. Values of significance-F are less.

TABLE V. ANALYSIS OF VARIANCE FOR POWER

	df	SS	MS	F	Significance F
Regression	14	5582178.84	398727.06	44.826	000
Residual	13	115634.82	8894.986		
Total	27	5697813.66			

df= degree of freedom, SS = sum of square, MS = mean sum of squre

TABLE VI. ANALYSIS OF VARIANCE FOR EXTRUDED LENGTH

	df	SS	MS	F	Significance F
Regression	14	1151.717	82.265	7.227	0.0005
Residual	13	147.964	11.381		
Total	27	1299.682			

TABLE VII. ANALYSIS OF VARIANCE FOR THICKNESS OF DIAPHRAGM

	df	SS	MS	F	Significance F
Regressio	14	0.0198	0.00142	0.80241	0.65676
Residual	13	0.0230	0.00177		
Total	27	0.0429			

TABLE VIII. ANALYSIS OF VARIANCE FOR THICKNESS OF NOZZLE

	df	SS	MS	F	Significance F
Regression	14	0.3081	0.022	2.2956	0.0716
Residual	13	0.1246	0.0095		
Total	27	0.4327			

V. RESULTS

Using empirical relation developed by response surface methodology, graphs are plotted and behavior of response against variation in process variables are recorded.

Power is most important performance measure. Extrusion force is most significant process variable observed, and shows higher influence on power. Fig. 3 shows variation in power against extrusion force. When forming force provided to the process is greater, relatively the power requirement also increases.

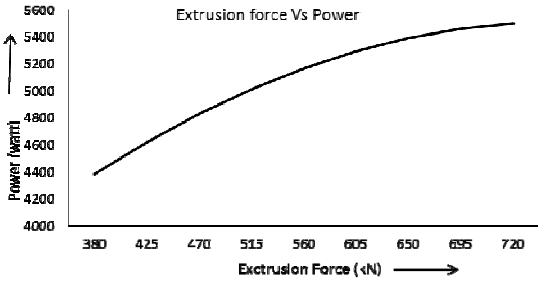

Fig. 3 : Behavior of power against extrusion force

Back pressure has influence in power requirement of the cold backward extrusion process. Fig. 4 show significant increment in the power as back pressure increases. Back pressure is a counter balance force use in formation of nozzle and diaphragm. As back pressure increase, effect to balance the force also significantly increase which ultimately results in increment of power requirement of the process. Stroke length and slug diameter also shows effect on power. Increment in the power requirement recorded as increment in slug diameter and stroke length.

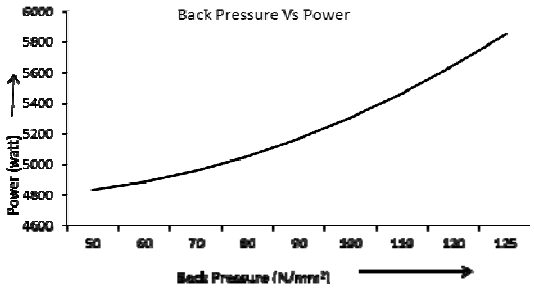

Fig. 4 : Effect of back pressure on power

As far as extrusion length is concerned, all four process variable shows significant influence on it. Effect of extrusion force and stroke length is successive and shown in Fig 5 and 6. As increase in extrusion force and stroke length take place the extruded length also increases.

When force applied on the material increase gradually, deformation of the part takes place. Due to greater deformation, strain generated in product get increased and extruded length increases. Increment in stroke length also results in elevated strain. Due to which increment in extrusion length take place.

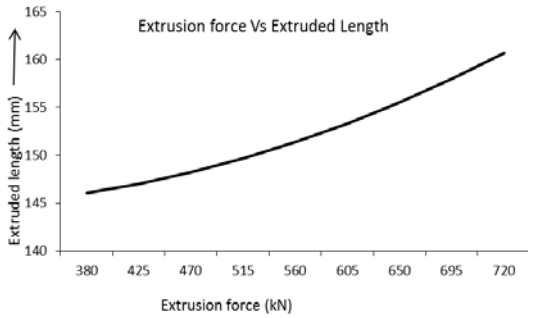

Fig. 5 : Behaviour of extruded length aginst stroke length

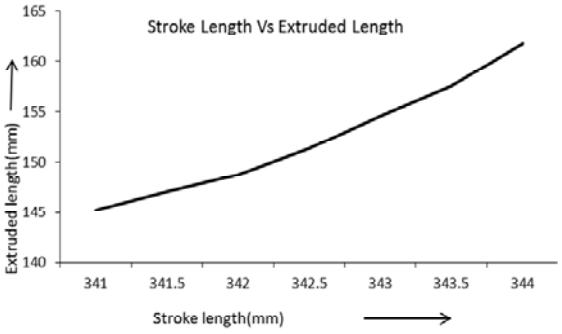

Fig. 6 : Behaviour of extruded length aginst stroke length

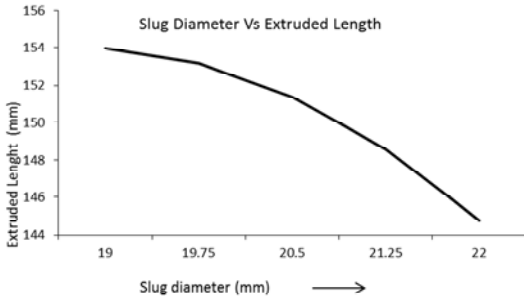

Fig. 7 : Behaaviour of extrusion length against slug diameter

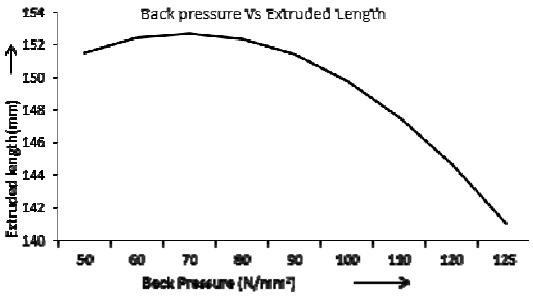

Fig. 8 : Behaviour of extruded length against back pressure

Process parameter like slug diameter and back pressure shows reverse effect on extrusion length. When increases in both process variables take place, successive decrement in extrusion length is observed. Fig 7 and Figure 8 shows behavior of slug diameter and back pressure on the extruded length.

Due to reduction in slug diameter, reduction ratio of extrusion process decrease. Force requirement of extrusion process is less at lower reduction ratio. So that deformation take place is greater in case of lower slug diameter. As far as back pressure is concern, back pressure decrease the forming effect of extrusion process. This results in reduction in extrusion length.

Thickness of diaphragm is one of the critical dimensions of test specimen. It has found from the empirical model that back pressure is on of the significant process parameter which shows highest influence on thickness of diaphragm. Behavior of response against back pressure is as shown in Fig 9.

Formation of diaphragm is function of back pressure. Due to elevated back pressure, force available for forming the diaphragm thickness increase. Forming force acts as a compressive strain accelerator. Due to which thickness of diaphragm get decreased.

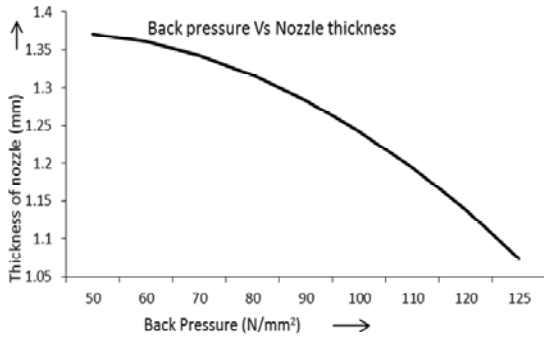

Fig. 9 : Behavior of thickness of diaphragm agaist back pressure

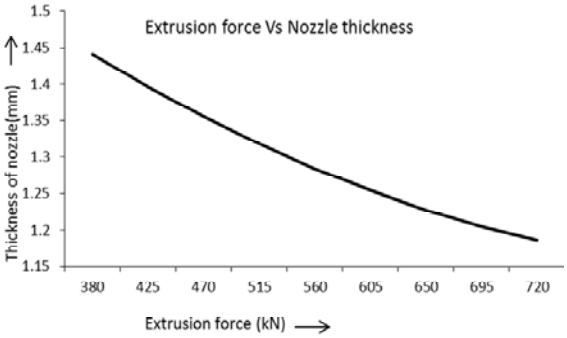

Fig. 10 : Behaviour of thickness of nozzle aginst extrusion force

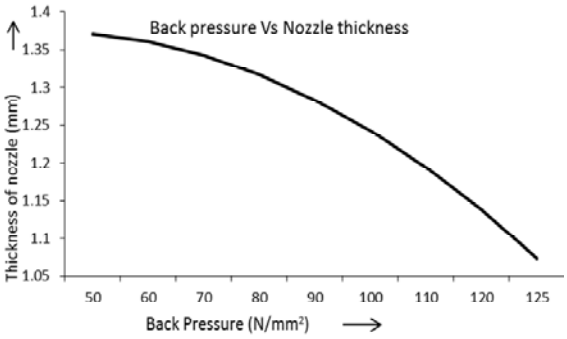

Fig. 11: Behaviour of thickness of nozzle aginst back pressure

Second critical dimetion of spesiman is nozzle thickness and it shows variation, significanly influence by back presure and extrusion force. Like diaphragm thickness, behaviour of nozzle thickness curve is also reverse and shows decreament with respect to increament in process variable. As extrusion force increases decreament in thickness of nozzle take place as shown in Fig 10 and 11.

All the response have influnece of process paramenter and showing variation as changing values of input variable.

VI. CONCLUSION

Response surface methodology (RSM) approach is used for data collection and defining empirical relation between process variable and performance measures. RSM shows good fit for experimentation.

Result reveals some of the interesting features of cold backward extrusion process used for manufacturing aluminum collapsible tubes. The facts observed from the results are as follows.

- Increment in power is observed with increment in all process parameters.
- Increment in extruded length is observed with increment in extrusion force and stroke length, whereas it decreases with increase in slug diameter and back pressure.
- Increment in thickness of diaphragm is observed with increment in extrusion force and back pressure whereas it decrease with increase in slug diameter and stroke length.
- Significance of slug diameter on thickness of diaphragm is less whereas back pressure shows high significance on thickness of diaphragm.
- Decrease in thickness of nozzle observed with increase in extrusion force, stroke length and back pressure whereas it increase with increase in slug diameter.
- Stroke length and back pressure are most significant parameters observed as far as thickness of nozzle is concern.

REFERENCES

[1] Klaus Siegert and Manfred Kammerer, 2002, “impact extrusion process”, Talat, Stuttgart, pp 02-19.

[2] Taylanaltan, Gracious Ngaile,GangshuShen, “Cold and hot forging: fundamentals and applications-vol. 1”,ASM international, pp 219-225.

[3] M. Plancak, A. Brameley and F. Osman, 1992, “Non-conventional cold extrusion”, journal of material processing technology, vol. 34, pp 465-472.

[4] J. Mstowski, P. Montmitonnet, F. Delamare, 1986, “Geometrical optimization of bi-layered plan bearing manufactured by cold backward co-

extrusion", journal of mechanical working technology, vol. 13, pp291-302.

[5] A. H. Elkholy, 1996 "Parametric optimization of power in hydrostatics extrusion", journal of materials processing technology, pp 111-115.

[6] K. Kuzman, E. Pfeifer, N. bay, J. Hunding, 1996,"Control of material flow in a combined backward can-forward rod extrusion", journal of materials processing technology, vol. 60, pp.141-147.

[7] M. Gierzynska-dolna, E. Krajewska-binczyk, 1992, "Criteria of optimization of extrusion of titanium alloys", journal of material processing technology, vol. 34, pp 405-410.

[8] J. Danckert, 2004, "The influence of the punch land in backward can extrusion" Manufacturing Technology, Volume 53, pp 227-230.

[9] S.O Onuh, M Ekoja and M.B Adeyemi, 2003,"Effects of die geometry and extrusion speed on the cold extrusion of aluminium and lead alloys" Journal of Materials Processing Technology, Volume 132, pp 274-285.

[10] M. Bakhshi-Jooybari, M. Saboori, S.J. Hosseinipour, M. Shakeri and A. Gorji, 2006, "Experimental and numerical study of optimum die profile in backward rod extrusion" Journal of Materials Processing Technology, Volume-177, pp 596-599.

[11] Myers, Raymond H., Montegomery, Douglas C., 1995," Response surface methodology: process improvement with steepest ascent, the analysis of response surface, Experimental designs for fitting response surface", New York: john wiley and sons inc, pp 183-351.

[12] Oehlert, Gary W., 2000, "Design and analysis of experiments: response surface design", New York: W H Freeman and company.

[13] M. M. Moshksar, R. Ebrahimi, 1998 "An analytical approach for backward extrusion forging for regular polygonal hollow components", international journal of mechanical science, vol. 40, pp 1274-1263.

[14] H. Long, 2006,"Quantitative evaluation of dimensional errors of formed components in cold backward cup extrusion", Journal of Materials Processing Technology, Volume 177, pp 591-595.

[15] R. Bihamta, Q.H. Bui, M. Guillot, G. D'Amours, A. Rahem and M. Fafard, 2011, "A new method for production of variable thickness aluminium tubes: Numerical and experimental studies", Journal of Materials Processing Technology, Volume 211, Pages 578-589.

◈◈◈

Strength Optimization of Pelton Turbine Runner under Dynamic Loading

Bharat P. Valand & Piyush P. Gohil

Department of Mechanical Engineering, Charotar Institute of Science & Technology,
Changa, Anand, Gujarat, India.

Abstract - This paper describes recent research in the field of Pelton turbine design optimization by considering the component structural stability point of view. Numerical method is useful tool to evaluate the structural stability of the pelton turbine runner under dynamic loading condition. Combined loads due to jet force by the nozzle jet on the blade and centrifugal force based on the rotational speed were considered. In order to increase the understanding of the loading condition, dynamic loading was to be considered as a time dependent loading. Numerical results are used to visualize the stress distributions in the pelton bucket and to predict structural stability of Pelton turbine at full load as well as at part loading due to rotation. In structural analysis, the finite element method has shown to be a strong numerical technique to provide good engineering accuracy. The optimized design is obtained based on structural strength of the pelton bucket using finite element analysis in ANSYS.

Keywords - *Pelton turbine runner; FEM model; Time-dependent loading; Strength optimization*

I. INTRODUCTION

Hydro power is eminent renewable energy source to suit higher energy demand of the world. Pelton turbine is useful to develop power using hydraulic energy in the case of high heads available. Numerical simulation is playing a very essential role for optimization of various components of Pelton turbine. [1]

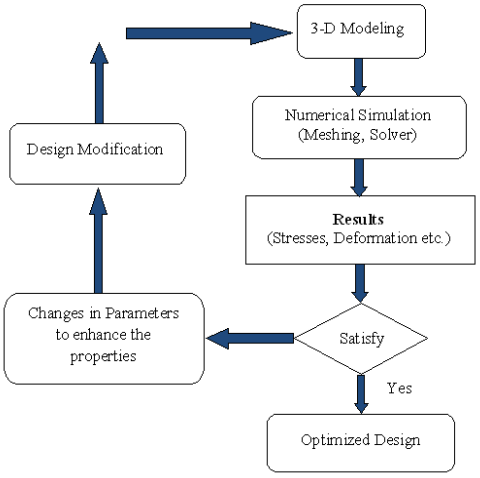

Fig. 1 : Optimization Cycle

Optimization cycle as shown in Figure 1 consists of design of each component using hydraulic calculation tools. After completion of basic design, 3-D model of each component has to be made. When looking at rehabilitation and maintenance processes to improve the performance of Pelton turbine runners, one needs to consider a number of steps. [2]

The stress analysis of the runner due to different loading is one of the most important tools that contribute its structural integrity evaluation. In structural analysis, the application of the finite element method has shown to be a strong numerical technique to provide good engineering accuracy. [2]

In the present work, the flow induced stresses in a Pelton turbine runner is presented by using the finite element analysis. Loads due to pressure on the blade and centrifugal force based on the rotational speed were considered.

In the present work, the strength optimization is presented by trial and error approach using finite element analysis. Loads due to jet force on the blade and centrifugal force based on the rotational speed were considered. Load due to jet force was derived from computations of the runner at different loading conditions. In order to increase the understanding of the loading condition, Gradual increment & decrement in the loading with respect to time is to be considered. [4]

II. PELTON TURBINE RUNNER

Pelton turbine runner was designed based on the following basic input parameters: [4]

Power to be developed (P)	: 4000 KW
Speed of the runner (N)	: 400 RPM
Head required (H)	: 350 m
Coefficient of velocity (C_v)	: 0.98

Coefficient of friction (μ) : 0.97

Geometrical modeling is first step of optimization loop. After designing the pelton turbine runner, the 3-D CAD model of pelton turbine runner was modeled using Pro-E wildfire 4.0.

The runner geometry was generated by a number of 3D sub models, one for each of the main components of the runner, rotor disc and pelton bucket.

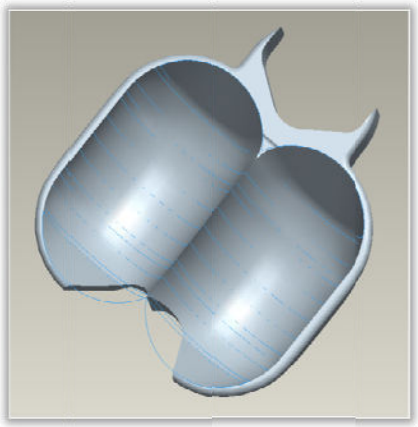

Fig. 2 : Pelton Bucket

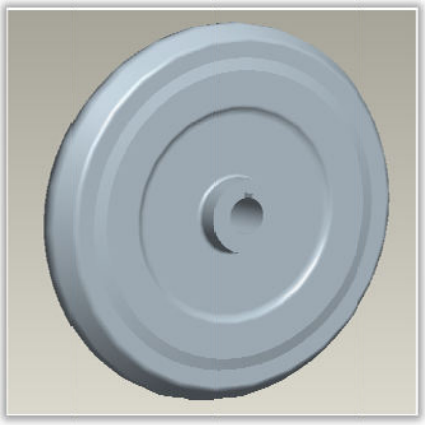

Fig. 3 : Rotor Disc

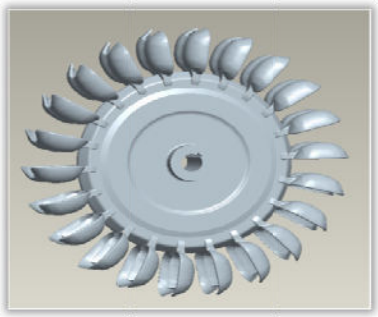

Fig. 4 : Assembly Model of Pelton Turbine Runner

The Pelton turbine runner was generated by mounting the number of buckets on the rotor disc which is represented in the Figure 2 Pelton bucket, Figure 3 Rotor disc of Pelton turbine runner and Figure 4 represents the Assembly model of Pelton turbine runner respectively.

III. FINITE ELEMENT MODEL

After generating the pelton turbine runner geometry, it is imported from the CAD software to generate the FEM model for finite element analysis. Because of periodic symmetry, only a sector of the domain was used for the finite element analysis. A sector of the runner was obtained by two main geometry sub-models; the first one was the definition of the Pelton bucket. The second sections were related to the rotor disc cross sections.

Once a sector of the runner was defined, a discretized model was generated. The number of finite elements was defined so as to obtain a three-dimensional element mesh of the Pelton bucket with a corresponding portion of the rotor disc. The Finite element mesh model of sector model of pelton turbine runner is shown in the Figure 5. It is well known, that from the fatigue life point of view, the bucket roots are the critical places of the Pelton runner where the maximum stress value can be generated. Finite element mesh with considerable element refinement in the bucket root area is shown in Figure 6.

Fig. 5 :FEM model of Sector of Pelton Turbine Runner

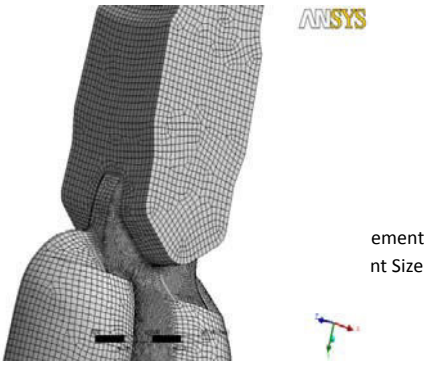

Fig. 6 : Mesh Refinement at Root Section of Pelton Turbine Runner

It is important to mention that during the meshing process, a compromise has to be done in order to evaluate the further solution and time of computations. It is important to achieve an exact solution by finite element method; the meshing of model needs to be performing very accurately as accuracy of results increases by increasing the no. of elements in the model.

The sector of the Pelton runner was modeled with 89126 solid elements (10-node Quadratic tetrahedron, 20-node quadratic hexahedron, wedge & pyramid).

IV. FORCE CALCULATION

Pelton turbine pressure energy of water is converted into kinetic energy at exit of injector. This high speed water jet is striking on bucket which makes it to rotate. [1] In Pelton turbine, the jet force from the nozzle act on the Pelton bucket for a limiting period in one revolution because Pelton buckets are moving through the jets, filling and emptying continuously during the rotation. [8]

Therefore, it is not continuous force condition. The total stress of the buckets is composed of the stresses resulting from the action of forces. [4]

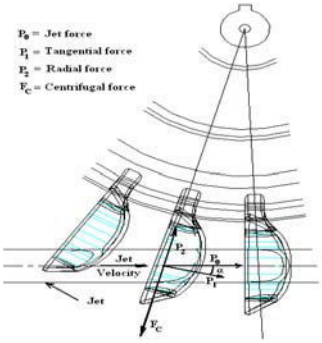

Fig. 7 : Forces acting on the Pelton Bucket

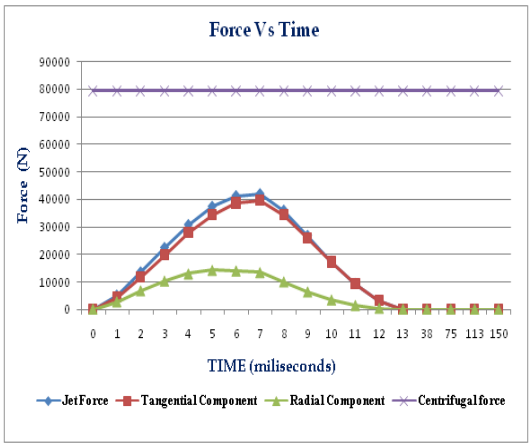

Fig. 8 : Dynamic Forces on Bucket Varying w.r.t. Time

The bucket is subjected to two kinds of forces, i.e. the centrifugal force due to rotary motion and the force of the jet as shown in the Figure 7. [4] Forces acting on the Pelton bucket have been calculated by considering the variation in time due to rotation of the Pelton runner which is represented in the Figure 8. Dynamic analysis was carried out by considering steady-state analysis under consideration of time dependent loads as its dynamic action of forces was converted into varying time loading. The stress resulting from the centrifugal force may be considered as static, the stress exerted by the force of the jet changes very rapidly with time. [4]

V. STRESS ANALYSIS

In this section, Stress analysis was performed by considering the combined loading due to Force of jet & Centrifugal force due to rotation of runner. Stress analysis was performed by considering the dynamic action of jet forces under time variation and the stress distribution over the bucket was evaluated in the dynamic loading. The material used in the pelton turbine runner designed was ASTM A743-CA6NM.

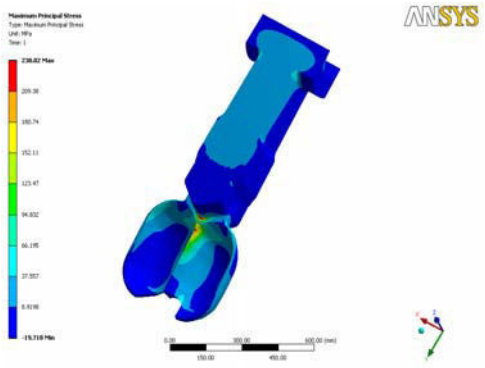

Fig.9: Stress Distribution over the Pelton turbine runner

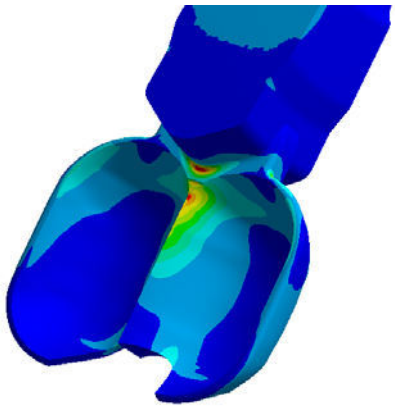

Fig. 10 : Front side View of Pelton Bucket

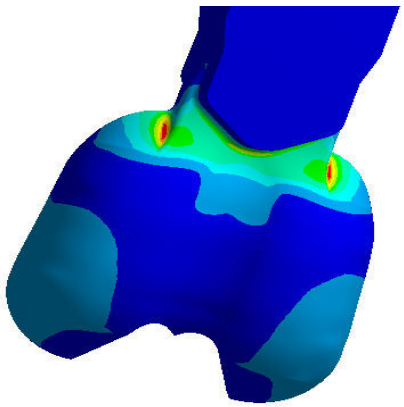

Fig. 10 : Back Side View of Pelton Bucket

From the structural analysis, stress distribution over the Pelton bucket under maximum loading condition is represented in Figure 9, 10 & 11.

During the dynamic action of forces on the pelton bucket, Maximum stress of magnitude of 238.02 MPa was generated during the period of 0.5042 milliseconds in which the full jet of force is acting on the pelton bucket.

As time is flowing, stress distribution in the Pelton bucket increases gradually and getting a maximum value at full load condition and then decreases gradually. As the load is varied with respect to time, the stresses generated in the pelton runner are also varying.

VI. OPTIMIZATION OF PELTON TURBINE RUNNER

The design of pelton runner which has been analyzed under time dependent loading is structurally in safe condition. But maximum stress magnitude is near by the designed stress of magnitude 275 MPa by considering the factor of safety.

Therefore some design modification has been done to increase the strength of the runner and its long life performance. From the structural analysis, the maximum stress is induced at the root section and fillet section of the pelton turbine runner. Therefore, to enhance the strength of the runner, the root of the pelton turbine runner is modified by changing in the shape of pelton turbine bucket geometry and the pelton rotor disc geometry.

A. Geometric Modification in Pelton Bucket

The optimization of the pelton runner has been done by making the following geometric modifications.

a) As from the analysis, the tensile stress was induced at fillet area of pelton bucket due to centrifugal force of pelton runner due to rotation. Hence, to reduce the stress at this section, the radius of the fillet was increased by 12 mm to 50 mm to achieve the smooth curvature and reduce also stress concentration at this section.

b) The material is also added to the back side of the pelton bucket to prevent the bending of the pelton bucket due to tangential jet force to reduce the tensile & compressive stress at root section.

c) Some dimensional modification has also been made at the contact area of pelton bucket and rotor disc to increase the contact area between the pelton bucket and rotor disc to improve the strength at the root section of the pelton runner. It's also a most critical portion of the pelton runner where the maximum tensile and compressive stresses are induced due to tangential jet force. Therefore, to reduce the stresses at this section, the contact area of the root section is increased from 189.20 mm to 196 mm.

B. Geometric Modification in Rotor Disc

The width of the rotor disc is changed to reduce the unnecessary weight of the runner and also shape has been modified to simplify the geometry to reduce manufacturing complexity and also reduce the material cost without compromising the structural strength of the pelton runner.

VII. COMPARISON OF NUMERICAL RESULTS FOR DESIGNED AND OPTIMIZED PELTON TURBINE RUNNER

After modifications in geometry, it was analyzed in the effect of dynamic loading condition. The comparison of numerical analysis results of designed model and new optimized model are shown as follows.

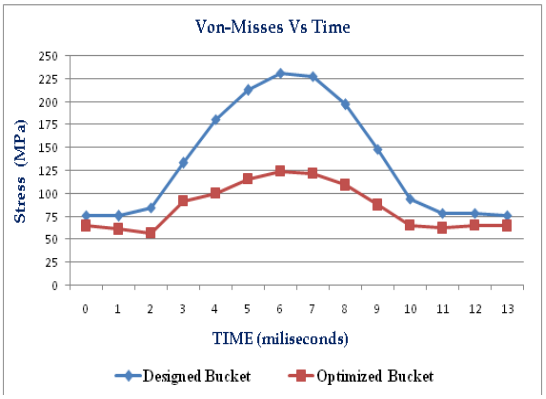

Fig. 12 : Von-misses Stresses in Designed & Optimized Pelton Turbine Runner w.r.t. Time

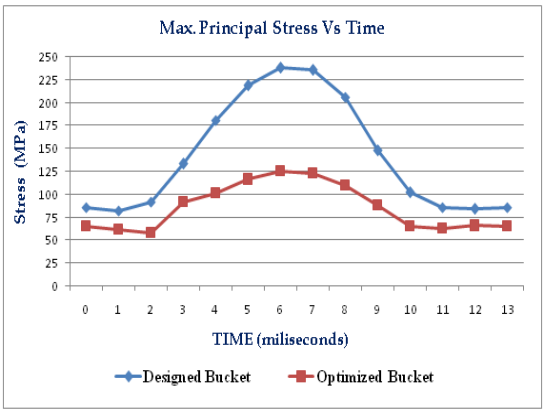

Fig. 13 : Maximum Principal Stresses in Designed and Optimized Pelton Turbine Runner w.r.t. Time

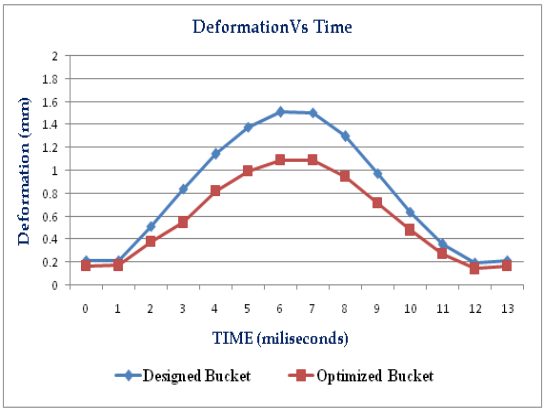

Fig. 14 : Deformation in Designed and Optimized Pelton Turbine Runner w.r.t. Time

VIII. RESULTS AND DISCUSSIONS

Numerical analysis result is very useful especially to understand behavior of designed under the operating condition. As from the results shown graphically, it can be seen that as time is varying, stress distribution in the Pelton bucket increases gradually and getting a maximum value at full load condition and then decreases gradually.

To validate numerical analysis result, the analytical procedure has been considered and it shows good agreement with analytical results. This validates the use of numerical analysis for future developments.

IX. CONCLUSION

From the analysis, it may conclude that the structural strength of the optimized model of pelton turbine runner under the dynamic loading condition is comparatively lower than the designed model.

The maximum stress distribution in optimized pelton turbine runner is below the $1/4^{th}$ of yield strength as compared to designed model of runner.

The optimized design of pelton turbine runner is structurally safe and may give the better performance and long life operation compared to designed pelton turbine runner based on the structural validation.

NOMENCLATURE

P	Power to be developed
N	Speed of the Pelton Runner
H	Head required
C_v	Co-efficient of Velocity
μ	Co-efficient of Friction
α	Angle between Jet Velocity and Peripheral Velocity
F_c	Centrifugal Force
P_0	Jet Force in Newton
P_1	Tangential Component of Jet Force
P_2	Radial Component of Jet Force
t	Time
σ_{uts}	Ultimate Tensile Strength of material used
σ_{ys}	Yield Tensile Strength of material used
f_s	Factor of Safety

REFERENCES

[1] K. Patel, B. Patel, M. Yadav and T. Foggia, "Development of Pelton Turbine using Numerical simulation", 25th IAHR Symposium on Hydraulic Machinery and Systems, IOP

Publishing, IOP Conf. Series: Earth and Environmental Science 12 (2010) 012048 doi:10.1088/1755-1315/12/1/012048.

[2] J. Veselý, M. Varner, "A Case Study of Upgrading of 62.5MW Pelton Turbine", CKD Blansko Engineering a.s., Czech Republic, 2000.

[3] J.S. Anagnostopoulos, D.E.Papantonis, "A Numerical Methodology for Design Optimization of Pelton Turbine Runners", Greece.

[4] M. Nechleba, "Hydraulic Turbines: their design & Installation", pages 374-431.

[5] J. lal, "A text book of Hydraulic machines including fluidics", pages 97-140, 2000, Calcutta.

[6] A. Perrig , M. Farhat "Flow in a Pelton Turbine Bucket: Numerical and Experimental Investigations", Journals of fluids engineering (Transactions of ASME), Vol. 128, March 2006.

[7] B. Zoppe, C. Pellone, T. Maitre, P. Leroy, "Flow Analysis inside a Pelton Turbine Bucket", Journal of Turbomachinery: Transactions of the ASME, July 2006, Vol. 128, Pages: 500-511, DOI: 10.1115/1.2184350.

[8] H. Keck, W. Michler, "Recent Developments in the Dynamic Analysis of water Turbines", 2nd IAHR International Meeting of the Workgroup on Cavitations and Dynamic Problems in Hydraulic Machinery and Systems Timisoara, October 24 - 26, 2007, Romania.

[9] John S. Anagnostopoulos, and Dimitrios E. Papantonis, "Flow Modeling and Runner Design Optimization in Turgo Water Turbines" World Academy of Science, Engineering and Technology 28 2007.

[10] A Santolin, G Cavazzini, G Ardizzon and G Pavesi, "Numerical investigation of the interaction between jet and bucket in a Pelton turbine", Proceedings of the Institution of Mechanical Engineers, Part A: Journal of Power and Energy 2009 223: 721, DOI: 10.1243/09576509JPE824.

◈◈◈

Thermal Analysis of Bellows Free Cryogenic Transfer line

Amit D. Thakkar & M. I.Vyas

Cryogenic Dept., L. D. College of Engineering, Ahmedabad, Gujarat, India

Abstract - Cryogenic transfer line is one of the major components used in any cryogenic system. This transfer line is used to transport cryogenic liquid from one system to the application at very low temp. Due to low temp, the cryogenic transfer line tends to contract. To avoid the thermal stress, bellows are generally used. But there bellows are not very reliable under the cyclic loads and they are weak points to have leaks. The reliability is essential in case of space technology and other closed systems which can not be opened easily. To make the system reliable, bellows free transfer line can be designed, which is now very challenging task. This paper describes the Thermo Structural design & Analysis of bellow free transfer line.

Keywords - *Ansys, Bellow free, Invar, Transfer lines*

I. INTRODUCTION

Cryogenic transfer line is one of the major components used in any cryogenic system. This transfer line is used to transport cryogenic liquid from one system to the application at very low temp. During the flow of the cryo-fluid, the transfer line should be well insulated otherwise required condition of cryo-fluid at the application can't be supplied. The insulation to these cryo transfer line is provided with the help of static vacuum. Among static vacuum insulated transfer lines, there are many different designs to choose from including flexible pipe, rigid pipe, internal bellows, external bellows and Invar. The most reliable transfer line is without bellows; which can be produced by using the INVAR material. Invar material can lead to bellow free transfer line. The unique feature of a static vacuum bellow free transfer line is that the performance over time does not change & there is no possibility of leaking. This type of transfer lines are used in small systems having very high reliability and within the constrained space for installation.

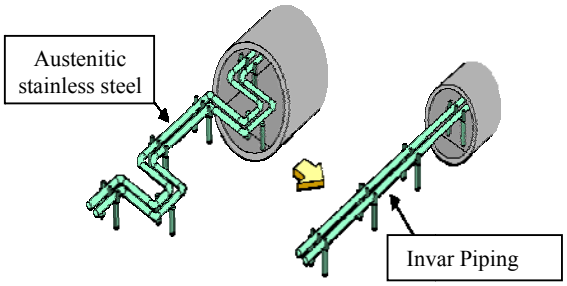

Fig. 1.1: Difference between the Austenitic line and Invar Transfer line [1]

II. MATERIAL- INVAR

The material has to be selected very carefully for cryogenic applications because of following reasons (i) The strength of the material changes. (ii) The thermal conductivity of the material changes. (iii) The material contracts and produces the thermal stress. (iv) Material modulus may change. (v) Many materials undergo phase changes (i.e. becomes brittle) etc. Hence all the above points should be checked as per the design criteria to select the proper material. The material should also be selected on the basis of fabrication, joining with other materials, cost and compliance with regulatory codes.

INVAR is used to make the bellow free transfer lines. Invar, also known generically as FeNi36 (64FeNi in the US), is a nickel steel alloy notable for its uniquely low coefficient of thermal expansion (CTE or α). It was invented in 1896 by Swiss scientist Charles Édouard Guillaume. He received the Nobel Prize in Physics in 1920 for this discovery, which shows the importance of this alloy in scientific instruments. "Invar" is a registered trademark of Arcelor Mittal, but FeNi36 is also manufactured by Japanese companies. Like other nickel / iron compositions, Invar is a solid solution; that is, it is a single-phase alloy. The name "Invar" comes from the word invariable, referring to its lack of expansion or contraction with temperature changes. The invar material has different composition as per their applications.

Table 1.1:Different Grades of the Invar materials

Grade	Ni	Co	Fe
Invar	36	< 0.4	Remainder
Invar-M93	36	< 0.2	Remainder
Inovar	36	< 0.1	Remainder
Microvar	36	0.25	Remainder
Inovco	33	4.5	Remainder

Invar-36 is used for cryogenic applications so It is used for bellows free transfer line.

III. PROBLEM FORMULATION:

Transfer line is required to cater the liquid from the storage tank to the point of application. Cryo transfer line can be from few meters to hundreds of meter. But bellow free transfer is generally used in the small length required by the system, because it is not very economic. But small systems are using bellow free transfer lines due to its high reliability.

3.1 Technical specifications required

(After technical discussion with I.P.R. Taken Data)

Type of transfer line : Bellow Free

Operating pressure : 2 bar

Operating temperature : 80 K

Cryogenic fluid used : LN2

Length of the transfer line : 5 m

Number of bends : 0 (Only straight transfer line)

Mass flow rate : 2000 litres/hour

Allowable pr. drop per meter : 50 Pa

Insulation : Vacuum & MLI

Configuration : Rigid

Cryogenic fluid condition : Sub-cooled

Max. Allowable deflection: 1 mm

3.2 Assumptions

a. Single phase liquid i.e. quality of the liquid does not change

b. Configuration of line should be completely straight without any bends

c. Only MLI and vacuum insulated lines are considered. No other type of insulation is considered.

d. Frictional, entry and exit loss is considered only

3.3 Fluid Properties

Liquid nitrogen is used as the working fluid, which is at the sub-cooled condition. The fluid properties are taken at 2 bar and 80 K. The following properties are necessary for the design point of view:

Density : 794.11 kg/m3

Viscosity : 1.45E-04 Pa-sec

Velocity of sound : 825.95 m/sec

Specific heat (Cp) : 2.05 kJ/kgK

Specific heat (Cv) : 1.06 kJ/kgK

Gamma (Ratio of Cp & Cv) : 1.93

3.4 Results

Table 3.1:Design summary & comparison of process lines designed for INVAR & SS

Sr. No.	Parameter Name	INVAR Transfer Line	SS Transfer Line
1	Contraction of the process line	-1.79 mm	-14.79 mm
2	Axial Stress	50.12 MPa	588.00 MPa
3	Bellow / U-Loop requirement	***NOT REQUIRED***	***REQUIRED***

IV. INPUT DATA FOR ANSYS ANALYSIS:

4.1 Technical Specification required:

a. Inner diameter of the INVAR line: 45 mm. (45 x 10-3 m)

b. Thickness of the line : 1.65 mm (1.65 x 10-3 m)

c. Outer diameter of the INVAR line: 48.3 mm (48.3 x 10-3 m)

d. Length of the INVAR line : 5m

4.2 Analysis :

a. Mode : Thermo – Structural

b. Type : Static

4.3 Element :

Solid45 element is used; this element supports both the thermal contraction, temperature and structural properties.

4.4 Model statistics:

Number of volume : 1

Number of areas : 6

Number of lines : 20

Number of key points : 16

Number of elements : 16000

Number of nodes : 32080

4.5 Loads:

Loads are given as the body loads and defined in terms of the temperature because here temperature is decreasing from 300 K to 80 K.

Reference temperature of the process line : 300 K

Uniform temperature of the process line : 80 K

4.6 Material Properties:

Material Number	: 1
Material type	: Isotropic
Young's modulus, EX	: 140E+9
Poisson's ratio, PRXY	: 0.3
Thermal Contraction, ALPX	: 1.62E-06
Density	: 8118 kg/m3

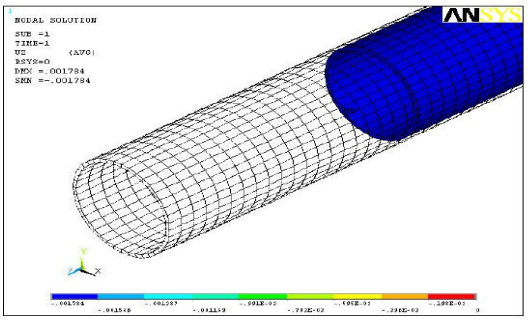

Fig. 4.1: Max. Displacement at the free end of process line

The maximum displacement at the free end as per above fig-4.1.= -0.001784 m = -1.784 mm

4.7 Thermal stress due to thermal contraction:

For the thermal stress , the other end of the process line is also constrained . The thermal contraction has to be restricted to get the thermal stress

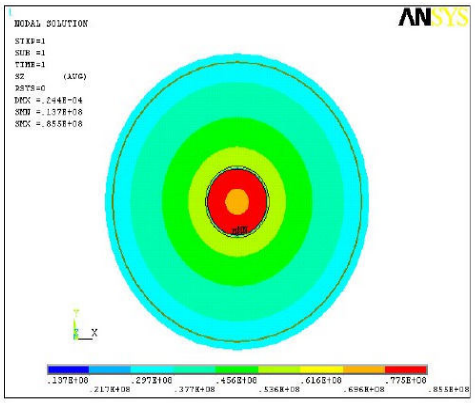

Fig. 4.2: Stress distribution of process line

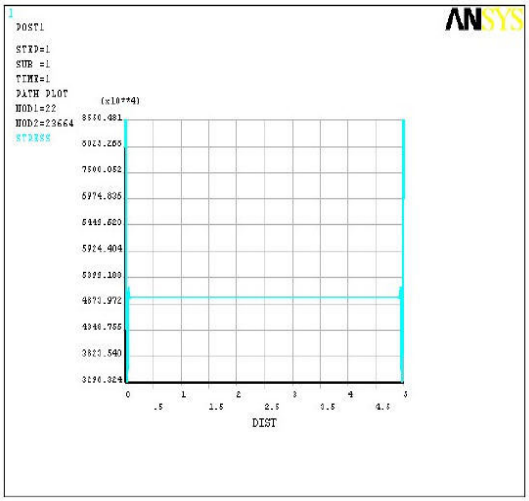

Fig. 4.3 : Stress Vs Length graph of process line

The above graph shows that the stress varies from 32.98 MPa to the 85.50 MPa. But these minimum and maximum stresses are at the ends only; hence these stresses will not be counted for the stress finding along the process line. The stress along the transfer line is between 48.73 MPa and 53.99 MPa. The exact value can be found out by checking the graph by magnifying the graph between the length 0.5 to 4.5 m and the stress value from 50 MPa to 52 MPa.

From range of 50 to 52 MPa; Stress value is between the 50 MPa to 50.20 MPa, which is shown in the figure 4.4.

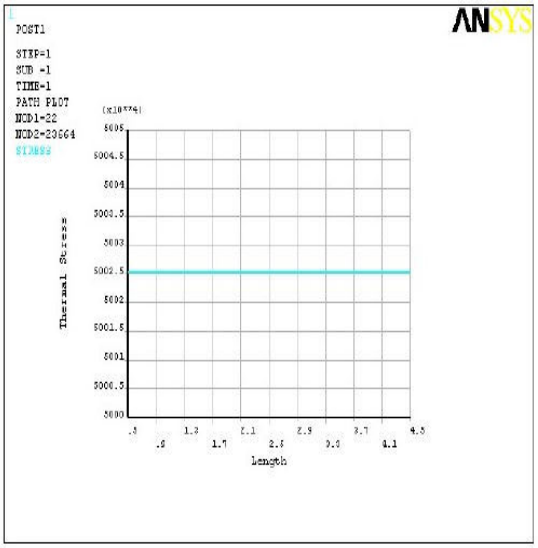

Fig. 4.4 : Magnification of Stress Vs Length graph of process line

4.8 Results

Table 4.1: Comparison of result between Analytical design & FE Analysis for INVAR (5 meter length)

Parameter	Analytical	FE Analysis	Ratio (Analytical/ ANSYS)
Thermal contraction	-1.79mm	-1.784mm	1.003
Thermal stress	50.12Mpa	50.02MPa	1.001

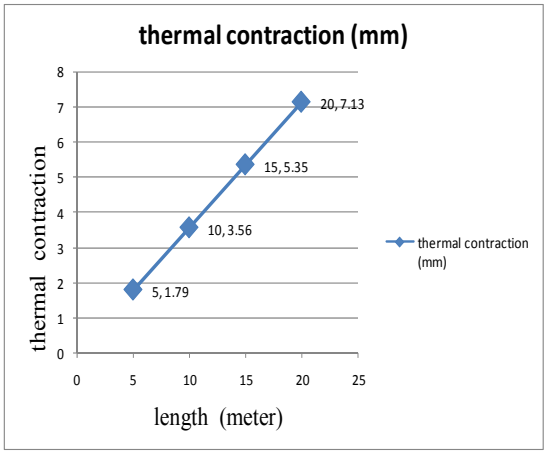

Fig. 4.5: Thermal stress vs Length Graph

Table 4.2: Result between FE Analysis for INVAR for Different length

Length	Thermal contraction	Thermal stress
5 m	-1.79 mm	50.02 Mpa
10 m	-3.56 mm	50.02 Mpa
15 m	-5.35 mm	50.02 Mpa
20 m	-7.13 mm	50.02 Mpa

After check result analyze the given curves are linear from any length. Thermal stress same for any length because all condition in same (ΔL/L*Y).Thermal contraction is increase with increase length.

V. CONCLUTION :

From the above result summary of design & analysis for the cryogenic transfer lines, it can be concluded that the SS transfer lines can be replaced with INVAR transfer lines. Both the type of transfer lines behaves same but the major difference in both the transfer line is requirement of bellows only. INVAR transfer lines do not require any bellow while the SS transfer lines requires bellow or U-loop

REFERENCES

[1] "Realization of Invar Alloy LNG piping" by Takehiko Edamitsu; Osaka Gas Co., Ltd. Shuji Yamamoto; Osaka Gas Co., Ltd. Muneji Ujita; Osaka Gas Co., Ltd.; Taketo Yamakawa; Kawasaki Heavy Industries, Ltd.; Setsuji Kishimoto; Kawasaki Heavy Industries, Ltd. Keiichi Nakamura; Sumitomo Metal Industries, LTD. Keiichi Yamamoto; Sumitomo Metal Industries.

[2] "Long, Bellows-Free Vertical Helium Transfer Lines for the LHC Cryogenic system" by Gruehagen H. LHC Division, CERN, 1211 Geneva 23, Switzerland, Posselt H & Weber J. LINDE AG, Linde Engineering Division, D-82049 Hoellriegelskreuth, Germany., Ahlers H. BABCOCK NOELL NUCLEAR GmbH, site D-46049 Oberhausen, Germany.

[3] "Cryogenic Engineering" by R.A. Barron.

[4] ASME Codes for the mechanical design etc.

[5] Technical Discussion with I.P.R BHAT Gandhinagar etc.

[6] Use analysis software ANSYS.

[7] Cryogenics – Research & Application By.Marshall sitting

◈◈◈

Green Supply Chain Management–Need of The Hour

Raaghavan.P , ShrinidhiVenkat, VivekNarayanji.S.G & *Adhithyan.S

Thiagarajar College Of Engineering, Madurai – 625015.
*Kalasalingam University, Krishnankoil– 626126.

Abstrac t- The term **e-waste**, expanded form **Electronic Waste**, term embracing all types of waste, referring electronic devices, surplus, broken or obsolete, which have been discarded. Computers, LCD / CRT screens, mobile phones, CFC foams etc. **They are** particularly significant because their disposal can result in toxic rubbish, as they contain dangerous metals like lead, cadmium and mercury, which can contaminate air and water. Concern about the environmental issues surrounding **e-waste** has led governments across the world to implement laws for its safe disposal. To address sustainable development concerns, there is a need to facilitate the recovery and reuse of useful materials from waste generated from a process, reducing the wastes destined for final disposal and to ensure the environmentally sound management of all materials. Green Supply chain management is the coordination and management of a complex network of activities involved in delivering a finished product to the end-user or customer. All stages of a product's life cycle will influence a supply chain's environment burden, from resource extraction, to manufacturing, use and reuse, final recycling, or disposal.

Keywords: *E-waste, Green Supply Chain Management.*

I. INTRODUCTION

Integrating environmental thinking into supply chain management, including product design, material sourcing and selection, manufacturing processes, delivery of the final product to the consumers, and end-of-life management of the product after its useful life.This process develops outputs that can be reclaimed and re-used at the end of their life-cycle thus, creating a sustainable supply chain." The whole idea of a sustainable supply chain is to reduce costs while helping the environment. In today's "sustainable" world the thinking should be what is the life cycle costs of this part, piece of equipment or supply chain process. Beyond this definition with adding the "green" component, it refers to green supply chain management (GSCM) which isdefined as "***green procurement+ green manufacturing+ green distribution+ reverse logistics***". The idea of GSCM is to eliminate or minimize waste (energy, emissions,and chemical/hazardous, solid wastes) along the supply chain. As a more systematic and integrated strategy, It has emerged as an important new innovation that helps organizationsdevelop "***win-win***" strategies that achieve profit and market share objectives by lowering their environmental risks and impacts, while raising their ecological efficiency. A set of performance measures is used to determine the efficiency and/or effectiveness of anexisting system, to compare competing alternative systems, or to design proposed systems by determining the values of the decision variables that yield the most desirable levels of performance.

GSCM improves operations by employing an environmental solution:

- Improves agility – It helps to mitigate risk and speeds up innovations.
- Increases adaptability – It often leads to innovativeprocesses and continuous improvements.
- Promotes alignment – It involves negotiating policies with suppliers andcustomers, which results in better alignment of business processes and principles.
- Core focus of the lectureship will be on the necessity of 'green' and on greenoperations (network design and reverse logistics, transportation, green manufacturingand re-manufacturing and waste management).

II. GREENSUPPLYCHAINMANAGEMENT

2.1 Green Procurement

It is defined as an environmentalpurchasing consisting of involvement in activities that include the reduction, reuse and recycling of materials in the process of purchasing. Besides green procurement is asolution for environmentally concerned and economically conservative business, and a concept of acquiring a selection of products and services that minimizes environmentalimpact. It includes,

- Supplier selection: Purchase materials or parts only from "Green Partners" who satisfy green partner environmental quality standards and pass an audit process in following regulations for the environment-related substances

- select suppliers who controlhazardous substances in company's standard lists and obtain green certificate achievements.

1.2 Green Manufacturing

It is defined as production processes which use inputs with relatively low environmental impacts, which are highly efficient, and which generate little or nowaste or pollution. Green manufacturing can lead to lowerraw material costs, production efficiency gains, reduced environmental and occupational safety expenses, andimproved corporate image.

- ***Hazardous substance control***: Lead free – replace other substances such as bismuth, silver, tin, gold, copper and rinse parts with clean water instead of using chemicals andReuse water for quality control in inputs at vendor site and recheck before processing
- ***Energy-efficient technology***:Reduce power consumption in products such as ramp load/unload technology in HDD, increase product life-span resulting in higher efficiency and productivity, improve machineuptime, improve machine performance, design product, for example compact design with Improved features yet using fewer resources to produce**,** Strive for higher percentage of recyclability and recoverability for products, using bio-based plastics achieves high level of fire retardancy.
- Promotes reuse/recycle of parts
- Enhance environmental consciousness
- Reduce indirect materials such as epoxy glue

2.3 Green Distribution

Green distribution are consists of green packaging and green logistics. Packaging characteristics such as size, shape, and materials have an impact on distribution because of their affect on the transport characteristics of the product. Better packaging, along with rearranged loading patterns, can reduce materials usage, increase space utilization in theWarehouse and in the trailer, and reduce the amount of handling required.

- Green packaging: downsize packaging.
- Use"green" packaging materials.
- Cooperate with vendor tostandardize packaging.
- Minimize material uses and time.

2.4 Reverse Logistics

It is the process of retrieving the productfrom the end consumer for the purposes of capturing value orproper disposal. Activities include collection, combinedInspection/selection/sorting,re-processing/direct recovery,redistribution, and disposal.

III. KEY DRIVERS FOR GREEN INITIATIVES

3.1 Government Compliance

The climate change is happening faster and will bring bigger changes quicker than titivated. Ironically market and the nature hitting the wall at once, is a sign that we need to find better ways to be more sustainable. Whether the drive is to comply with the government regulations or to meet the costumers' expectations companies are finding motivation to go green. Going green does not just impact company's thinking and strategy but influences supply chain as well. Righteously the focus is not just to attain cleaner water consumption and alternative energy sources for server farms, but to make supply chains more environmentally friendly.

3.2 Supply chain efficiency

Organizations are integrating their supply chains to reduce operating costs and improve their customer service Businesses that want to transition to a green supply chain should take the opportunity to review all their business processes to identify areas where adopting a greener outlook can actually improve their business. Companies should review each process along the

Supply chain to identify if a more environmentally sound approach will help cure the inefficiencies that occur Successful supply chain management is an iterative process that evaluates the cost/benefit trade-offs of operational components. The supply chain strategy constitutes the actual operations of that organization and the extended supply chain to meet aspecific supply chain objective. Most supply chain management strategies focus on driving down operational costs and maximizing efficiencies. An organization may choose a supply chain approach directed at supplier and vendor management as a means to remain competitive

3.3Corporate Responsibility

Green initiatives are tied to the larger issue of corporate social responsibility (CSR), the idea that companies have obligations not just to their investors but also to their stakeholders, society, and the environment. Many corporations driven to comply with increasing government regulations and pressure from shareholders are turning to the International

Organization for Standardization (ISO) for guidance with implementing green and CSR programs.

IV. SUGGESTION

To obtain efficient and effective in GSCM, collaborativeamong important stakeholders in industry must bestrongly concerned. After making discussion about researchresults with experts and manufacturers, some importantsuggestions are noted here:

- **Promote Eco design**: Eco design as an activity thatintegrates environmental aspects into product design anddevelopment, the integrated activities lead to continualimprovement of the environmental performance of the entireproduct through technological innovation.
- Developingenvironmentally friendly products
- Design the products to extendlifetime of product, it can be improved, repair, and re-use ofproducts such as modular design
- Designfor recycling /disassembly, after end of life products that can bemore recovery
- Control hazardous substances: complying with RoHSand other regulations.
- Set rules for disposing electronics waste and considermore investment in recycle plants
- Propagate GSCM knowledge and encourage usingenvironmentally friendly goods and services
- Set a direct responsible unit to take in charge ofelectronics waste only which will increase reverse logisticsefficiently
- Promote refurbishing and recycling throughcampaigns/ activities to raise reuse/recycle awareness inelectronics consumption
- Set a database unit to collect and record informationAbout production, import/export data, and wastemanagement (do traceability)
- Encourage team building and train skilled labours forreverse logistics management
- Raise the applications in Extended ProducerResponsibility (EPR); EPR is an environmental protectionstrategy based on the "polluter pays" principle, by making themanufacturer of the product responsible for the entirelife-cycle of the product and packaging they produce
- Promote Product Service System (PSS); services andproduct-service combinations are recognized as a potentiallypowerful concept for sustainable development. Aproduct-service system (PSS) is a new trend that has thepotential to minimize environmental impacts of bothproduction and consumption. Thus, more traditional materialintensive ways of product utilization are replaced by thepossibility to fulfil consumers' needs through the provisionof more dematerialised services

V. GAINING SUSTAINABILITY THROUGH GREENSUPPLY CHAIN MANAGEMENT

Sustainable development is development that meets the needs of the present without compromising the ability of future generations to meet their own needs. Implementing a sustainable development approach within a company is a horizontal task, is as much as it impacts on almost all the company's functions. Green is a subset of the broader world of sustainability. Sustainability incorporates endeavours such as fair labour practices, human rights, and community responsibility, while green includes things that impact the environment.

VI. KEY FINDINGS

- Retail chain GSCM mandates bring business and environmental benefits to the entire consumer products supply chain.
- Best-in-Class (BiC)firms report improvements in distribution efficiency, service differentiation, cost reduction, and customer retention as a result of adopting GSCM practices in distribution activities.
- GSCM practices are strategically important for retail chains and CPG manufacturers, withImplementation mainly driven by high transportation and energy cost coupled with the need to differentiate distribution services.
- Many retail chains and CPG manufacturers are seeing improvements in energy usage, wasteReduction, packaging reduction, and greenhouse gas (GHG) emissions reduction in distribution activities.

REFERENCES

1. Q. Zhu, J. Sarkis, and K. Lai, "Green supply chain management:pressures, practices and performance within the Chinese automobile industry," *Journal of Cleaner Production*, vol.15, 2007, pp.1041-1052.
2. A. A. Hervani, M. M. Helms, and J. Sarkis, "Performance measurementfor green supply

chain management," *Benchmarking: AnInternational Journal*, vol. 12, no. 4, 2005, pp. 330-353.

3. R.I. Van Hock, "From reversed logistics to green supply chains,"*Logistics Solutions*, vol.2, 2000, pp.28-33.
4. H.K. An, T. Amano, H. Utsumi, and S. Matsui, "A framework for greenSupply chain management complying with RoHS directive,"Available:http://www.crrconference.org/plaintext/downloads/2006kyunganamanoutsumimatsui.pdf
5. J. Sarkis, "A strategic decision framework for green supply chainmanagement," *Journal of Cleaner Production*, vol.11, 2003,pp.397-409.
6. B.M. Beamon, "Designing the green supply chain," *LogisticsInformation Management*, vol.14, no.4, 1999, pp.332-342.
7. M.A. Salam, "Green procurement adoption in manufacturing supplychain," *Proceedings of the 9th Asia Pasific Industrial Engineering & Management Systems Conference* (APIEMS2008), 3-5 December2008, Indonesia, pp.1253-1260.
8. M. Atlas, and R. Florida, "Green manufacturing," *Handbook ofTechnology Management*, 1998
9. K. Kamigaki, "Generation of green brand," Asian Electrical andElectronic Green Society International Conference, 7-9 October 2009, Thailand.
10. J.C. Ho, M.K. Shalishali , T. Tseng, and D.S. Ang, "Opportunities ingreen supply chain management," *The Coastal Business Journal*, vol.8, no.1, 2009, pp.18-31. Available: http:// www. coastal.edu/ business/cbj/pdfs/ articles/ spring2009/ ho_shali shali_ tseng_ ang.pdf.

◈◈◈

Fabrication & Experimental Analysis On Self Generated Electricity Room Cooler

Vijay B. Patel, Kishor R. Watkar & Gautam R. Ramteke

Mechanical Engineering Dept., Government College of Engineering, Chandrapur,
Dist- Chandrapur, Country – India

Abstract **-** Problem of load shedding is not new for all. Most of the underdeveloped & developing countries like ours are really facing the scarcity of electricity. India's 70% population resides in village where power failure is around 6-8 hours a day. In summer this much power shortage directly led's to the incomfortness as well as physical and mental stresses to people as they can't use their comfort providing devices like fans, Room coolers, A.C.'s etc. Keeping this problematic statement in mind, we developed an assembly of a general room cooler which will also work in the absence of power. Our paper thus reflects the unambiguous scenario of such a room cooler along with its constructional features and working of the same. Further it deals with some of the mathematical analysis which we had taken assuming constant load conditions. At the end, some expected future modifications are well discussed.

Keywords – *D.C. motor, dynamo, rotor, coupling, rectifier*

I. INTRODUCTION

Global Warming and increment in environment's temperature is a matter of serious concern. Earth's temperature is increasing day by day. Talking about India & particularly about Maharashtra, some of the backward districts like Chandrapur, Akola, Nagpur etc have recorded temperature of more than 45º C in summer. The graph below shows the annual temperatures of Nagpur, one of the biggest districts in vidharbh region in Maharashtra. Around April to June, temperature is at its peak above 40º C (Refer Fig. 1). At this temperature human beings cannot carry out his day-to-day activities. In fact it's somewhat very much difficult to survive at this temperature. Problem of sun stroke, cramps etc are common in this period. To survive at this hot temperature, some basic inventions had taken place which includes Ceiling fan, Air Conditioners, Room Coolers etc. All of which requires continuous power supply.

On the other hand, underdeveloped & developing countries like India can't produce power as per its consumption rate which ultimately leads to the problem of load shedding. In order to provide comfort at this time, we developed an arrangement in the assembly of a general room cooler & named it as "Self generated electricity room cooler".

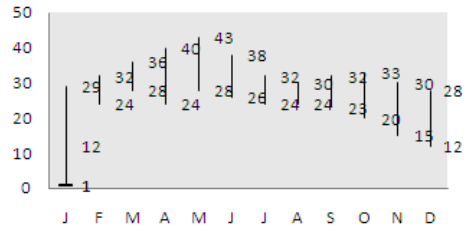

Fig. 1: Line graph showing annual temperature distribution of Nagpur district

The arrangement made is such that it will run on internal (D.C.) & external (A.C.) power source. In normal load shedding period, there is unavailability of electricity of 3-4 hours. At this time internal (D.C.), drives the whole cooler assembly & provides comfort to human beings whereas at the time of availability of electricity, we can drive it with external (A.C.) power source and at the same time it will also charge the battery (as shown in the schematic arrangement).

III. PARTS OR COMPONENTS OF SELF COOLER ASSEMBLY

A. D.C. Motor

The internal configuration of D.C. motor is designed to harness the magnetic interaction between a current – carrying conductor and an external magnetic field to generate rotational motion. Every DC motor has six basic parts – axle, rotor, stator, commutator, field magnet and brushes. The principle of operation is based on simple electromagnetism. A current – carrying

conductor generates a magnetic field which will experience a force proportional to the current in the conductor and to the strength of the external magnetic field (refer table 1 for specification).

B. Dynamo

It is an electric device used to D.C. current & to charge the battery. If a rotor (rotating part) is rotted in between line of force, it cuts the magnetic lines and produces current according to the faradays laws of electromagnetic induction and current produce in rotor (refer table 2 for specification).

C. Battery

A common lead – acid storage battery is used to store the D.C. power produced by dynamo and provide the same when needed. It is made up of plates (electrode), lead, lead oxide & electrolyte solution with a 35%sulphuric acid and 65% water.

D. Coupling

Coupling is a device used to connect two shafts to transmit torque, motion etc. It can adjust itself to misalignment of two shafts connected by it. When motion transmission is important, the misalignment should not affect the velocity & acceleration of the shaft. Thus, it is the media which assist in combination & used to transfer the torsional motions in rotation part.

E. Rectifier

A rectifier is an electrical device that converts alternating current to direct current. This process is known as rectification. Rectifiers are used as components of power supplies. They are made of solid state diodes, vacuum tube diodes, mercury arc valves & many other components.

F. Exhaust bracket

Exhaust fan is nothing but an outcome of sophisticated fan technology which is designed meticulously. Flawless performance of this transair exhaust fan brings in comfort of fresh air by driving out stale air, round the clock.

Table 1: Specifications of D.C. Motor

Sr. no.	specifications	Ratings
1	Input volts	12 volts
2	Current input	2.9 amp
3	Power	5.2 watt
4	Cost	1000
5	Operating speed	1800 rpm

Table 2: Specifications of Dynamo

Sr. no.	Specifications	Ratings
1	Output	0-40 volts d.c.
2	Current	16 amps
3	Max peak current	12 amps
4	Power to charge battery	19 watt,15v*20 amp
5	Operating temp.	82 c
6	Cooling	air
7	Shaft bearings	Ball
8	Wire lead length	12
9	Wire lead size	12 awg
10	No of poles	4
11	Generator type	Permanents magnets
12	Operating speed	1600 RPM
13	cost	2300 rs.

Table 3: Specifications of D.C. Water Pump

Sr. no	specifications	Ratings
1	input	12 volts
2	current	0.4 amp
3	power	9 watt
4	Pump head	2.5 m
5	Flow rate	240 L/H

G. D.C. Water Pump

Water pump is the device which is used to lift the fluid from low level side to high level side. It is a hydraulic machine which converts mechanical energy into hydraulic energy. It works on the principle that when certain mass of liquid lifts upward from low level to high level due to the rotation of the rotator placed inside the motor, the motor converts mechanical energy to hydraulic energy (ref table 3).

III. BLOCK DIAGRAM AND WORKING OF THE SETUP

A. Construction

Fig. 2, shows the construction and assembly details of our self generated electricity cooler. It consists of number of parts which are already mentioned above.

- D.C. motor is attached to the dynamo with the help of rigid coupling.
- The fan or blades are mounted on the front of shaft of the D.C.motor.

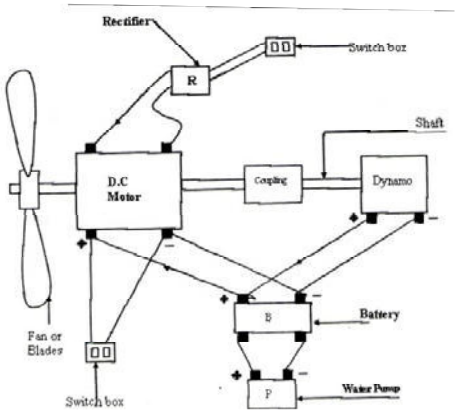

Figure 2: Block diagram of self generated room cooler

- The negative terminal of the motor is connected with negative terminal of the battery & same terminal is connected to the negative terminal of dynamo with the help of single wire.
- The positive and negative terminal of the motor is connected to positive & negative terminal of the rectifier and same terminal connected to the switch box.
- The two terminal of the battery is connected to the two terminal of the water pump.

B. Working

Condition 1:- When AC current is supplied to the rectifier from external power supply, then rectifier converts AC into DC and the DC current drives the motor (refer fig. 3)

DC motor will utilize the current and rotates at high speed, due to rotation of the motor the shaft of the dynamo will also rotates.

When shaft of dynamo rotates then electro-magnetic flux gets cut by the conductor and it produces current, the current produced by the conductor is stored in the battery.

Condition 2:- In the absence of power supply i.e. at the time of load shedding or power cut, the external source of electricity will be totally closed. At that time, cooler will run itself by utilizing the stored power of battery.

The external power circuit should be switched OFF and internal power circuit should be made ON. Now battery provides sufficient current to run DC motor and DC motor will once again rotates the shaft of dynamo.

Dynamo produces DC current that will be stored in battery and simultaneously pump will utilize the required current.

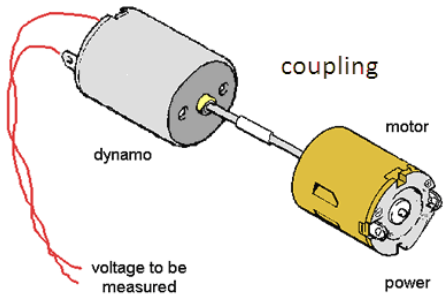

Figure 3: dynamo & motor arrangement coupled with rigid coupling

IV. ASSEMBLY PROCEDURE

- First of all DC motor has been taken out and kept in semicircular 'D' base plate which is fixed & clamped over it with the help of nut and bolt and then this assembly is fitted with circular disc with the help of nut and bolt.
- Then dynamo has been taken and kept on semi-circular 'D' type base plate and attached on the back side shaft of the DC motor & front side shaft of the dynamo with the help of coupling and fitted on two bolts. After that the 'c' clamp over the dynamo is fastened with base plate.
- Now, the exhaust bracket has been taken and whole assembly is prepared by fixing the exhaust bracket with the help of four bolts and nuts.
- Then fan is mounted on front side of the motor by only one bolt and make it free to rotate.
- In next step whatever assembly is prepared is fitted inside cooler body fastened with nut & bolts. Inside the nut rubber washers are used for absorbing vibrations.
- The battery set up in bottom side of the room cooler body is fixed on hanged bracket.
- The battery has two terminals, as same as like motor and dynamo i.e. positive and negative terminals.
- Now the, positive terminals of the dynamo is connected to positive terminal of the battery and then some terminals attached to the positive terminals of the DC motor with the help of single wire, and thus the circuit gets completed.
- On the other hand, the negative terminals of the dynamo is connected to the negative terminals of

the battery and then same terminal is attached to the negative terminal of the DC motor with the help of single wire. This completes the second circuit.

- After this the rectifier inside the cooler body is fixed with the help of clamp and nut & bolts.
- In next step, switch and pin box was set-up on the outermost top side of the cooler body by means of nuts and bolts. Switches and pin box has also positive and negative terminals.
- The positive terminal of the rectifier is connected to the positive terminals of the DC motor and same terminal of rectifier is connected to positive terminal of switches box by the single wire and then completed the one circuit.
- Now the negative terminal of DC motor is connected to the negative terminal of the rectifier and same terminal is attached to the negative terminal of switches and pin box, by the single wire which completes the second circuit.
- Now, water pump is connected to the terminal of the battery and water pump is set-up on the bottom side of the cooler body.
- In next step, a flexible pipe is used whose one end connected to the bottom end of the water pump and another end is connected to the top side of cooler body
- At last, Given outer wiring is connected to the cooler by the positive terminal of the switches and pin box to connect the sample single wire
- The negative terminal of the switches and pin box was connected to a simple another single wire and another end of the wire is free.
- This completes the fabrication of "Self operated Electricity room cooler".

V. MATHEMATICAL READINGS AND CALCULATIONS

Calculation of Motor speed = ?

Motor Specifications (D.C. shunt motor 4 pole)

V = 12 volt (voltage),
Ra = 0.2 ohm (Armature resistance),
Rsh = 200 ohm (Shunt field resistance)
Ish = ? (Shunt field current)

When motor is running free

N1 = 1800 RPM (speed of motor),
Il1 = 2.9 Amp (load current),
Ia1 = ? (Primary armature current)
Eb1 = ? (Induced electromotive force)

Φ1 (flux generated)

When motor is running with load

Il2 = 36 Amp (load current)

N2 = ? (Speed of motor)

Ia2 = ? (Secondary armature current)

Eb2 = ? (Induced electromotive force)

Φ2 (flux generated)

Calculations of speed of motor when loaded: -

1) Ish = V/Rsh
= 12/200
= 0.06 Amp.

2) Il = Ia + Ish
Ia = Il – Ish
Ia1 = Il1 - Ish
= 2.9 – 0.06
= 2.84 Amp
Ia2 = Il2 – Ish
= 36 – 0.06
= 35.94 Amp

3) Eb1 = V – (Ia1 × Ra)
= 12 – (2.84 × 0.2)
= 11.432 volt
Eb2 = V – (Ia2 × Ra)
= 12 – (35.94 × 0.2)
= 4.812 volt

4) N1/N2 = Eb1/Eb2 × Φ1/Φ2
1800/N2 = 11.432/4.812
.... (Assuming the fluxes to be constant)
N2 = 757.66 RPM

Thus, the speed of the motor when subjected to load of shaft, dynamo etc. is 757.66 RPM

B. Calculation for current produced by dynamo = ?

Dynamo Specifications: -

P2 = 0.19 KW= 190 Watt (output power)

N = 757.66 RPM (as both the motor & dynamo are coupled with a common shaft, hence their speeds are same)

V = 12 volt (Voltage)

Ra = 0.05 ohm (armature resistance)

Rsh = 110 ohm (shunt field resistance)

Rse = 0.06 ohm (series field resistance)

η = 85% (overall)

Il =? (load current)

Ish =? (shunt field current)

Ia =? (armature current)

P1 =? (Input power)

Calculations of current produce: -

1) Il = P2/V
= 190/12
= 15.83 Amp

2) Ish = V/Rsh
= 12/110
= 0.1090 Amp

3) Ia = Il + Ish
= 15.83 + 0.1090
= 15.939 Amp

Thus, the current produced by dynamo neglecting losses is 15.939 Amp.

VI. ADVANTAGES

- It can run in absence of electricity.
- Less expensive as compare to other alternative power sources which are used to run the cooler.
- It is power efficient assembly.
- By using high capacity part we can run other equipment.
- It is very economical as compare to other cooling devices.
- It generates the electricity for its requirements.
- Circuit is quite simple.
- Easy in operation.
- Rigid in construction.
- Less noisy as compare to other cooling equipments.
- Less vibration & shock absorbing device because the rubber bushes are used for absorbing the shocks vibrations.

VII. PRECAUTIONS AND MAINTENANCE

It should be noted that cooler have the arrangement of running on A.C. as well as on D.C. current as per the requirement & there are respective switches for both but precaution is to be taken that both of them should not be switched ON at the same time because it will damage the internal arrangement of the cooler and cooler will not work.

On the other hand following maintenance should be carried out time to time to ensure the smooth running and proper functioning of the cooler. These are: -

- Proper lubrication to motor & water pump is to be done.
- Battery capacity should be check periodically (acid-liquid level).
- All the internal parts should be check from time to time.

VIII. FUTURE MODIFICATIONS

Further we can try to develop this work by modifying it for various other electrical appliances. By applying this concept & using with high rating high capacity part we can develop such models which will produce much electric energy so that it may be capable of driving the other domestic appliances like radio, lights, mobile charger, T.V. & fan. Hope that it can be visible to see in the near future.

IX. CONCLUSIONS

Thus, our objective to modify a general room cooler in "self generated electricity room cooler" was successfully fulfilled & we got fruitful results when we done analysis on it. The following table shows some readings obtained on constant speed/load conditions.

Table 4: readings obtained on constant speed/load conditions

Sr. No.	Name of parts	Input	Output
1	D.C. MOTOR	2.9 Amp	758 RPM
2	DYNAMO	758 RPM	16 Amp
3	STORAGE BATTERY	16 Amp	3.4 Amp (as per our requirement)
4	RECTIFIER	2.9 Amp	2.9 Amp
5	D.C. PUMP	0.4 Amp	240 litre/hour

In general cooler there is more power consumption as it uses A.C. motor whereas in self generated Electricity cooler this problem is sort out to some extent by using D.C. motor.

At last, our basic aim of providing comfort at the period of load shedding is also fulfilled partially, as this arrangement is 50% efficient of running in the absence of electricity. That means if the cooler runs for 8 hours in the presence of electricity after which there is power failure than it will run for around 4 hours at this period in the absence of electricity by utilizing the power from storage battery.

REFERENCES

[1] Climatic Parameters of Nagpur". India Meteorological Department Regional Meteorological Centre, Nagpur. http:// web.archive.org/web/ 20060713205120/ http://www.imd ngp.org/cfnagpur.htm. Retrieved 4 July 2006

[2] Nagpur sizzles at 47.6 °C, TNN, Times of India (Bombay), pg 1, 23 May 2005

[3] Mr. V.V. Pangave - Applied electronics, pp. 2.1-2.30

[4] Mr. Manohar Prasad - Refrigeration and air conditioning, pp. 575-591

[5] Mr. K.B. Lal – Automobile Engineering, pp. 292-301 & 322- 332

◈◈◈

Design and Dynamic Characterization of Reciprocating Compressor Piston

Hiren Prajapati[1], U V Shah[2] & A. P. Bhabhor[3]

[1&2]L D Engineering College, Ahmedabad, India
[3]LDRP Engineering College, Gandhinagar, India

Abstract - Abstract: In today's scenario air is used for many purpose all over the world and for that Air-compressor manufacturers try to make best compressor which fulfills all most all requirements of industry. They are only option for many applications such as very high pressure and light gases (for example hydrogen, etc). Worldwide installed reciprocating compressor horsepower is approximately three times that of centrifugal compressors. In reciprocating air compressor reciprocating parts are one of the major reasons for vibration. The Primary unbalanced Forces can be partially reduced just by adding the balancing weight on the crank shaft. Secondary unbalanced forces result from the acceleration and deceleration of the piston which cannot be reduced through use of counterweights. The effective vibration reduction can be possible by designing the weight of reciprocating parts (e.g piston). The C-language program for piston design also presented.

The modal analysis is best tool for effective characterization of dynamic behavior of the piston. This paper include the design and modal analysis of 15 hp reciprocating air compressor piston.

Keywords - *Design, Reciprocating air compressor, Vibration, Modal analysis, Mode shapes.*

I. INTRODUCTION

The piston is the heart of the reciprocating air compressor. The piston reciprocates vertically within the cylinder. The two extremes of this motion are referred to as Top Dead Center (TDC) and Bottom Dead Center (BDC) referred to Fig.1 Top Dead Center is the position of the piston that creates the smallest volume in the cylinder, which is defined as the clearance volume, Vc. The Bottom Dead Center is when the piston creates the largest volume in the cylinder. The distance between TDC and BDC is referred to as the stroke and the volume, which the piston displaces during this moment, is called the displacement volume, V_s.[5]

The piston is connected to the crankshaft via the connecting rod, which allows rotation at both onnections. The crankshaft converts the rotational motion of the motor shaft into linear motion of piston. To translate rotational motion into linear motion the crankshaft has an offset rotation

The design of modern reciprocating compressor is required to make noise and vibration as light as possible. In reciprocating air compressor reciprocating parts are one of the major reasons for vibration. The Primary unbalanced Forces can be partially reduced just by adding the balancing weight on the crank shaft. Secondary unbalanced forces result from the acceleration and deceleration of the piston which cannot be reduced through use of counter weights. In order to successfully control the noise and vibration, the vibration of reciprocating compressor piston this can cause vibration and noise of the compressor. So early in design stage, computations of natural frequencies and mode shapes piston are indispensable. Thus, an accurate model for prediction of the vibration of a piston is essential for reciprocating compressor.

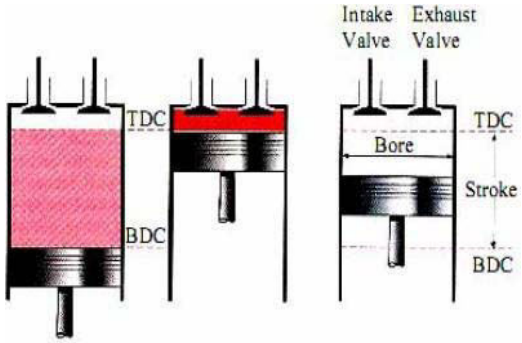

(a) Displacement (b) Clearance Volume
(c) Nomenclature Volume

Fig. 1 : Cross Section of a Reciprocating Engine

In this paper, The piston design is explained after finding bore diameter of cylinder by performing thermal analysis. The piston is then modeled in Pro-e Wildfire-5. The iges data transfer formate used to import three dimensional model from Pro-E to ANSYS. The ANSYS package effectively used for performing the modal analysis of piston of Law pressure side (L.P.side).

II. PISTON DESIGN

The elements of a piston are shown in Fig. 2. The head thickness based on strength can be calculating assuming the head to be a flat of uniform thickness and fixed at the edges. The air load is considered as a uniform load over entire cross section.

The thickness of the piston head (t_h), according to Grashoff's formula.

$$t_h = 0.443 \times D \times \sqrt{\frac{P_{max.}}{f_t}}$$

Where t_h is thickness of the piston head, $P_{max.}$ is maximum gas pressure or explosion pressure, D is cylinder bore and f_t is allowable stress in bending (tensile) stress for the material of the piston. It may be taken as 50 to 90 MPa for aluminum alloy [8].

The radial thickness (t_1) of the ring may be obtained by considering the radial pressure between the cylinder wall and the ring.

$$t_1 = D\sqrt{\frac{3 \times P_w}{f_t}}$$

Here D is cylinder bore, P_w is pressure of gas on the cylinder wall (0.025 MPa to 0.042 Mpa), and f_t is allowable bending (tensile) stress (84 MPa to 112 MPa for cast iron rings). The axial thickness (t_2) of the rings may be taken as 0.7 t_1 to t_1. The minimum axial thickness (t_2) may also be obtained from the following empirical relation is given by [7]

$$t_2 = \frac{D}{10 \times z}$$

Where z is number of rings. In air compressor piston mainly two types of rings are used. One is piston or seal ring and other is guide or rider ring. The piston rings are used to impact the necessary radial pressure to maintain the seal between the piston and cylinder bore. guide ring serves only to keep the piston from contacting the cylinder. The guide ring must be made wide enough to keep bearing pressure between rider and cylinder very light, since tolerance for wear will be less than for piston rings.[4]

The width of the top land is made larger than other ring lands to protect the top ring from high air load existing at the top of the piston.

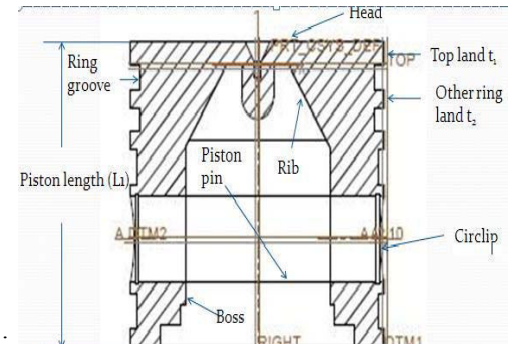

Fig. 2 : Elements of piston

So width of top ring land is given by

$$b_1 = t_h \text{ to } 1.2t_h$$

The width of other ring lands in the piston may be made equal to or slightly less than the axial thickness of the ring (t_2) .The lands between the piston rings are loaded by the forces of the gases, of inertia of the piston rings, and of friction.

$$b_2 = 0.75t_2 \text{ to } t_2$$

The depth of the ring grooves should be more than the depth of the ring so that the ring does not take any piston side thrust. The gap between the free ends of the ring is given by $3.5t_1$ to $4\ t_1$ .The gap when the ring is in the cylinder, should be 0.002 D to 0.004 D. The maximum thickness (t_3) of the piston barrel may be obtained from the following empirical relation.

$$t_3 = 0.03D + b + 4.5$$

Where b is radial depth of piston ring groove, D is the bore diameter.

$$b = t_1 + 0.4$$

The piston wall thickness (t_4) towards the open end is decreased and should be taken as 0.25 t_3 to 0.35 t_3. The portion of the piston below the ring section is known as piston skirt. It acts as a bearing for the side thrust of the connecting rod. The side thrust (R_t) on the cylinder liner is usually taken as 0.03 to 0.1 times of the maximum gas load on the piston [7].

Maximum side thrust on the cylinder, is given by

$$R_t = \mu \times \frac{\pi}{4} \times D^2 \times P_{max.}$$

The side thrust (R_t) is also given by:

$$R = P_b \times l_s \times D$$

Where ls is length of the piston skirt and Pb is the bearing pressure. Now the total length of the piston (L) is given by:

L= Skirt length + Ring section + top land

The length of the pin in the connecting rod bushing will be about 0.45 of the cylinder bore allowing for the end clearance of the pin etc. The piston pin should be designed for the maximum gas load or the inertia force of the piston, whichever is larger.

The outside diameter of the piston pin (d_p) is obtained

$$P_{max.} = l_p \times d_p \times P_b$$

Where, d_p is outside diameter of the piston pin, l_p is length of the piston pin in the bush of the small end of the connecting rod (0.3D to 0.45D), P_b is bearing pressure at the small end of the connecting rod bushing. Assume allowable bearing pressure is 15 to 30 MPa, for larger size of piston smaller value is taken. Here, the piston diameter is 138 which is too large so take P_b= 16 MPa.

The piston pin may be checked in bending by assuming the gas load to be uniformly distributed over the length l_p with supports at the centre of the bosses at the two ends. Therefore, the maximum bending moment at the centre of the pin,

$$M = \frac{P_{max.} \times D}{8}$$

The maximum bending moment is,

$$M = \frac{\pi}{32} \times d_p^3 \times \sigma_t$$

Where, σ_t is allowable bending stress 84 Mpa for case hardened steel and 140.0 Mpa for heat-treated alloy steel.

Inner diameter of pin,

$$d_i = 0.6 \times d_p$$

III. MODAL ANALYSIS

A. The establishment of piston model:

The PRO-E Wildfire-5 software is applied to do the three-dimensional solid modeling of reciprocating compressor piston.

B. FEM equation of modal analysis:

The goal of modal analysis in structural mechanics is to determine the natural mode shapes and frequencies of an object or structure during free vibration. It is common to use the finite element method (FEM) to perform this analysis because, like other calculations using the FEM, the object being analyzed can have arbitrary shape and the results of the calculations are acceptable. The types of equations which arise from modal analysis are those seen in eigensystems. The physical interpretation of the eigenvalues and eigenvectors which come from solving the system are that they represent the frequencies and corresponding mode shapes. Sometimes, the only desired modes are the lowest frequencies because they can be the most prominent modes at which the object will vibrate, dominating all the higher frequency modes.

For the most basic problem involving a linear elastic material which obeys Hooke's Law, the matrix equations take the form of a dynamic three dimensional spring mass system. The generalized equation of motion is given as:

$$m\ddot{x}+c\dot{x}+kx= F(t)$$

Where m is the mass matrix, $\ddot{x}$ is the 2nd time derivative of the displacement x (i.e., the acceleration), $\dot{x}$ is the velocity, c is a damping matrix, k is the stiffness matrix, and F(t) is the external force vector. However, for vibration modal analysis, the damping is generally ignored, leaving only the 1st and 3rd terms on the left hand side:

$$m\ddot{x}+kx=o$$

$$\ddot{x}+\omega_i^2 x=0$$

where, $\omega^2_i=k/m$

According to simple harmonic motion,

$$x=A \sin(\omega_i^2 t)$$

In this eq. A is i-order modal vibration vector(eigenvector):ω_i^2 is i-order modal natural frequency(eigen value). We can conclude the following equation:

$$(k-\omega_i^2 m)A=0$$

Thus, basic equation of solving the typical undamped modal analysis becomes the classical problem of eigenvalue. abow equation getting nontrivial solution is on condition that its determinant of coefficient equals zero, that is,

$$\det(k-\omega_i^2 m)=0$$

C. Modal analysis of the piston

1) The modeled components are exported to IGES formate, which is able to retrieve by ANSYS for preprocessing of the part.

2) Meshing

ANSYS provides the meshing module MESH in preprocessor phase within the package. This process divid the whole geometry in number of elements. Here for meshing of piston 10 nodes tetrahedral elementwas used. A total of 29769 elements and 49657 nodes were generated with 3.5 mm element length which is shown in figure 3.

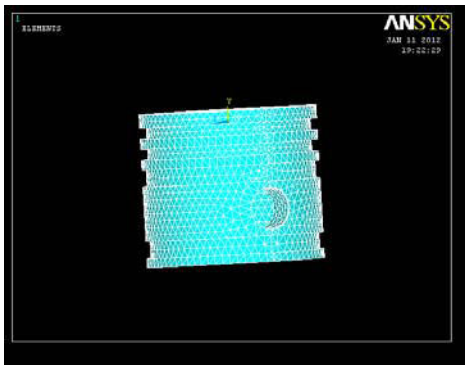

Fig. 3 : Meshing of piston

1) Load constraints

This phase becomes very important in which define different forces acting on piston with their location. The main forces which acts on piston are compressed air force, inertia force, connecting rod thrust etc. In modal analysis free forced vibration measured so no need to define loads.

2) Boundary condition constraints

According to actual working condition, boundary condition is constrained in ANSYS. The degree of freedom in X and Z co-ordinate fixed along the ring groove and degree of freedom in Y constrained on upper of semi-circular surface of pin hole.

3) The results of modal analysis

The first 10 mode shapes of piston are listed in Table 1

Table 1. The result of modal analysis

Degree	Natural Frequency
1	0.00
2	214.96
3	238.09
4	409.74
5	431.62
6	437.62
7	614.01
8	628.27
9	649.28
10	690.32

The corresponding mode shapes as shown below.

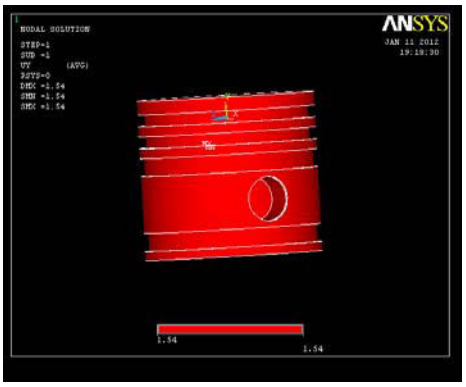

(a) First mode shape of piston

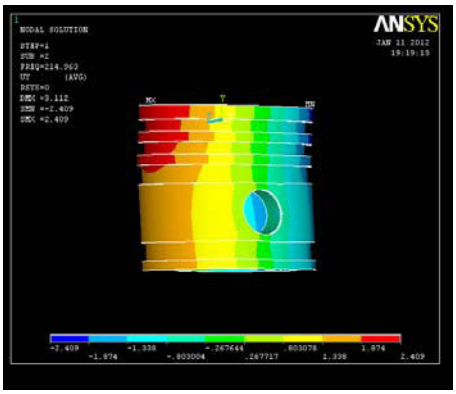

(b) Second mode shape of piston

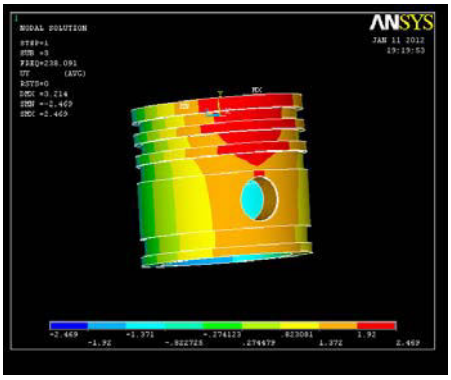

(c) Third mode shape

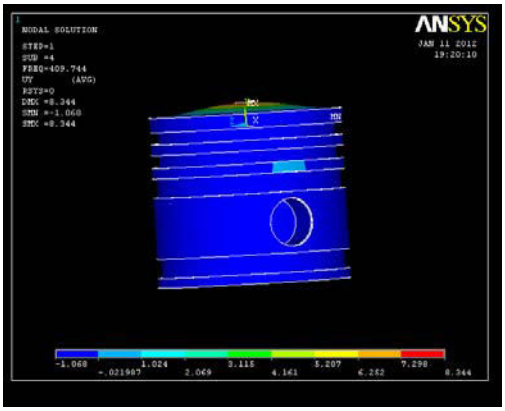

(d) Fourth mode shape

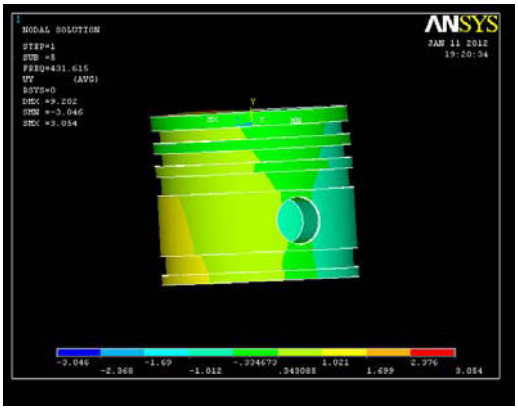

(g) Seventh mode shape

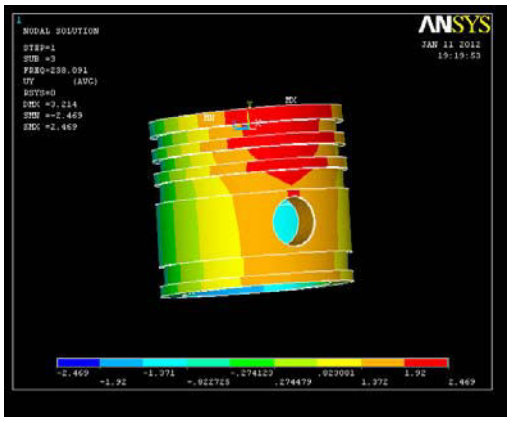

(e) Fifth mode shape

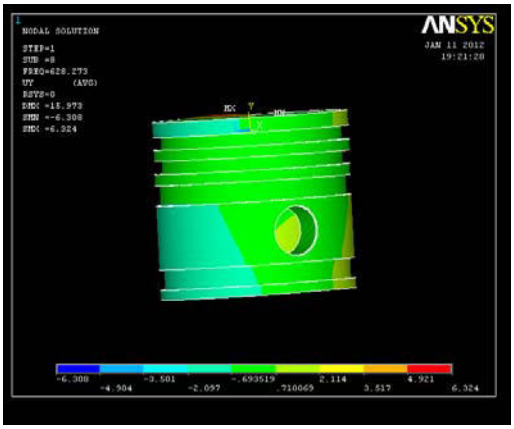

(h) Eighth mode shape

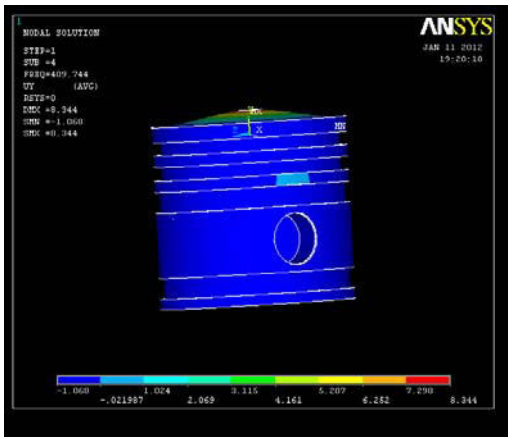

(f) Sixth mode shape

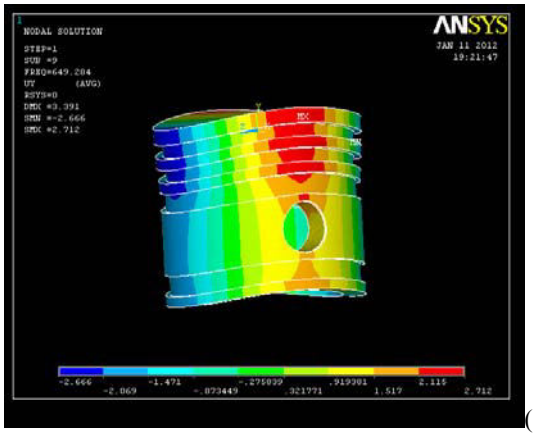

i) Ninth mode shape

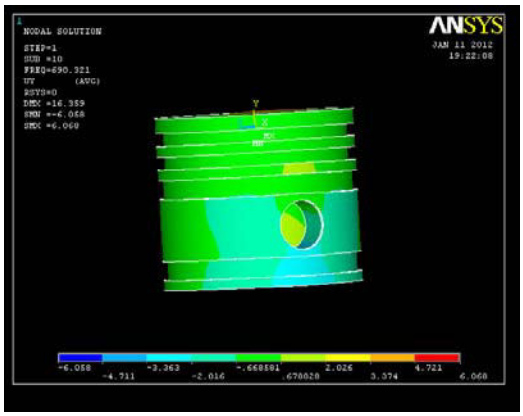

(j)Tenth mode shape

IV. CONCLUSION

In design procedure of 15 hp air reciprocating compressor piston, structural rigidity combined with lightness must always be the first consideration. The fundamental design procedure for piston design has been studied in this paper. When a piston is designed, care should be taken to have a minimum weight with strength to withstand pressure and inertia forces. Piston designs for this compressor by selecting aluminum alloy have also been evaluated.

Modal analysis shows second natural frequency as 214.96 Hz which is far away from the compressor excitation frequency 12.5 Hz (750 rpm). So there will be no chance of resonance to occur. This piston is safe from vibration point of view.

Here, also present the C-language program for piston design whose outputs are shown below. This will make design of component so fast and rapid.

OUTPUT:

Enter the bore diameter, stroke length, allowable tensile strength of material, maximum explosion pressure or discharge pressure

88

100

50

1

The piston head thickness the is 5.513170

Thickness of rib is 2.297154

Enter the maximum wall pressure, allowable tensile strength of ring material: 0.036 26

Radial thickness of piston ring is 5.671630

Enter the number of rings: 4

Axial ring thickness is 4.820886

Width of top land is 6.064487

Width of other ring land is 4.218275

Barrel thickness at ring section is 13.211630

Barrel thickness at open end is 3.963489

Enter the allowance between maximum gas load and thrust pressure, bearing pressure as per piston material 0.1 0.25

Total skirt length is 27

Length of piston is 65

Length of entire pin is 79.199997

Length of pin at bearing is 39.599998

Enter the bearing pressure at pin 20

bending moment at pin66869.437500

Enter the allowable bending stress at pin

84

The outer diameter of pin is 19

The inner diameter of pin is 11

Inner diameter of boss = 19

outer dia of boss = 38

Length of boss = 17.600000

ACKNOWLEDGMENT

Authors of this paper thankfully acknowledge the generous and continuous support of the Dintech.pvt.lmt, Naroda-GIDC, A'bad, Gujarat, India.

REFERENCES

[1] Yabin Tian, Xueyi Qi, Xiaobin Ji(2011)."Analysis of vibration failures caused by imbalanced mass of machinery under high speed". Lanzhou University of technology, Lanzhou, Gansu, china.

[2] Manning P., & Aiken S. C.(2002)."Reciprocating Compressor Vibration", A General Discussion, Presentation, September 13, 2002, Technical Associates, Ingersoll Rand Company.

[3] Gajjar H."A Balanced Compressor in a World of Unbalanced forces And Couple's", Director-Southern Region Technical Product Support, Weatherford Compression.

[4] Paul C. Hanlon, compressor handbook, mcgraw-hill.

[5] Patel V L, Patel R N,"Fluid power engineering", Third Edition, Mahajan Publication.

[6] Mathur M.L., Sharma, "A Course in Internal Combustion Engine",R.P. Dhanpat Rai Publication 1997 (i, ii, iii).

[7] J.S.Soni,"Design of machine elements (part-2)", Nirali and roopal prakashan. Dr. P.C. Sharma, Aggarwal, R.D.K, , "A Text Book of Machine Design", S. K. Kataraia and sons, New Delhi. 2004.

Torsional Vibration Analysis of a Typical Three Cylinder Turbocharged Intercooled Diesel Engine Crankshaft

Vijay Mahangade[1] , Khalil Nadaf[2] & S.G. Joshi[3]

[1&2]Mahindra Engineering Services Limited, Pune, Maharashtra, India
[3]Dept. of Mech. Engineering, Walchand College of Engineering, Sangli, Maharashtra, India.

Abstract - Diesel engine torsional vibrations mainly depend upon crankshaft design which in turn depends upon crankshaft balancing and crankshaft stiffness. Degree of crankshaft balancing as well as stiffness depends upon number of cylinders. Crankshaft of a three cylinder engine is more unbalanced compared to a four cylinder engine while a three cylinder crankshaft is more rigid than a four cylinder crankshaft. These inherent characteristics with increased engine loading due to turbocharging have effect on crankshaft torsional vibrations. In this paper, the torsional vibration analysis of a three cylinder crankshaft is carried out when a four cylinder naturally aspirated diesel engine is converted to three cylinder turbocharged intercooled diesel engine to meet stricter emission norms while maintaining higher power output. Due to this, loading per cylinder in a three cylinder engine is more than that of a four cylinder engine. Natural frequencies of crankshaft are determined using the Holzer and Finite Element Methods. The results of analysis are compared. The crankshaft critical orders and speeds have been determined using Campbell diagram. The results of gas torque and inertia torque harmonic analysis of crankshaft are compared with those of experimental analysis. The torsional vibration amplitude of the crankshaft is calculated by analytical method as well as by experimental method and results are compared. From this study, it has been observed that the crankshaft is safe in view of torsional vibrations and there is no need of installation of torsional vibration damper for this engine application.

Keywords - *Three Cylinder Engine Crankshaft, Turbocharged Diesel Engine, Torsional Vibration, Finite Element Analysis*

I. INTRODUCTION

Automotive diesel engine technology is governed by parameters called technology drivers viz. emission regulations, fuel efficiency, noise regulations, alternate fuels and cost. Stricter emission regulations lead the diesel engine aspiration transition from natural to turbocharging to turbocharged intercooling. To meet stricter emission norms while maintaining same power output, it is customary practice to reduce engine size during upgradation of engine aspiration. For an off-road vehicle, reduction of engine size by 25% along with increased combustion pressure to meet stricter emission norms of TREM-IIIA has lead to engine powertrain load increase by approximately 50%. For each cylinder of a three cylinder engine, product of varying instantaneous gas pressure and effective crank radius leads to turning moment which varies throughout the cycle. This leads whole rotating crankshaft system to move backwards and forwards relative to its mean rotating position as the instantaneous torque of the total engine falls below and later exceeds mean torque. This also produces relative instantaneous movements between various masses due to changing relative torques on each crank throw due to firing intervals among three cylinders. The natural frequencies of torsional vibrations of the crankshaft may coincide with a few of the harmonic torque frequencies depending on individual cylinder harmonic torque components and phasing of cylinders. In such a case, torsional vibration amplitude will build up on resonance leading to crankshaft system failure. Many researchers have carried out work in crankshaft torsional vibration on six cylinder or, four cylinder inline and V-engines and very little work is carried out on three cylinder inline engines as a complete crankshaft system torsional vibration study from natural frequency estimation, torque harmonic analysis up to TV amplitude calculations and measurements. Burla et al. [1] have developed three-dimensional parametric finite element model of crankshaft which estimates natural frequency and mode shapes.

II. THE CRANKSHAFT ASSEMBLY MODEL

A typical crankshaft assembly considered here consists of crank gear on front side and flywheel on rear side of crankshaft itself. The subject crankshaft is a three cylinder crankshaft with crankpins 120° apart and firing order of 1-3-2. Fig. 1 shows a mathematical model for this system shown as 5-DOF Torsional Vibration System. The crankshaft design is verified for static and fatigue loading in bending and torsion. In the subsequent sections, a torsional vibration analysis of a crankshaft assembly is presented. The results of theoretical analysis have been compared with those of experimental analysis.

[*] The numbers in bracket indicate the reference numbers.

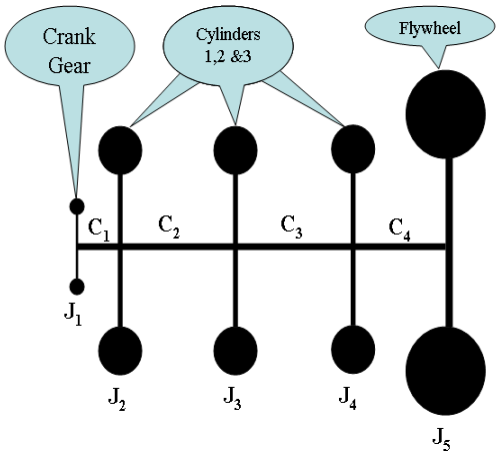

J_i – Moments of Inertia, C_i – Stiffnesses of Shaft,

$Ø_i$ - Amplitude of Torsional Vibration

Fig. 1: Typical Three Cylinder Crankshaft Assembly Model

III. CRANKSHAFT TORSIONAL VIBRATION (TV) ANALYSIS

Crankshaft TV analysis is carried out in steps of natural frequency calculation, crankshaft harmonic analysis, crankshaft critical orders and speeds, TV actual amplitude calculation and TV measurement on running engine. The crankshaft natural frequencies have been determined by Holzer Tabulation Method and FEM (Refer Table I). The polar moments of inertia and stiffnesses of crankshaft crank-throws are calculated using IDEAS software. Since the Holzer table gives relative deflections at each mass corresponding to the assumed unity angular deflection at the free end of the crankshaft, the mode shapes are also obtained. The natural frequencies of first and second mode of torsional vibrations of the crankshaft were obtained as 388.9 hertz, and 952.63 hertz respectively. For this analysis, the values of J1, J2, J3, J4 and J5 were respectively taken as 0.000582kgm2, 0.0263kgm2, 0.0115kgm2, 0.0307kgm2 and 0.4297 kgm2 while values of C1, C2, C3 and C4 are respectively taken as 7.65x105Nm/rad, 5x105Nm/rad, 5.07x105Nm/rad and 7.97x105Nm/rad.

A. Crankshaft Modal Analysis

The Finite Element Analysis (FEA) method has been used to determine natural frequencies and mode shapes. Modal analysis allows the design to avoid resonance vibrations or to vibrate at a specified frequency. The modal analysis has been performed before trying any other dynamic analysis. Crankshaft natural frequencies and mode shapes have been determined using IDEAS 11NX version in which Normal Mode Dynamics–Lanczos method was used. The three conditions used to study modal analysis of crankshaft are: free-free analysis of crankshaft alone, modal analysis of crankshaft alone in constrained conditions and modal analysis of crankshaft assembly consisting of crank gear, crankshaft and flywheel in constrained conditions. The consolidated results of crankshaft modal analysis are presented in Table I.

Table I: Modal Analysis Results of a Three Cylinder Crankshaft

Component or assembly →	Crankshaft		Crankshaft		Assembly (Crankshaft+ Crank Gear + Flywheel)	
Boundary Conditions →	Free - Free		Constrained		Constrained	
Modal Analysis Type →	Normal Mode Dynamics – Lanczos method					
Modes	Nat. Freq. (Hz)	Mode Shape	Nat. Freq. (Hz)	Mode Shape	Nat. Freq. (Hz)	Mode Shape
1ST Mode	385	Bend.	695	Bend.	459	Bend. & Tors.
2nd Mode	418	Bend.	980	Tors.	540	Bend.
3rd Mode	555	Bend.	1432	Bend.	917	Bend.
4th Mode	766	Tors.	1783	Bend. & Tors.	971	Tors.

B. Gas Torque and Inertia Torque Harmonic Analysis

Harmonic analysis is a study of individual behavior of gas loads and inertia loads by representing them in mathematical form and then adding them to calculate total load.

Harmonic analysis of gas torque is carried out as follows.

Using High-speed data measurement of engine, the variation of gas pressure in the cylinder against crank-angle i.e. P-θ curve is plotted. For this purpose, Gas Torque, (T_g) is given as [5],

$$T_g = F_g.R\left(Sin(\theta+\beta)/Cos\beta\right) \quad \text{.....(1)}$$

Where, Gas Force, $F_g = P.(\pi D^2/4)$ and, θ= Crank-angle, β= Con-rod angle from Cylinder axis, R= Crank radius. The equation (1) can be represented as,

$$T_g = T_{gm} + \sum_{\substack{n=0.5 \\ \theta=0^\circ}}^{\substack{n=42 \\ \theta=360^\circ}} [A_n.Sin(n\theta) + B_n.Cos(n\theta)] \quad \text{.....(2)}$$

Where, T_{gm} = Mean Gas Torque, n= Harmonic order no. and, A_n, B_n are the Harmonic coefficients of Gas Torque. The Gas Torque has order numbers in multiples of 0.5 as gas torque cycle repeats after every two crankshaft revolutions. Now,

$$A_n = (2/m)\frac{2}{m}\sum_{i=1}^{i=m}[Y_{gi}Sin(nX_{gi})],$$

$$B_n = (2/m)\sum_{i=1}^{i=m}[Y_{gi}Cos(nX_{gi})]$$

where, Y_{gi} = Instantaneous gas torque values at each crank angle X_{gi}. Accordingly, Gas torque at engine speed of 1400 rpm has been calculated by harmonic analysis as well as by actual pressure measurement and the results are presented in column 3 and 5 of *Table II* (Also refer Fig. 2).

Table II : Gas Torque Calculation from Harmonic Analysis and Actual Measurement at Engine Speed of 1400 rpm

Sine Amplitude (An)→		-203	418	…	0.1	**Colu-mn 1**	**Column 2**	**Colu-mn 3**	**Column 4**
Cosine Amplitude (Bn)→		-208	86	…	-0.3	**Mean Tangential Effort**	**Gas Torque From Harmonic Analysis, Tg**	**Meas-ured Pres-sure**	**Gas Torque From Measu-red Pressu-re, Tg**
Cra-nk Angle (°)	**Con-rod Ang-le (°)**	**Orders**							
		0.5	**1**	**…**	**42**	**(Nm)**	**(Nm)**	**(Bar)**	**(Nm)**
0	0	-208	86	…	-0.3		-0.27	2.33	0
60	14.8	-282	405	…	-0.3		42.19	1.08	44.7
120	14.8	-280	318	…	-0.3		25.1	0.94	28.59
180	0	-203	-86	…	-0.3		-0.37	1.64	0
240	-14.8	-71	-405	…	-0.3		-80.94	2.61	-79.85
300	-14.8	79	-318	…	-0.3		-434.01	10.44	-433.85
360	0	208	86	…	-0.3	100.8	2.67	128.0	0
420	14.8	282	405	…	-0.3		1324.1	31.84	1322.43
480	14.8	280	318	…	-0.3		353.23	11.56	353.19
540	0	203	-86	…	-0.3		-0.09	7.23	0
600	-14.8	71	-405	…	-0.3		-107.25	3.59	-109.76
660	-14.8	-79	-318	…	-0.3		-137.57	3.31	-137.62
718	-0.59	-205	71	…	-0.2		-5.23	2.47	-4.65

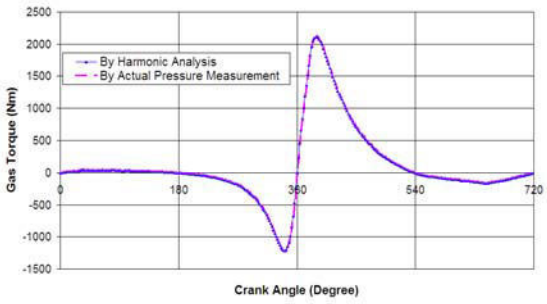

Fig. 2 : Gas Torque vs Crank Angle at Engine Speed of 1400rpm

Harmonic analysis of inertia torque is carried out as follows.

Inertia torque can be represented as,

$$T_i = T_{im} + \sum_{\substack{\theta=0° \\ n=1}}^{\substack{\theta=360° \\ n=42}} C_n.Sin(n\theta) \quad \text{.....(3)}$$

Where, T_{im}= Mean Inertia Torque, n = order no. and C_n= Harmonic Coefficient of Inertia torque is given as

$$C_n = (2/m)\sum_{i=1}^{i=m} Y_{ii}.Sin(nX_{ii})$$

Where, Y_{ii} = Instantaneous inertia torque and X_{ii}= Crank angle. The inertia torque will have only integer order number as inertia torque cycle repeats in every one crankshaft revolution and beyond 4th order; coefficients are negligibly small and hence omitted. The inertia torque values are calculated by harmonic analysis as well as actual torque formula and the results at engine speed of 1400 rpm have been presented in *Table III* (Also refer Fig. 3).

Table III: Inertia Torque Calculation from Harmonic Analysis and Actual Measurement at Engine Speed of 1400 rpm.

Crank Angle (°)	Sine Components (Cn)				Sum of Sine Components - Inertia Torque by Harmonic Analysis (Nm)	Inertia Torque by Torque Formula (Nm)
	Orders					
	1	2	…	42		
0	0	0	…	0	-4.02E-15	0
60	38	38	…	-8E-14	43.76	43.76
120	-51	51	…	2E-13	-59.1	-59.1
180	0	0	…	-2E-29	-1.16E-14	0
240	-51	51	…	-4E-13	59.1	59.1
300	38	38	…	-6E-13	-43.8	-43.76
360	0	0	…	-2E-28	-5.51E-14	0
420	38	38	…	1E-12	43.76	43.76
480	-51	51	…	8E-13	-59.1	-59.1
540	0	0	…	-2E-28	-2.71E-14	0
600	-51	51	…	2E-12	59.10	59.1
718	0	1	…	7E+00	-7.27	-7.27

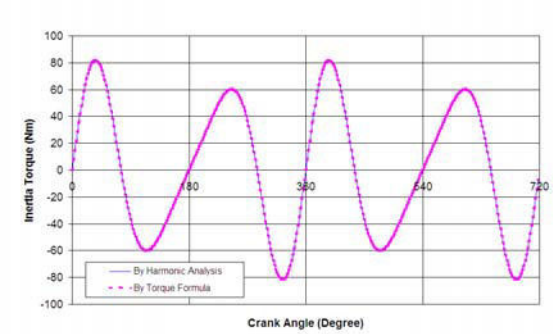

Fig. 3: Inertia Torque vs Crankshaft Angle at Engine Speed of 1400rpm

Summation of Gas Torque and Inertia Torque gives Total Torque (T_{tn}) as shown by equation [6] i.e. Total Force at each order,

$$T_{tn} = \sqrt{(A_n + C_n)^2 + B_n^2} \quad \text{.....(4)}$$

Accordingly, values of total torque have been calculated for engine critical speeds viz. 1400rpm, 2200rpm and 2860rpm. For example, the results at engine speed of 1400 rpm are presented in *Table IV*.

C. *Estimation of Critical Orders and Speeds*

Engine order numbers which are multiples of half the number of cylinders, i.e. 1.5, 3, 6, 9, 12, etc. are called major orders. Engine revolutions multiplied by the order number equals the forcing frequency. When the forcing frequency with major order matches with natural frequency, the torsional vibration amplitude is likely to be increased due to resonance. This is shown in Campbell diagram in Fig. 4.

From Campbell diagram, it is evident that major orders 9, 10.5 and 12 cut the first mode natural frequency line with corresponding engine operating speeds of 2600 rpm, 2200 rpm and 1900 rpm. These speeds are critical speeds. Engine operating speed range is from 850 rpm to 2400 rpm. Considering the over speed limit of 30% above rated power speed of 2200rpm, the engine is design protected for maximum speed of 2860 rpm in worst conditions. Engine speed of 2600 rpm does not fall between engine operating speed range. Based on expertise inputs, it was decided to check the actual amplitude at 2200 rpm (Rated Power Speed), 1400 rpm (Maximum Torque Speed) and 2860 rpm (Engine Overspeed). These three speeds have been considered critical for torsional vibration amplitude measurement during harmonic analysis.

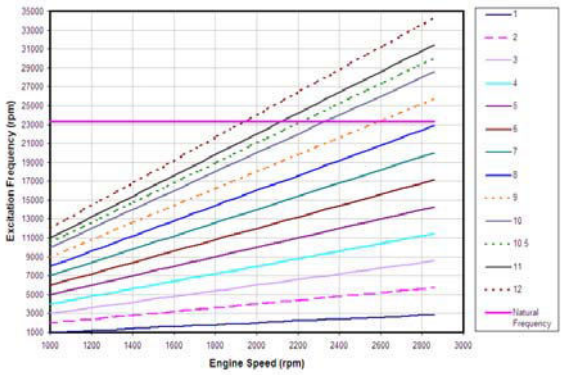

Fig. 4: Campbell Diagram for Three Cylinder Engine Diesel Engine Crankshaft

D. *Torsional Vibration (TV) Amplitude Estimation*

First, the Equilibrium (i.e. static) amplitude ($Ø_{en}$) is calculated by equating maximum kinetic energy at mean

Table IV: Actual Torsional Vibration Amplitude Calculation at Engine Speed of 1400 rpm

Order	Gas Torque (Tg)		Inertia Torque (Ti)	Total torque (Ttn)	Vectorial addition of angle of twist according to crank throw arrangement and firing order (θ)	Equilibrium amplitude	Dyn. magnifier	Actual amplitude with Dynamic magnifier (θ)
	sine	cosine	sine	--				
	Nm	Nm	Nm	Nm	Rad	Rad	--	deg
1.5	-348	16.5	0.0	348.9	1.94	0.00339	1.008	0.196
3	208	-53.3	27.6	242.0	1.94	0.00235	1.033	0.139
4.5	-100	42.7	0.0	108.9	1.94	0.00106	1.079	0.065
6	43.2	-24.5	0.0	49.7	1.94	0.00048	1.149	0.032
7.5	-16	9.6	0.0	19.3	1.94	0.00019	1.254	0.013
9	4.5	0.3	0.0	4.5	1.94	0.00004	1.411	0.004
10.5	-1.6	-4.2	0.0	4.5	1.94	0.00004	1.658	0.004
12	1.8	5.0	0.0	5.3	1.94	0.00005	2.076	0.006
							Max.	0.196
							Min.	0.001

Engine Speed =	1400 Rpm
Damping Factor =	0.0023033
Nat. Freq. =	23336 Rpm

position and maximum potential energy at maximum deflected position [6]. Thus, $T_{tn}\phi_r = \phi_{en}\omega^2 \sum_{i=1}^{i=3} J_i\phi_i^2$ from which one can write,

$$\phi_{en} = T_{tn}.\phi_r \Big/ (\omega^2 \sum_{i=1}^{i=3} J\phi^2) \quad \text{.....(5)}$$

Where, $\sum_{i=1}^{i=3} J\phi^2$ = Sum of products of moment of inertia and square of angle of deflection Øi for each crank-throw, ωc = Natural frequency and $Ø_r$ = Vectorial addition of angle of twist according to crank-throw arrangement and firing order. $\sum_{i=1}^{i=3} J\phi^2$, ω_c and $Ø_r$ are taken from Holzer table. T_{tn} is taken from gas and inertia torque harmonic calculations. Values of θ_{en} have been calculated for critical engine speeds viz. 1400 rpm, 2200 rpm and 2860 rpm. For example, values of T_{tn} at engine speed of 1400 rpm are presented in *Table IV*. Dynamic magnifier is a ratio of actual amplitude to equilibrium amplitude and is calculated by equation,

Where, $Ø_{an}$ is actual amplitude, ω is forcing frequency = crankshaft angular velocity= (2πN/60) x Order No. (n), ω_c is natural frequency in Hz, N is crankshaft speed in rpm and,

$\xi = K/K_c$ .....(7) is a damping factor or relative damping coefficient where, K = Specific viscous damping coefficient (Nms/rad) and, Kc= Critical Damping Coefficient (Nms/rad) = $2\omega_c \sum J$....(8)

Substituting numerical values of ω_c=2443.8 rad/s and, J=0.916718kgm^2 in Eq. (8), we get K_c=4480.5 Nms/rad while substituting numerical values of K=3.44 Nms/rad per cylinder in Eq. (7), we get ξ = 0.0023033.

Using the values of dynamic magnifier, actual amplitude values have been calculated for all engine critical speeds viz. 1400 rpm, 2200 rpm and 2860 rpm. For example, the results at engine speed of 1400 rpm are presented in *Table IV*.

E. Torsional Vibration Measurement on Engine

Torsional vibration measurements were carried out on the engine without damper. Engine was rigidly coupled with the hydraulic dynamometer through universal joint. Adapter was designed to mount the pickup on the crankshaft front end. Torsional vibration measurement equipment with magnetic encoder was mounted on crankshaft nose end and vibration amplitude measurements were carried out at full load and at various speed steps as well at 0.5 to 12 vibration orders. The measurement results have been presented in Fig. 5.

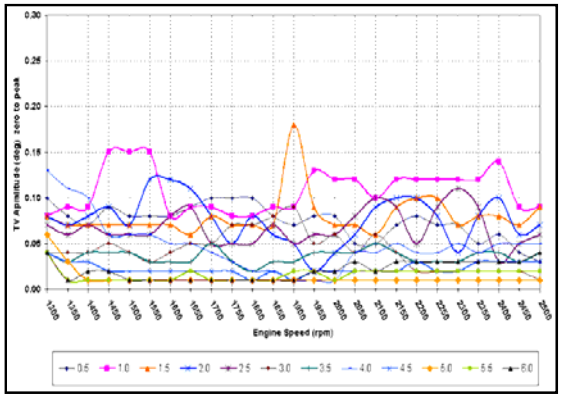

Fig. 5 : Torsional Vibration Amplitude Measurements

F. Discussion of Results

The analytical results show that the first mode or fundamental natural frequency is 388 hertz or 23336 revolutions per minute. Order number corresponding to first mode frequency is 10.1. While second mode natural frequency is around 952.63 hertz or 57158 revolutions per minute. Order number corresponding to second mode frequency is 24.8.

Campbell Diagram depicts that the order numbers 9, 10, 10.5, 11 and 12 are intersecting natural frequency line at crankshaft speeds 2600, 2300, 2200, 2100 and 1900 rpm respectively. Hence, these orders are the Critical Orders. However, 9, 10.5 and 12 are the major orders and are Major Critical Orders. Rest of critical orders are minor critical orders. However being typical diesel engine off-road application, torsional vibration measurement is carried out at (i) maximum torque point (1400 rpm) due to predominant gas load and vehicle field operation speed while at (ii) overspeed (2860 rpm) due to predominant inertia loads in addition to (iii) rated speed (2200 rpm) conditions.

From modal analysis results, it is seen that the fundamental natural frequency of crankshaft in free-free conditions is 385 Hertz or 23100 revolutions per minute (rpm). When the crankshaft assembly including crank gear, crankshaft and flywheel are constrained, natural frequency is observed 459 Hertz or 27540 rpm. Natural frequency of crankshaft assembly calculated using Holzer Table is 15% lower than that measured using FEA modal analysis method.

When the harmonic analysis of gas torque (Tg) and inertial torque (Ti) is carried out up to 42 orders, the calculated results match with actual measured results. Maximum torsional vibration amplitude values at engine speeds of 1400rpm, 2200rpm and 2860rpm are 0.195°, 0.191° and 0.158° respectively. These values are below

acceptable limit of 0.20° maximum. Fig. 4 presents the results of Torsional vibration measurement on engine. It is seen that all orders from 0.5 - 6.0 have torsional vibration amplitude levels below 0.20° at Crankshaft front end. Results of 6.5 - 12.0 orders were observed in the range of 0.01° to 0.02°. Maximum torsional vibration amplitude of 0.18° was observed at 1900rpm with order 1.5. Actual amplitude values as per analytical and experimental results are below the acceptable limit of 0.20° which implies that there are no major torsional vibration problems and there is no need of installation of torsional vibration damper for this engine application.

IV. SUMMARY / CONCLUSIONS

Natural frequency of crankshaft assembly calculated using Holzer Table is 15% lower than that measured using FEA modal analysis method. The difference in results could have reduced if the FEA modal analysis had considered clutch along with flywheel. Harmonic analysis results of gas load and inertial load match with measured or calculated results when harmonic analysis is carried out up to 42 orders. The analytical and experimental results of torsional vibration amplitude are below the acceptable limit of 0.20°. It implies that there are no major torsional vibration problems. Thus crankshaft is safe in view of torsional vibrations and there is no need of installation of torsional vibration damper for this engine application. Hence the crankshaft design is safe.

REFERENCES

[1] Ravi Kumar Burla, P. Seshu and H. Hirani, P.R. Sajanpawar and H.S. Suresh, "Three Dimensional Finite Element Analysis of Crankshaft Torsional Vibrations using Parametric Modeling Techniques", SAE International Technical Paper Series, 2003.

[2] H. Okamura, T. Morita, "Simple Modeling And Analysis For Crankshaft Three-Dimensional Vibrations Under Firing Conditions" (Downloaded from Internet).

[3] Dr. Ch. Ratnam, B. Sridhar and K.N.S. Prakasa Rao, "Frequency Analysis of a Multi-cylinder Four-stroke Diesel Engine Crankshaft by using the Transfer Matrix and Finite Element Methods", Journal of The Institute of Engineers (India), Vol. 86, pp. 1-6, 2005.

[4] W. Ker Wilson, "Practical Solution of Torsional Vibration Problems", Vol. 2, Chapman and Hall Ltd., London, 3rd Edition, 1963.

[5] A. Kolchin and V. Demidov, "Design of Automotive Engines", MIR Publishers Moscow, English translation, 1984.

[6] Bernard Challen and Rodica Baranescu, "Diesel Engine Reference Book", Society of Automotive Engineers Inc., USA, Second Edition, 1999.

◈◈◈

Design and Development of Liquid Nitrogen Storage Vessel

Salot Vimalkumar P & R.K. Patel

L. D. College of Engineering, Ahmedabad, India

Abstract **-** Conventional cryogenic fluid storage vessel consists of inner vessel, outer vessel, fill and drain line. Here the novel concept of interposing radiation shield in between inner and outer vessel is introduced. Thus this new design consists of two insulation gaps instead of one. The insulation used is vacuum alone. Theoretical analysis shows good result. The prototype of ten litre capacity is developed and it shows considerable saving of ten percent in boil off rate of liquid nitrogen, as compared to vessel without radiation shield.

Keywords **-** *liquid nitrogen, vacuum, radiation, heat transfer.*

I. INTRODUCTION

After the cryogenic fluid has been liquefied, it is necessary to store it in such a way that it results in minimum boil-off rate. Spherical vessels have most effective configuration as far as heat in leak is concerned, and they are often used for large volume storage in which the vessel is constructed on the site. Cylindrical vessels are usually required for transportable trailers and railway cars. For small laboratory vessels, cylindrical configuration is preferred for their easiness and economical fabrication. Small laboratory vessels are widely used for long time storage of cryogenic fluids, for the preservation of biological samples, for cooling of small samples and to cool detectors for space telescopes.

II. SELECTION OF MATERIAL

Some materials like carbon steel performs ductile to brittle transition when they are exposed to liquid nitrogen temperature and they become very brittle. So this type of materials cannot be used for the construction of inner vessel. But material like Stainless Steel retains their properties even at lower temperature because of martensitic transformation[3][6]. Some other desirable properties for constructional materials are:

- compatibility for high vacuum
- low emissivity
- low thermal contraction coefficient
- good weldabiity
- low out gassing rate
- available in standard shape and size
- economical

Considering all these requirements S.S. 304 is best suitable material and is selected for the construction of inner vessel, outer vessel and radiation shield.

III. PROBLEM FORMULATION

Here small laboratory vessel of 10 litre capacity is developed with radiation shield interposed between inner and outer vessel.

A. Technical specifications

Capacity: 10 litre

Ullage space: 10%

Cryogenic fluid to be stored: LN_2

Absolute design pressure: 238 kPa

Type of insulation: Vacuum

Vacuum intensity: 2 mPa

TABLE I. PROPERTIES OF LIQUID NITROGEN

Temp.(K)	P_{sat} (kPa)	Density (kg/m^3)	Latent heat h_{fg} (kJ/kg)
75	76	818.1	202.3
77.36	101.3	807.3	199.3
80	136.7	795.1	195.8

B. Design Methodology

1) Mechanical analysis and design: It determines minimum thickness required for inner vessel and outer vessel. It is done according to ASME Boiler and Pressure Vessel Code, section VIII, Div-I.

2) Thermal analysis and design: It determines insulation requirements and heat transfer rate.

IV. DESIGN OF INNER VESSEL

A. Height of the vessel:

The design of inner vessel is done accrding to ASME design standards[1]. Height of the vessel is determined by the total volumetric capacity of the

vessel. It is made from NPS 6 schdule 5 with following dimensions:

Inner diameter (D_{ii}) = 162.7 mm

Outer diameter (D_{oi}) = 168.3 mm

Thickness (t_i) = 2.8 mm

ASME standard 2:1 elliptical head is used as bottom cap.

The height of the vessel can be found by

$$V = V_{cyl} + V_{head} \quad (1)$$

Where V = total volume of the vessel = 11 lit

V_{cyl} = volume of the cylindrical portion

V_{head} = volume of head

h= height of the vessel

Fig. 1 shows assembly drawing of inner vessel which includes cylindrical portion, bottom head, top flange and standard KF.

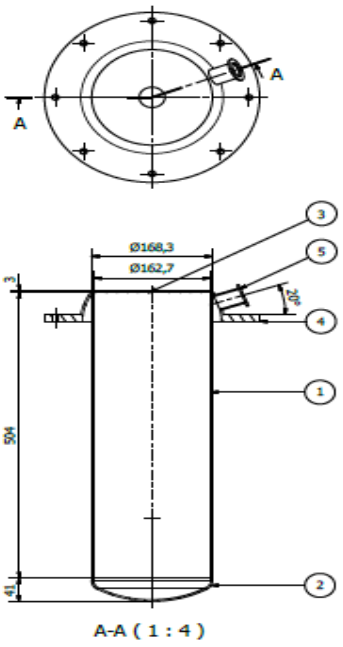

Fig. 1 : Inner vessel assembly drawing

V. RADIATION SHIELD

It appears that the dominant heat transfer mode is radiation in the isolating cavity[4]. This can be reduced by interposing radiation shield between inner and outer vessel.

NPS 7 schedule 5 pipe, S.S. 304 is used as radiation shield with flat bottom head. The following are dimensions:

Inside diameter (D_{is}): 189 mm

Outside diameter (D_{os}): 193 mm

Thickness (t_s): 2 mm

The gap maintained between inner vessel and radiation shield is 10 mm in order to fulfill the condition that free mean path should be larger than this gap.

Fig. 2 shows details of radiation shield which includes cylindrical portion and top flange.

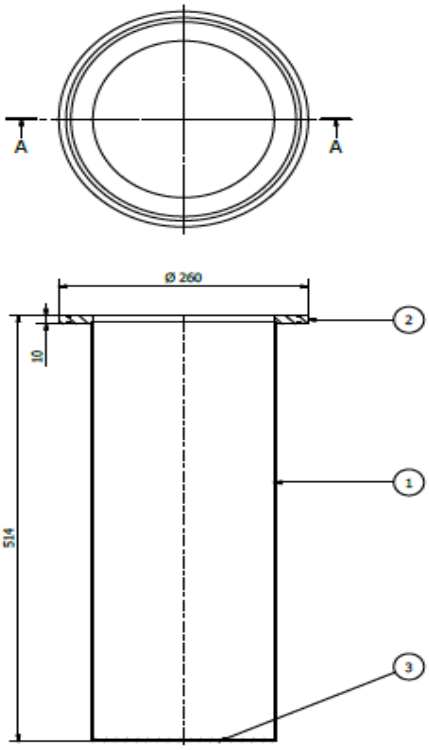

Fig. 2 : Assembly drawing of radiation shield

VI. FREE MEAN PATH

In order for free molecular conduction to occur, the mean free path of the gas molecules must be larger than the spacing between two surfaces. To check this condition, the mean free path may be determined from

$$\lambda = (\mu_1/p) \times (\pi RT/2g_c)^{1/2} \quad (2)$$

where

μ_1= gas visocity, Pa-s

p = vacuum pressure = 2 mPa

R = specific gas constant = 287 J/kg K

A. check this condition for inner vessel and radiation shield:

$\mu_1 = 16 \times 10^{-6}$ Pa-s at 253 K

□ = 2.94 m

The gap between inner vessel and radiation shield = 10.35 mm, thus □ is geater than gap.

B. check this condition for outer vessel and radiation shield:

μ_1=18.47×10^{-6}Pa-s at 300K, hence □=3.39m

VII.DESIGN OF OUTER VESSEL

It has to withstand only atmospheric pressure. So it may fail from the view point of elastic instability or buckling. It is designed by considering four times atmospheric pressure acting on it[1][2].

NPS 8 schedule 5 pipe, S.S. 304 is used as outer vessel with following are dimensions:

Inside diameter (D_{io}): 213 mm

Outside diameter (D_{oo}): 219 mm

Thickness (t_o): 3 mm

The gap maintained between outer vessel and radiation shield is 10 mm in order to fulfill the condition that free mean path should be larger than this gap.

Fig. 3 shows assembly drawing of outer vessel which includes cylindrical portion, bottom head, top flange and standard KF.

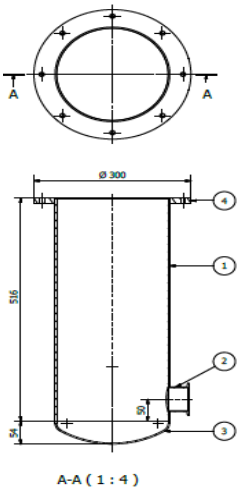

Fig. 3 : Outer vessel assembly drawing

Fig. 4 shows assembly drawing of whole vessel.

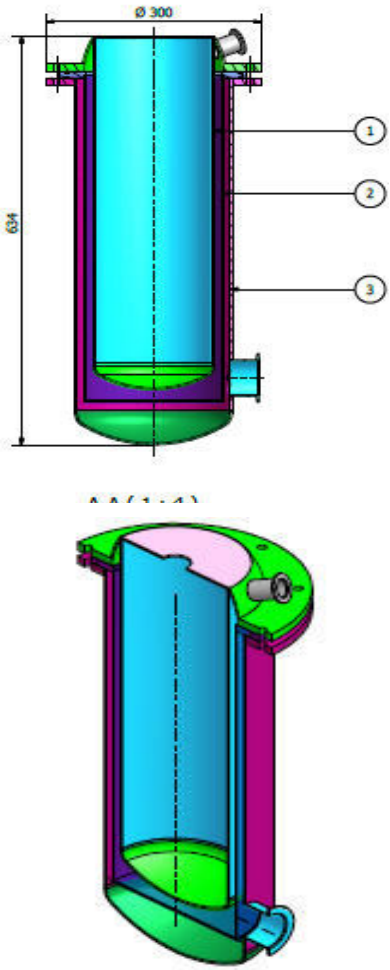

Fig. 4 : Assembly drawing of vessel

VIII. HEAT TRANSFER BY RADIATION

The radiant heat transfer rate between two surfaces is given by the modified Stefan-Boltzman equation,

$$Q_r = F_e \times F_{1-2} \times \sigma \times A_1 \times (T_s^4 - T_1^4) \text{ [5]} \qquad (2)$$

Where

F_e = emissivity factor

F_{1-2} = configuration factor

σ = Stefan-boltzman constant = 56.69×10^{-9} W/m^2 K^4

T_s = temperature of radiation shield = 252 K

T_1 = temperature of inner vessel = 78 K

Total heat transfer through cylindrical portion and head by radiation,

Q_r = 0.4645 W

IX. HEAT TRANSFER BY MOLECULAR GAS CONDUCTION

Heat transfer through residual gas conduction is given by

$$Q_g = G \times p \times A_1 \times (T_s - T_1) \quad (3)$$

Where

$$G = (\gamma+1)/(\gamma-1)\ (g_c R/8\pi T)^{1/2} \times F_a \quad (4)$$

R = specific gas constant

γ = specific heat ratio = C_p/C_v = 1.4

F_a = accommodation co-efficient

Total heat transfer through cylindrical portion and head by residual gas conduction,

Q_g = 0.0578 W

Total heat transfer by radiation and residual gas conduction (with radiation shield),

$Q = Q_r + Q_g = 0.4645 + 0.0578 = 0.5223$ W

Total heat transfer by radiation and residual gas conduction (without interposing radiation shield),

$Q = Q_r + Q_g = 2.3114 + 0.0784 = 2.3898$ W

Fig. 5 shows experimental set up.

Fig. 5 : Experimental set up

X. BOIL OFF RATE

The total heat energy required to evaporate the full content of the vessel is given by,

$E_t = \rho_f \times h_{fg} \times V = 807.3 \times 199.3 \times 10 \times 10^{-3} = 1608.95$ kJ

Where,

ρ_f = density of liquid nitrogen

h_{fg} = latent heat of evaporation

The total energy transfer to the vessel content during one day is,

$E_d = Q \times t_d \quad (5)$

$= (0.5223 \times 10^{-3})\ (3600$ s/hr) (24 hr/day)

= 45.12 kJ/day

The fraction of the full vessel content that is evaporated during one day is given by, E_d/E_t. Following is the summary of results.

TABLE II. RESULT

	With radiation shield	Without radiation shield
Boil off rate of liquid nitrogen	2.80% per day	12.83% per day

XI. CONCLUSION

This experiment shows good result of using radiation shield in between inner and outer vessel. The saving achieved in boil off rate is about 10% which justifies the additional cost. For higher volume to surface area still better results may be obtained.

REFERENCES

[1] ASME Boiler and Pressure Vessel Code,Section VIII, Unfired Pressure Vessels, American Society of Mechanical Engineers, New York, 1983.

[2] Barron R. F, "Cryogenic Systems," second edition, oxford university press, 1985.

[3] Mohsen Botshekan, Suzanne Degallaix and Yannick Desplanques,"Influence of martensitic transformation on the low-cycle fatigue behavior of 316LN stainless steel at 77 K", 1997.

[4] O.Khemis, M.Boumaza, M.Ait Ali and M.X.Francois,"Experimental analysis of heat transfer in a cryogenic tank without lateral insulation", Universite de constantine, constantine, Algeria,2003.

[5] Seo Young Kim, Byung and Ha Kang,"Thermal design analysis of a liquid hydrogen vessel", Korea institute of science and technology, South Korea, 2000.

[6] Wigley, D.A.,"The mechanical properties of Materials at Low Temperatures", Plenum Press, New York, 1971

◈◈◈

Failure Prevention in Rotating Machinery using Vibration Analysis

Varanasi Shri Aditya & L Praveen

Mechanical Engineering, SMBS, VIT University, Vellore, India
Rotary Maintenance Department, Indian Oil Corporation Limited, Gujarat Refinery, Vadodara, India

Abstract - Preventive maintenance is an effective approach for reliability enhancement. Time-based and condition-based maintenance are two major approaches for Preventive maintenance. In contrast to time based maintenance, condition-based maintenance that is often called as predictive maintenance can be a better and more cost-effective than time-based maintenance. Preventive maintenance using vibration analysis has achieved significant results in successfully diagnosing machinery problems. Vibration is an effective tool in detecting and diagnosing some of the incipient failures of machines and equipment. A vibration signature measured on the external surface of a machine or a structure contains a good amount of information, which, if properly interpreted, can reveal the running condition of the machine. Two types of analysis are widely used to detect machinery problems. The first is velocity measurement, to pick up low frequency problems such as misalignment, unbalance, and looseness in the machine. These measurements are typically in the 1x to 10x operating frequency where 'x' is the rotating speed in cycles per minute or more commonly in RPM. Acceleration enveloping is the second analysis type used and its primary function is to detect problems in the high frequency range or bearing frequencies. These frequencies are greater than ten times of the operating speed. A case study is done to illustrate how machine failures are diagnosed with the help of vibration signatures. This paper deals with the basic principles and also compares the vibration signature before and after the diagnosis is performed. The Case Study is done with cooperation of Indian Oil Corporation Ltd. and SKF at Gujarat Refinery, India.

Keywords: *Preventive maintenance; Predictive maintenance; Vibration analysis; Case study; Fault diagnoses; reliability.*

I. INTRODUCTION

Predictive maintenance is a condition-driven preventive maintenance program. This philosophy consists of scheduling maintenance activities only when a functional failure is detected. Mechanical and operational conditions are periodically monitored, and when unhealthy trends are detected, the troublesome parts in the machines are identified and scheduled for maintenance. If left unattended, these failures could result in costly secondary failures. One advantage of this approach is that the maintenance events can be scheduled in an orderly fashion. It is nowadays seen as the means of improving productivity, product quality, and overall effectiveness of manufacturing and production plants.

Instead of relying on industrial or in-plant average-life statistics (i.e., mean-time-to-failure) to schedule maintenance activities, predictive maintenance uses direct monitoring of the mechanical condition, system efficiency, and other indicators to determine the actual mean-time-to-failure or loss of efficiency for each machine-train and system in the plant [1].

Many techniques have been developed over the years to predict the health or condition of various machines, but the scope of this paper restricts to vibration analysis. Predictive maintenance using vibration signature analysis is predicated on two basic facts: (1) all common failure modes have distinct vibration frequency components that can be isolated and identified, and (2) the amplitude of each distinct vibration component remains constant unless the operating dynamics of the machine change [2].

II. MATERIALS AND METHODS

The technique of condition monitoring through vibration is built up on the following principles:

- Any malfunctioning or deterioration in the operation of a machine component causes increase in vibration level.
- Vibration emanating from a component consists of certain frequencies depending on its nature of operation. This frequency information does not get changed or lost during transmission of vibration; however, their vibration level may be attenuated.
- Mixing of different vibrations does not cause any loss of the individual's frequency information.
- Every individual component or system has its own frequency, called its natural frequency, which changes only when the system parameters get effected.

Fig.1 illustrates some of the principles enunciated above. The unbalance in the coupling generates

vibrations with frequency equal to the rotational speed, the bearing generates vibration of frequency depending on the number of balls and the gear generates vibrations of tooth-meshing frequency. These vibrations mix with one another during transmission, and the mixed signal is picked up by the transducer. The mixed signature has all the frequencies of the individual vibrations, i.e. no information regarding frequency is lost in mixing or transmission.

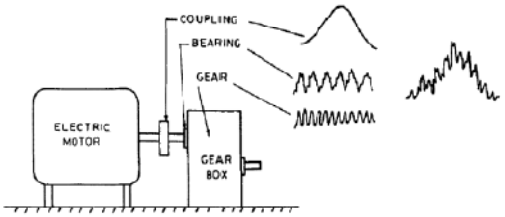

Figure 1. Vibration generation and transmission.

A. Equipement Details

The following are the specifications of the equipment used to carry out the case study.

- SKF Microlog Analyzer

  GX series

  CMXA 75

  Portable data collector / FFT analyzer
- SKF Vibration Sensor

  CMSS 786T-IS

B. Test bed

Fluid catalytic cracking (FCC) is the most important conversion process used in petroleum refineries. It is widely used to convert the high-boiling, high-molecular weight hydrocarbon fractions of petroleum crude oils to more valuable gasoline, olefin gases, and other products.

An air pre-heater (APH) is a general term to describe any device designed to heat air before another process with the primary objective of increasing the thermal efficiency of the process. It is usually placed in the furnace circuit; heat given out by the flue gases is used to reheat in the feed circuit. It can be found at many units in a refinery as auxiliary equipment.

The following are the details and specifications of the test bed, on which the case study was done.

- RefineryUnit– Fluidized Catalytic Cracking (FCC)
- Equipment type- Air Pre-Heater Blower (APH)
- Equipment Identity Number-820-APH-01
- Running Speed- 1500 RPM

Fig.3 shows the sequential arrangement of the test bed. The positions are marked where the vibration signals were recorded, in the figure.

III. RESULTS

The Vibration signal was analyzed using SKF Microlog Analyzer and Vibration Sensor. The measurement was made at particular sites, marked by position numbers in Fig. 3.

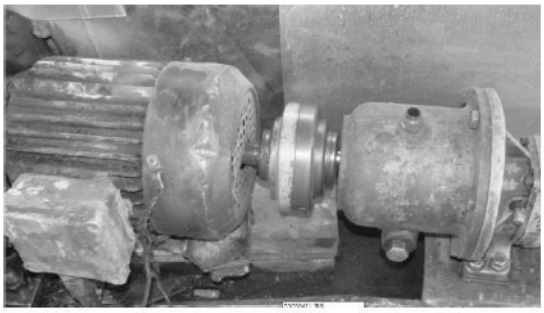

Figure 2. Test Bed

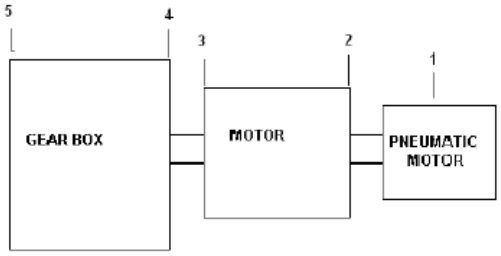

It was made in the velocity spectrum. The results are enlisted in Table 1, both before and after predictive maintenance (PdM) are mentioned for better comparison. Air Motor mentioned in the Table 1 is same as Pneumatic Motor shown in the Fig. 3. H, V, A means Horizontal, Vertical, Axial respectively. Motor has two connections, one being Drive End (DE) where it is connected through coupling and other being Non Drive End (NDE) where coupling is absent. Readings at both ends of the Motor are analyzed for appropriate conclusion.

TABLE I. VIBRATION MEASUREMENT VALUES (MM SEC^{-1})

No.	*Location*	*Before PdM*	*After PdM*
1.	Air motor H	64	6.8
2.	Air motor V	42	4.5
3.	Air motor A	37	2.8
4.	Motor NDE 2 H	53	4.2
5.	Motor NDE 2 V	25	2.7
6.	Motor NDE 2 A	14	3.4
7.	Motor DE 3 H	28	6.6
8.	Motor DE 3 V	27	1.8
9.	Motor DE 3 A	16	1.6
10.	Gear Box 4 H	11.3	6.7
11.	Gear Box 4 V	4.6	1.5
12.	Gear Box 4 A	5.6	1.3
13.	Gear Box 5 H	13.5	5.1
14.	Gear Box 5 V	6.1	1.3
15.	Gear Box 5 A	6.1	1.2

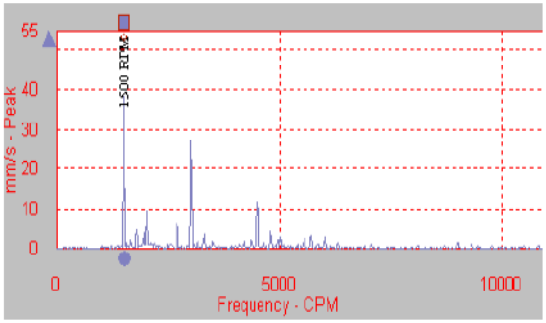

Figure 4. Motor NDE Horizontal- Before PdM

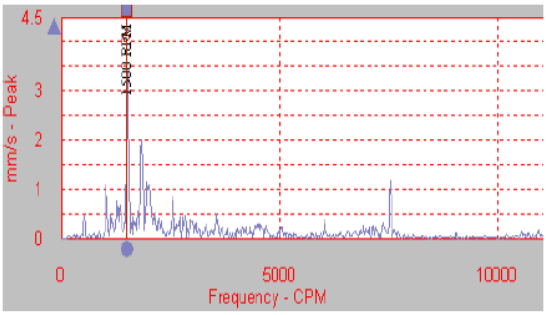

Figure 5. Motor NDE Horizontal- After PdM

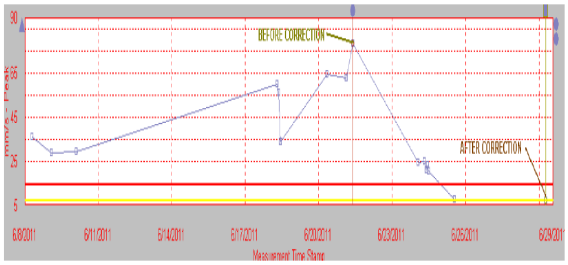

Figure 6. Trend Vibration Signals analyzed at different dates.

DISCUSSION

The Air Pre Heater unit in the FCC is scheduled to have the regular maintenance checks every third day, during its running operation. On 17th of June 2011 it started showing increasing signals at the Non Drive end of the Motor. The sensor probe was placed horizontally on the motor. From 20th June 2011, a recommendation for increasing the frequency of the scheduled maintenance from every third day to every day was placed. This equipment was indicating an ALERT condition with maximum vibration amplitude of 64mm/sec PEAK as recorded in the Motor NDE bearing location. Misalignment and coupling inaccuracies were observed. Initial recommendations given were on 22nd June 2011:

- Check coupling.
- Precise alignment to be carried out.
- Motor base support to be done.
- Further analysis will be carried out once the above mentioned action is carried out.

A possible cause for the vibration was chosen as Misalignment since the equipment was giving maximum vibration at the running frequency that is 1500RPM. It can be clearly seen in Fig.4.

Mechanical unbalance, misalignment, bowed shaft, hydraulic unbalance, shaft run out, excessive bearing clearance, looseness of bearing caps all these are possible defects when there is high amplitude vibration at the running frequency. According to the condition of the machine and its state visible to the naked eye, Misalignment was finalized. Causes can be loose foundation bolts, flexible base plate, piping loads, bearing degradation and incorrect axial setting for flexible coupling.

Misalignment was found out when Easy Laser apparatus was setup at the NDE of the motor. Predictive maintenance was done using laser alignment. Easy Laser apparatus is used for aligning shafts to the

maximum possible accuracy. After the PdM, the vibration signals dropped between 2 to 6 mm sec-1.

V. CONCLUSION

Vibration is a very effective tool for diagnosing many mechanical defects. It however needs expert knowledge and experience for fault-tracing. When vibrations are used for condition monitoring, it is always advisable to start with simple instrumentation and before applying the technique to plant or machinery maintenance, the economical viability must be assessed [3]. Trend of overall frequencies and vibration spectrum provides useful information to analyze defects in rotary equipment. Vibration domain spectrum identifies amplitudes corresponding to defect frequencies and enables to predict the exact defect. The paper demonstrates how vibration monitoring and analysis is used to aid predictive maintenance in industry to minimize unexpected machinery failures as well as to reduce maintenance costs.

VI. ACKNOWLEDGMENTS

We would like to extend our sincere gratitude to SKF and Indian Oil Corporation Limited for its continuous cooperation and support. We would also like to thank Mr. V J Rao and Ms. Atima Goel, Deputy General Manager, Indian Oil Corporation Limited and B Tech Mechanical & Energy respectively for proof reading the paper.

VII. REFERENCES

[1] Robert Bond Randall. Vibration-Based Condition Monitoring Industrial, Aerospace And Automotive Applications. Reading, Mass. 1st Edn., John Wiley & Sons, 2011

[2] [2]. M Amarnath, R Shrinidhi, A Ramachandra, S B Kandagal. Prediction of Defects in Antifriction Bearings using Vibration Signal Analysis. IE(I) Journal-MC 85, 2004, pp.88-92.

[3] [3]. H. Mohamadi Monavar, H. Ahmadi and S.S. Mohtasebi. Prediction of Defects in Roller Bearings Using Vibration Signal Analysis. World Applied Sciences Journal 4 (1) , 2008, pp.150-154

◈◈◈

Finite Element and Experimental Stress Analysis of an Automotive Hollow Stabilizer Bar

Gangadhar A. Jagdale[1] & S. G. Joshi[2]

[1]Dept. of Mechanical Engg., Sinhgad Education Society's SKN College of Engg., Pune, India
[2]Dept. of Mechanical Engg., Rajarambapu Institute of Technology, Sakharale, India

Abstract - A stabilizer bar or an anti-roll bar has been used in passenger cars, light trucks etc. for improvement of running stability and decreasing body roll. The use of stabilizer bar results in a vehicle weight penalty in order to achieve the desired roll control. However, it is possible that for the saving of material and energy, a hollow stabilizer bar will be advantageous over the solid stabilizer bar. As such, in this paper, results of the stress analysis of a hollow stabilizer bar of a typical road vehicle using finite element method are presented. The experimental stress analysis using strain gauge technique has been performed to correlate the Finite Element Analysis (FEA) results. The effect of material weight saving on the magnitude and location of peak stress has been studied. To decide the fatigue analysis approach, the modal analysis of the hollow stabilizer bar has been carried out and the effect of material weight saving on fatigue life of the hollow stabilizer bar has been discussed. It is observed that the peak stress value of a hollow stabilizer bar obtained by FEA is in good agreement with that measured in experimental stress analysis. With the increase in material weight saving, magnitude of peak stress increases and its location moves away from the inside of the main bend. The stress distribution pattern of the hollow stabilizer bar is not symmetric unlike the solid stabilizer bar. Static fatigue can be used for the estimation of fatigue life of the hollow stabilizer. Fatigue life of the hollow stabilizer decreases with the increase in material weight saving and the fatigue failure occurs near the centre of main bend. Thus, an automotive hollow stabilizer bar can be designed to meet the requirements of saving of material and energy.

Keywords - *hollow stabiliser bar; FEA; experimantal stress analysis; peak stress; material saving; fatigue life*

I. INTRODUCTION

The stabilizer bar is an important part of the automotive suspension system and has been widely employed to tune ride and handling by managing lateral weight transfer and reducing body lean during cornering. Typically, it is connected to both lower control arms and the front cross member of a road vehicle. Stabilizer bars have been used for passenger cars, light trucks and recently the application has been extended for heavy-duty trucks. However, stabilizer bar usage results in a vehicle weight penalty in order to achieve the desired roll control. The stabilizer can be either solid or hollow, with hollow stabilizers lighter but more expensive. It has been found that design of hollow stabilizers is different than solid stabilizers because of the different stress distribution [1] and design challenges increase as material stress increases. Stabilizer bar improves the riding stability and decreases the rolling, when the automobile makes its turn. However, stabilizer bar has minimal effect on the ride stability [2]. In recent years, with the increase in consciousness over energy and saving of natural resources, there has been a corresponding demand for weight saving in the manufacturing of automobiles. And as for the stabilizer, the application of the tube (hollow stabilizer) instead of the solid bar has become manufacturing requirement. Hollow stabilizers can be 35 to 50 % lighter than equivalent rate solid bars [3]. Stabilizer bars in a suspension are supported with bushings by a frame structure. To prevent the axial movement of the stabilizer bar within the bushing several new stabilizer bar bushing systems have been designed. Relative merits and demerits of these features in terms of the roll stiffness and the fatigue life are evaluated using CAE tools [4]. The new system introducing permanent mechanical bond between the bar and the bushing has been also invented [5]. It eliminates the different design features on the bars and bushings. Stabilizer bars are subjected to the wide band of random loads in service. Hence, they are prone to fatigue failure. The fatigue damage correlation of a stabilizer bar between laboratory and road has been studied [6] in order to determine the fatigue damage imposed on a front suspension stabilizer bar.

In this paper, stress analysis of a hollow stabilizer bar of a typical road vehicle using Finite Element Analysis has been performed and the effect of material weight saving on the magnitude and location of peak stress is studied. To validate FEA results, experimental stress analysis using strain gauge technique has been carried out. For this purpose, a suitable experimental setup was developed. To decide the approach of fatigue analysis, modal analysis of the hollow stabilizer bar is performed. Based on the results of finite element stress analysis of the hollow stabilizer bar, its fatigue analysis

is carried out and the effect of material weight saving on its fatigue life has been discussed.

II. MAGNITUDE AND LOCATION OF PEAK STRESS

Finite element analysis (ANSYS-11) was performed to study the stress distribution pattern of an automotive hollow stabilizer of a typical road vehicle. To study the effect of material weight saving on the magnitude and location of the peak stress, the analysis was carried out for five different stabilizer bars, with dimensions as shown in Table I.

TABLE I : DIMENSIONS OF HOLLOW STABILIZER BAR

Sr. No.	Outside Diameter d_2 (mm)	Bend Radius R (mm)	Displac-ement, f (mm)	Thickness t (mm)	Thickness ratio, t/d_2
1	25.4	50	37.5	2.5	0.10
2				2.8	0.11
3				3.0	0.12
4				3.5	0.14
5				3.8	0.15

Among these, 3.00 mm thickness hollow stabilizer is of a typical road vehicle. As the frequency of loading is very small (1.6 Hz), loading condition can be simulated as a static case [7].The wall of hollow stabilizer was modeled as a mid-surface area. Two bushes were modeled in the form of volumes. Element types along with input material properties and real constants are given in Table II.

The critical areas where failure likely starts to occur were meshed with lesser element length i.e. dense meshing. (Fig. 1) It helped to achieve the desired accuracy of magnitude and location of the peak stress, so that in the experimental stress analysis strain-rosette could be bonded exactly at the maximum stress point.

TABLE II : ELEMENT TYPES ALONG WITH INPUT MATERIAL PROPERTIES AND REAL CONSTANTS

Sr. No.	Component	Material	Material Property	Element Type	Real Constant
			Young's Modulus, E (MPa)	*Poisson's Ratio, ν*	*Coeff. of Friction, μ*		
1	Hollow Stab Bar	Alloy Steel	$2x10^6$	0.3	0.15	SHELL 63	Thickness
2	Bush	Rubber	2	0.4		SOLID 92	None

Contact condition between stabilizer bar and bushings was prescribed to simulate the contact interaction. The selected contact elements have been summarized in Table III.

TABLE III : CONTACT ELEMENTS

Sr. No.	Contact Type	Component	Contact Element Type
1	Rigid-to-Flexible, (Surface-to-Surface)	Hollow Stab Bar	TARGE 170
2		Bush	CONTA 174

The outer lateral surfaces of the bushes were constrained with all degrees of freedom and a vertical displacement load of 37.5 mm, which is equivalent to a transverse acceleration of 0.4 g was applied in the opposite directions at the two ends of the hollow stabilizer bar, in all the cases.

From the Fig. 2, it can be seen that the peak stress occurs at a location near the centre of main bend, in all cases. From Fig. 3, it is observed that the stress distribution curve of a hollow stabilizer bar is not symmetric, unlike the solid stabilizer bar. As the thickness of hollow stabilizer bar becomes smaller (i.e. weight saving ratio increases) the peak stress value becomes larger and its location moves away from the inside of the bend. The peak stress occurs around the location of $\alpha \approx 60°$ to $70°$. The stress results have been summarized in Table IV.

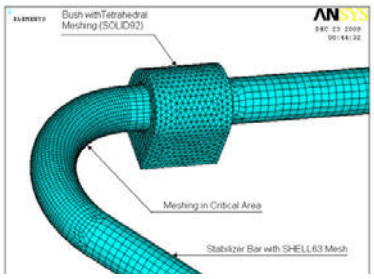

Fig. 1: FEA model of hollow stabilizer bar

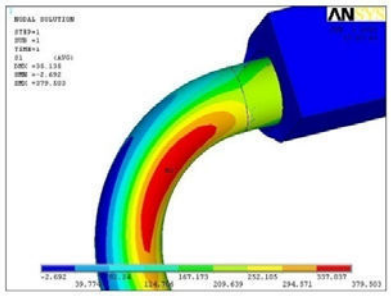

Fig. 2 : Stress distribution pattern of hollow stabilizer bar with thickness, t=3.0 mm

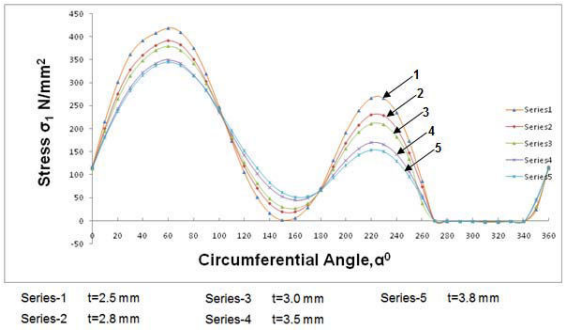

Fig. 3 : Variation of stress along the cross section of hollow stabilizer bar near the main bend

TABLE IV : RESUTS OF STRESS ANALYSIS OF THE HOLLOW STABILIZER BARS

Sr. No.	Outside Diameter, d_2 (mm)	Thickness, t (mm)	Max. Stress, σ_1 (N/mm^2)	Max. Stress Location, $\alpha°$
1	25.4	2.5	418.749	70
2		2.8	390.814	68
3		3.0	379.503	65
4		3.5	349.8	62
5		3.8	344.552	60

III. EXPERIMENTAL SETUP AND STRAIN MEASUREMENTS

Experimental Stress Analysis of the hollow stabilizer by using strain-gauge technique was carried out to validate its finite element stress analysis. As the directions of principal stresses (or strains) were not known in advance, three-element rectangular strain gauge rosette was particularly suited in such a situation. Hence bonded electrical resistance type metal-foil gauges (rosette), make Coya Instruments, Japan, type 0°/45°/90°, with standard resistance of 120± 0.5 Ω, gauge length of 5 mm and gauge factor K=2.0 have been selected for the purpose.

Fig. 4 : Rectangular strain –rosette with connecting wires

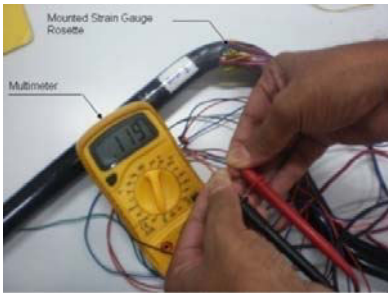

Fig. 5 : Checking of gauge resistance for gauge continuity

Fast curing cynoacrylate was used as an adhesive, for bonding the strain-rosette to the hollow stabilizer bar specimen. Wheatstone quarter-bridge circuit was selected for strain gauge circuit. To achieve temperature compensation a dummy gauge of the same type and of the same resistance was used in the strain gauge circuit. The Wheatstone quarter-bridge circuit with temperature compensating dummy gauge is as shown in Fig. 6.

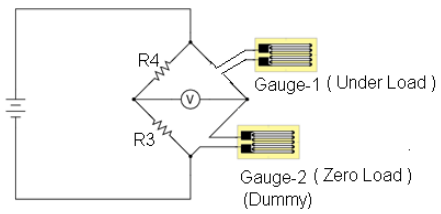

Fig. 6 : Temperature compensation with dummy gauge

To apply the displacement loads, a heavy fatigue-testing machine, Fig. 7, was employed and for the measurement of strains, digital strain-indicator was used.

Three specimens of the hollow stabilizer bar of the same dimensions were selected for the test purpose. The bars were made by forging, followed by quenching. To induce compressive residual stress, the bars were submitted to shot peening surface treatment. Bars were free from any tool scratch, scale and surface defects and were 100% crack tested. Finally, individual bar was mounted on the rubber bushes in the developed experimental test setup.

Fig. 7 : Experimental setup for experimental stress analysis

1. Mounted strain-rosette
2. Supporting bush with bracket
3. Hollow stabilizer bar
4. Loading point
5. Pivoted lever
6. Fatigue testing machine
7. Digital strain indicator
8. Experimental setup platform

With the help of a heavy fatigue-testing machine, a constant reversed displacement load of 37.5 mm was applied gradually at both the ends of hollow stabilizer bar. Three active strain gauges from the rectangular rosette were brought in Wheatstone quarter-bridge circuit one by one and the strain induced in each of the gauge was measured with the help of digital strain indicator. To avoid strain hardening effects, the strain measurements were done for loading as well as unloading cases. From the measured values of strains, principal strains have been calculated and from those values, principal stresses have been evaluated. The observations and results have been presented in Table V and Table VI.

The variations observed in the first principal stress values may be because of measurement system inherent error or other factors related to stabilizer bar itself. The system error was evaluated by using statistical technique of multiple regressions and it was found to be 0.491292786 N/mm^2, a negligible value. Thus, the variation observed in experimentally calculated stress values is mainly not because of measurement system error and it may be attributed to other factors such as slight variations in bend dimensions, manufacturing processes, surface conditions, loading speed and the overhanging length of the bar, etc.

TABLE V : STRAIN MEASUREMENT RESULTS

Stabilizer Bar	**Sr. No.**	**Loading**			**Unloading**		
		ε_a	ε_b	ε_c	ε_a	ε_b	ε_c
		(in microstrain)			***(in microstrain)***		
Stab Bar-I	1.	233	1236	1613	221	1231	1629
	2.	234	1246	1600	223	1223	1642
	3.	235	1226	1593	228	1224	1630
Stab Bar-II	1.	177	1164	1575	170	1142	1561
	2.	175	1164	1566	171	1143	1589
	3.	178	1165	1565	173	1150	1604
Stab Bar-III	1.	141	1243	1605	124	1214	1626
	2.	141	1244	1612	121	1243	1640
	3.	137	1242	1608	123	1243	1619

TABLE VI : STRESS VALUES FOR LOADING AND UNLOADING FOR HOLLOW STABILIZER BAR-I, II AND III

Stabilizer Bar	Sr. No.	Loading						Unloading					
		ε_x	ε_y	γ_{xy}	ε_1	ε_2	σ_1 (MPa)	ε_x	ε_y	γ_{xy}	ε_1	ε_2	σ_1 (MPa)
Stab Bar-I	1	233	1613	626	1680.67	165.32	380.27	221	1629	612	1692.62	157.37	382.24
	2	234	1600	658	1675.10	158.89	378.63	223	1642	581	1699.16	165.83	384.37
	3	235	1593	624	1661.25	166.74	376.10	228	1630	590	1689.54	168.45	382.43
Stab Bar-II	1	177	1575	576	1632.00	119.99	366.59	170	1561	553	1613.94	117.05	362.42
	2	175	1566	587	1625.39	115.60	364.85	171	1589	526	1632.20	123.79	366.88
	3	178	1565	587	1624.55	118.44	364.85	173	1604	523	1650.28	126.71	371.05
Stab Bar-III	1	141	1605	740	1693.19	52.80	375.61	124	1626	678	1698.96	51.03	376.76
	2	141	1612	735	1698.70	54.29	376.92	121	1640	725	1722.07	38.92	381.04
	3	137	1608	739	1695.59	49.40	375.91	123	1619	744	1706.39	35.60	377.37

IV. MODAL ANALYSIS OF HOLLOW STABILIZER BAR

The modal analysis of the hollow stabilizer bar (wall thickness, t=3.00 mm) of a typical road vehicle was carried out to find its fundamental frequency and to decide the approach of fatigue analysis accordingly. As the excitation frequency (1.6 Hz, first natural frequency of the spring mass of the vehicle) of the hollow stabilizer bar was less than one third of its fundamental frequency (83.5 Hz), static fatigue analysis approach was followed and static stress analysis results were used as input data for this analysis [7].

The input materials properties for modal analysis and obtained natural frequencies have been tabulated in Table VII and Table VIII respectively.

TABLE VII : INPUT MATERIAL PROPERTIES FOR MODAL ANALYSIS OF THE HOLLOW STABILIZER BAR (T = 3.00)

Component	Material	Material Property	
		Young's Modulus, E (MPa)	*Density, ρ Kg/m^3*
Hollow Stab Bar	Alloy Steel	2x10^6	7830
Bush	Natural Rubber	2	1180

TABLE VIII : NATURAL FREQUENCIES OF THE HOLLOW STABILIZER BAR (T=3.00 MM)

Natural Frequency Number	Natural frequency, Hz	Natural Frequency Number	Natural frequency, Hz
1	83.577	9	530.23
2	109.4	10	571.73
3	114.10	11	630.28
4	159.64	12	649.29
5	200.75	13	715.21
6	323.80	14	718.64
7	365.32	15	719.34
8	502.97		

V. FATIGUE ANALYSIS OF HOLLOW STABILIZER BAR

Before fatigue analysis, the modal analysis of the hollow stabilizer bar (wall thickness, t=3.00 mm) of a typical road vehicle was carried out to find its fundamental frequency and to decide the approach of fatigue analysis accordingly.

Stabilizer bar being a part of automotive suspension system is subjected to loads with variable amplitude and frequencies and it may lead to its fatigue failure. Fatigue analysis of the hollow stabilizer bars was performed to estimate their fatigue lives and also to study the effect of

material weight saving on their fatigue lives. The modal analysis of a hollow stabilizer bar (of thickness, 3 mm) showed that its excitation frequency (1.6 Hz) is very less than its fundamental frequency (83.5 Hz).Hence its static fatigue analysis was performed. Static stress analysis results were used as the input data for static fatigue analysis. The IDEA-software was used to serve the purpose of FEA-fatigue analysis. Static fatigue analysis of five different hollow stabilizer bars with same outside diameter and varying material thickness was performed. The dimensions of hollow stabilizer bars for fatigue analysis are as shown in Table IX.

TABLE IX : DIMENSIONS OF HOLLOW STABILIZER BARS FOR FATIGUE ANALYSIS

Sr. No.	Outside Diameter d_2 (mm)	Main Bend Radius, R (mm)	Thickness t (mm)	Thickness ratio, t/d_2	Weight saving, S (%)
1	25.4	50	2.5	0.10	53
2			2.8	0.11	51
3			3.0	0.12	50
4			3.5	0.14	44
5			3.8	0.15	41

The fatigue failure of the Hollow Stabilizer bar occurred at main bend as shown in Fig. 8.

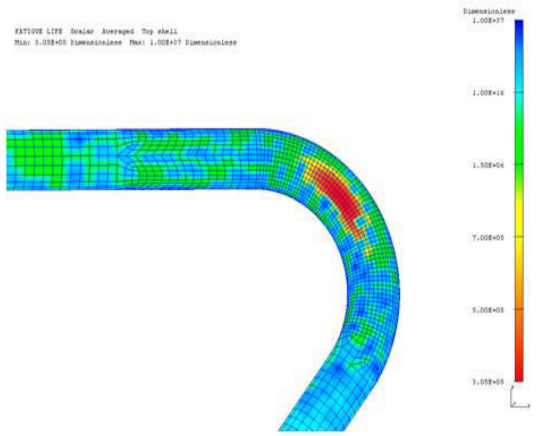

Fatigue Life- 3.05X10^5 Cycles

Fig. 8 : Fatigue life pattern of hollow stabilizer bar of wall thickness, 3.0 mm

The fatigue lives of the respective hollow stabilizer bars are summarized in the Table X.

TABLE X : FATIGUE LIFE OF HOLLOW STABILIZER BARS

Sr. No.	Outside Diameter, d_2 (mm)	Thickness, t (mm)	Weight saving, S (%)	Fatigue Life, N (Cycles)
1	25.4	2.5	53	$1.77x10^5$
2		2.8	51	$2.51 x10^5$
3		3.0	50	$3.05 x10^5$
4		3.5	44	$4.42 x10^5$
5		3.8	41	$5.35 x10^5$

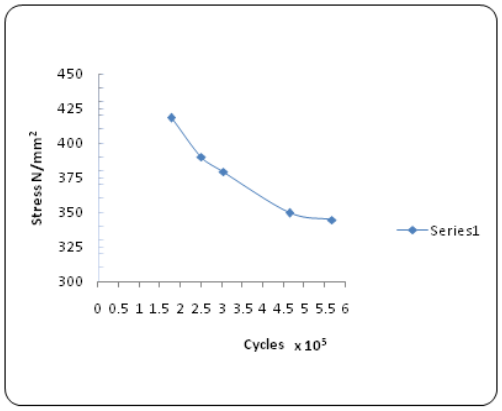

Fig. 9 : S-N Curve

Fatigue life of hollow stabilizer bar decreased with decrease in wall thickness ratio i.e. in other words it decreased with increase in weight saving ratio. The laboratory fatigue test data for the hollow stabilizer bar with wall thickness 3.00 mm showed the occurrence of failure at the main bend at around $2.5x10^5$ cycles. FEA fatigue analysis of the hollow stabilizer bar also showed the occurrence of failure at the same location but at $3.05x10^5$ cycles. It can also be seen from Fig. 8, that the fatigue analysis data for the five specimens can be expressed by one S-N curve.

VI. CONCLUSION

1. The solid stabilizer bar can be replaced by the equivalent rate hollow stabilizer bar with the advantage of material weight saving.
2. The peak stress value of a hollow stabilizer bar obtained by FEA is in good agreement with that measured in experimental stress analysis.
3. With the increase in material weight saving, magnitude of peak stress increases and its location moves away from the inside of the main bend. The stress distribution pattern of the hollow stabilizer bar is not symmetric unlike the solid stablizer bar.

4. Static fatigue analysis approach can be used for the estimation of fatigue life of the hollow stabilizer bars. Fatigue life of the hollow bar decreases with the increase in material weight saving and the fatigue failure occurs near the centre of main bend.

REFERENCES

[1] Kanji Inoue, Hiroshi Koyama and Akira Ohno, "Design of the hollow stabilizer bar", SAE-820763.

[2] Pinas Barak,Natraj Pankanti and Tarun Desai, "Effect of chasis design factors on the ride quality using a seven degree of freedom vehicle model", SAE-2004-01-1555.

[3] SAE Spring Committee, Spring Design Manual, Society of Automotive Engineers, U.S.A., 1996.

[4] L.N.B. Gummadi, H.Cai, S.Lin, X.Fan and K.Cao, "Bushing characteristics of stabilizer bars", SAE-2003-01-0239.

[5] X.Fan, H.Cai, S.Lin, L.N.B.Gummadi and K.Cao, "Non-linear analysis of tunable compression bushing for stabilizer bars", SAE-2004-01-1548.

[6] Ernani S.Palma and Edvaldo S.dos Santos, "Cummulative fatigue damage in an automobile stabilizer bar: correlation between laboratory and road experiments", SAE-2001-01-3175.

[7] Nitin S. Gokhale, Sanjay Deshpande, Sanjeev V. Bedekar and Anand N. Thite, Practical Finite Analysis, Finite to Infinite, 2008

[8] Ian Czaja and Mohammad Hijawi, "Automotive stabilizer bar system design and reliability", SAE-2004-10-155.

◈◈◈

FEM Simulation of Crack Initiation and Propagation to Predict the Quality of Product in Blanking Process

O. M. Tavare & S. G. Joshi

Department of Mechanical Engineering, Rajarambapu Institute of Technology, Rajaramnagar, Islampur- 415 414 Maharashtra, India

Abstract - An approach to predict quality of the product in the sheet-metal blanking using a ductile fracture initiation criterion and numerical modeling for simulating automatic crack propagation are presented. The normalized Cockroft-Lathem ductile fracture criteria in mixed tension and sliding fracture mode and its relative accuracy for predicting and quantifying fracture initiation sites in conjunction with experiments and finite element method (FEM) are investigated. From the moment of crack initiation to the complete rupture of the sheet, a 2D remeshing procedure in problem specific FEM code combined to deletion-and-replacement method with the maximum circumferential stress criterion is used to predict the direction of crack advancement and updating the explicit geometric description of evolving cracks. In the investigation, the shearing mechanism was studied by simulating the blanking operation of a JIS 2550 steel sheet. The FEM results of the present paper are in good agreement with experimental results.

Keywords - *Blanking simulation; FEM; Crack growth simulation; Experimental validation; Quality prediction.*

I. INTRODUCTION

Sheet-metal working by material shearing mechanisms is one of the most frequently used processes in industry. Stamping is an important process in sheet metal work. The operations associated with the stamping are blanking, piercing, forming, and drawing. Depending on the position of the sheared surface with respect to the workpiece coordinates, various shearing processes such as blanking, piercing and cutting off are used. Contrary to other operations such as forming, drawing and, folding, where the aim is to plastically deform the sheet, blanking operations lead to the total rupture of the sheet.

Blanking is a constrained shearing operation that involves elastic deflection, plastic deformation and fracture of the work material. As the process is performing, the material whose behavior is non-linear is subjected to a complex state of stress and strain. Before the complete rupture occurs, the material is subjected to crack propagation and damage.

Nowadays, it is observed that product specifications are getting more severe, since the sizes of the high-tech products are becoming smaller and smaller. This can lead to lengthy trial and error procedures in developing industrial blanking applications and a proper model of the blanking process is desired. Because of the constantly changing loading situations in the material, the process is too complex for an analytical approach. Instead, the finite element method (FEM) has been used to simulate the blanking process, with varying success. It is possible to drastically reduce the lead time of new parts and products by proper implementation of a simulation technique into the product development and research.

In recent years, numerical simulations of the shearing process of sheet metals have been performed based on the finite element method (FEM) to reduce the time and cost for production and optimize the blanking processes [1]. However, there have been few numerical studies which deal with the mechanism of crack initiation and crack propagation or the formation of shear zone geometry characteristics during the blanking process of sheet metals. But, from a manufacturing point of view, the shear zone geometry characteristics are often the most important quality parameters. Furthermore, from a numerical point of view, a good description of the crack initiation and propagation requires the development of reliable algorithms and implementation, FE model. This is important because fracture initiation determines the shear zone geometry characteristics thus the product shape and final quality of product [2]. Fig.1 shows schematic of the shear zone geometry characteristics of a typical cut-profile of a blanked sheet.

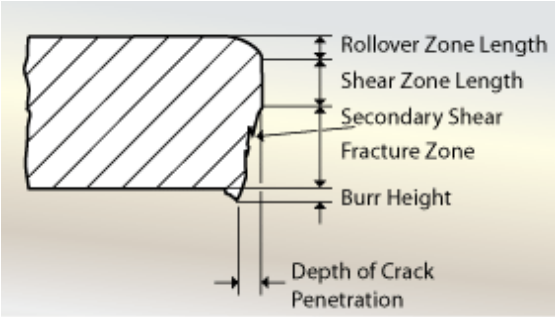

Fig. 1 : Schematic of shear zone geometry characteristics.

The objective of the present work is to evolve a methodology to predict the quality of the blanking product by the FEM simulation of crack initiation and propagation in the blanking process using problem specific commercial finite element code.

II. FEM SIMULATION FOR LARGE DEFORMATION

The blanking process is a classical elasto-plastic large deformation. The blanking process is divided into three phases with fundamentally different physical behavior and numerical treatment [2]. The first phase is elastic deformation. After contacting the sheet metal, the punch will compress the sheet and the sheet will undergo elastic compression and tensile and bending deformation. With the penetrating of the punch, the sheet material will reach the elastic limit and begin plastic deformation, which is the second phase. This phase begins when the stresses within the deformation zone increases until the yield limit of the material is reached. In this phase, the extruding depth of sheet increases gradually, whilst the tensile stress and bending moment in the material continue to increase. The material in the deforming section will suffer work hardening. The blanking force continues to increase until cracks occur in the sheet near to the cutting edges. When the cracks appear, this phase will be over and the third phase, namely fracture separation, will begin. The punch still continues to penetrate into sheet, and the cracks near to cutting edges of the punch and the die become larger and expand into the material. When the cracks at top and bottom meet and coincide, the sheet will be fractured.

Two challenges in the simulation of the blanking process are plastic deformation and ductile fracture separation of the sheet. The FEM simulation for large plastic deformation includes the elasto-plastic FEM and the rigid–plastic FEM. The elastic deformation in the blanking process is negligible. In this research, the simulation for the plastic deformation of the sheet is carried out by the rigid–plastic FEM. In the rigid–plastic FEM, the objects are treated as elastic objects until the yield point is reached. Then any portions of the objects that reach the yield point are treated as plastic, while the remainder of the object is treated as elastic. The material deforming plastically beyond the limiting strain rate of the objects is specified with a material flow stress [3].

Material and geometry non-linearity exist simultaneously in blanking simulation. From the viewpoint of numerical formulation for large deformation, the FEM may be divided into two major approaches: the Lagrangian approach and the Eulerian approach. In the Eulerian approach is more suitable for fluid-flow problems involving a control volume. The Lagrangian approach, on the other hand, a natural approach for solid-mechanics analysis, the FE mesh consists of material elements that cover the region of analysis exactly. Compared with the Eulerian approach, the Lagrangian approach is very attractive for blanking, where the boundaries of the workpiece are mostly traction-free, and the boundaries that are not free on the punch face are changing during the course of analysis.

III. DUCTILE FRACTURE MODELING

A. Ductile fracture initiation criterion

Ductile fracture in metals is caused by the growth and coalescence of voids [2]. These voids are holes in the material caused by dislocation pile-ups, second phase particles or other imperfections. Under the influence of plastic deformation, the voids can grow until a number of voids coalesce to initiate a crack. So far, the ductile fracture has been predicted by local failure criteria mainly. These criteria predict the onset of failure at a material point by studying the stress and strain history of this point. Various criteria have been evaluated by, for instance, Clift et al., Bolt, Gurson, Rice and Tracey, McClintock and Oyane et al. [2, 3]. However, it has been found that the criterion suggested by Cockroft and Latham [5] predicts the most reasonable fracture strain in metal forming processes.

B. Cockroft-Latham's Criterion

Crack initiation is a local phenomenon and in this methodology it is postulated that a crack is initiated at the point of the sheet whose effective strain first reaches the fracture strain of the work material. This criterion states that fracture takes place when the following relation is satisfied:

$$\int_0^{\varepsilon^{-f}} \sigma^* d\bar{\varepsilon} = C \qquad (1)$$

Where is the maximum principal tensile stress, ε^{-f} the fracture strain, and C the material constant. The effective stress and effective strain are represented by $\bar{\varepsilon}$and $\bar{\sigma}$ respectively. In the shearing operation, deformation is concentrated along the shear band the stress ratio ($\sigma^*/\bar{\sigma}$) is not expected to change along the shear band. Thus the equation is formulated as equation 2 and called as Normalized Cockroft-Latham's Criterion.

$$\int_0^{\varepsilon^{-f}} \left(\frac{\sigma^*}{\bar{\sigma}}\right) d\bar{\varepsilon} = C \qquad (2)$$

Therefore, Cockroft and Latham's criterion may be approximated by ε^{-f} = C* at the shear band. Consequently, it may be assumed that fracture takes

place at a given effective strain. During the blanking operation it is observed that when the punch penetrates the sheet, the metal lying between the edges of the punch and the die (shearing gap) deforms severely, and finally cracks are initiated.

IV. NUMERICAL SIMULATION

A. Geometry Model

The problem can be simulated as 2D or 3D depending on the computation time and accuracy required. In this work we have analyze it for 2D; considering it as a plane stress problem.

In all the case studies of this work, the blanked part to be analyzed for blanking is assumed to be axisymmetric for simplification. The 2D geometry representation is shown in Fig.2.

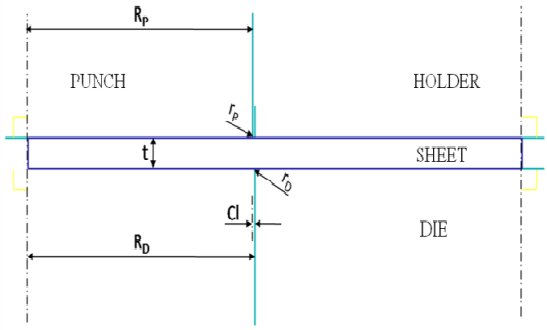

Fig. 2. Representation of type of geometry used in blanking simulation

In this simulation, a few assumptions are made for the analysis. The material of the sheet metal is considered as a plastic object, while the punch and die are defined as rigid bodies. The geometrical parameters of the die, the punch and the sheet are shown in Table 1.

TABLE I. DIMENSIONS CORRESPONDING TO MODEL IN FIGURE.2

t mm	Cl mm	R_P mm	R_D mm	r_P mm	r_D mm
1	0.1	10	10.1	0.05	0.05

B. Meshing

The adaptive remeshing strategy module is used in the FEM program as a solution to excessive element distortion problem in simulating forming process with free surfaces, using the common Lagrangian FEM. In adaptive remeshing frequent updating of the mesh is done, in which the element topology is changed and remeshed.

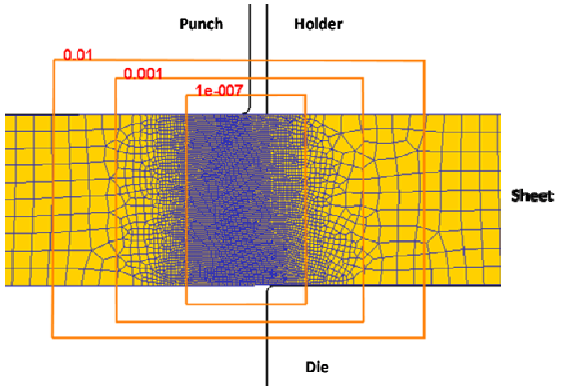

Fig. 3 : Different mesh densities in different zones of the sheet

The objects undergoing large plastic deformation will be remeshed when the mesh becomes unusable (negative Jacobian). During the simulation, if an object satisfies any of its remeshing criteria, a new mesh is generated, the solution information from the old mesh being interpolated onto the new mesh and the simulation then continuing. In the present simulation, the element meshes of the sheet consist of isoparametric quadratic elements.

In Fig.3, the density of the meshes near to the deformation zone is greater than that of other zones, for the material within the punch–die clearance suffers several shear deformation, whilst the material outside the region is almost unformed.

In automatic mesh generation, it is necessary to define mesh density windows (Fig.3), which specify some areas in space that will move with the punch. When a remeshing procedure begins, the system will discretize the sheet with these specific densities.

C. Boundary Conditions and Contact formulation

The Contact between tool and the blank is enforced by the kinematic contact condition, using pure master-slave surface pairs. The master and slave designation must be chosen so the rigid tools forms the master surface and the surfaces defined on the blank acts as the slave. The friction contact between sheet and tools follows Coulomb's law. The punch displacement of 1.25mm and punch velocity is applied as 1 mm/sec and the holder. The nodes at the symmetry line are locked in the radial direction by the displacement boundary condition when the axisymmetric definition is adopted, no material flow in the angular direction is presumed.

D. Crack Propagation Mechanism

To express described process of the crack propagation, it is common to adopt element-deletion and node-separated approach [3]. However, the shape of the

crack is largely affected by the size and shape of the mesh in these two techniques. The delete-and-fill remeshing method is adapted in this study to simulate the crack growth after its initiation. First, a group of mesh in the vicinity of the crack tip is deleted. Then, the crack is extended after the direction and length of the crack is calculated by FEM, the local domain is refilled with new elements for the new crack tip. There are three critical techniques in this approach: the crack growth criteria, the evaluation of fracture parameters and sewing between the new generated mesh and the remained ones. The fracture in blanking process is tension and shearing mixed mode fracture because large rotations of material elements in the narrow shear band between the punch and die.

In this study, maximum circumferential stress criterion based on stress intensity factors (SIFs) is adapted to the implementation of crack growth criteria and predict the direction of crack propagation. The crack propagates in the direction perpendicular to the maximum principal stress, and the stress intensity, energy release rates and crack tip opening angle are also calculated to evaluation of fracture parameters in the developed procedure.

To model the crack growth explicitly, the fine mesh in the vicinity of the crack tip and smooth transformation have to be carried out from the fineness near the tip to coarseness in remained mesh. As a consequence of the remeshing on the region around the discrete crack, the history dependent variables need to be mapped form the old mesh to the new mesh configuration. As stated above, the crack growth processes have been simulated by the presented fracture models without user intervention.

E. Material Data Model

In this work, a JIS 2550 steel sheet of 1mm thickness is used. The material data such as plastic data, elastic data and fracture data is specified in the problem specific FEM software simulation. To generate the necessary input data for the simulation tensile tests have been performed for the material. This data is provided to the FEM software to get flow stress data which will be used for the all the FE-model analysis. The flow stress equation for JIS 2550 used is given with a constitutional model as below:

(3)

where is the effective stress, the effective strain, effective strain rate and temperature T.

V. EXPERIMENTAL ANALYSIS AND VALIDATION

A. Correlation Technique

The comparison of the FEM results has been carried out to validate the results concerning the quality of the blanked component. The quality of blanked component is described by the edge profile and characteristics zones of cut edge.

To generate the necessary data for the validation of simulation results SEM (Scanning Electron Microscope) test has been performed on the blanked component generated from blanking process for stampings for an electric stator-rotor assembly.

B. Comparison of Experimental Vs. FEM Results

Fig.4 (a) shows experimental edge profile and Fig.4 (b) shows simulated edge profile. It is seen there is a fairly good agreement in the results of experimental and simulated edge profile.

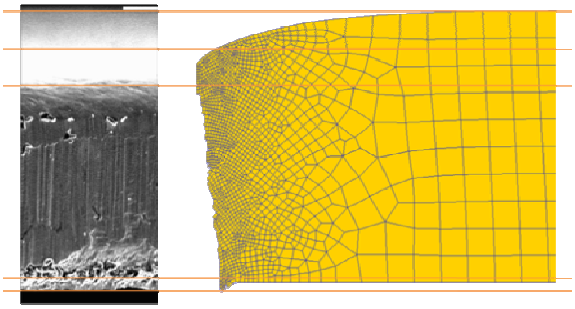

(a) (b)

Fig. 4 : Experimental and simulated edge profile comparison

It can be seen from the picture of the experimental edge profile that the rollover was over predicated in the simulations. When comparing the edge profiles the spatial orientation of zones differs as an effect of the larger rollover zone that was formed in experiments. The shorter rollover zone in simulations also causes a longer fracture zone than one being measured in the experiments. Although the rollover zone and fracture zone were slightly different from those of the experimental results, the FEM results show the potential of this method for simulating the shear surface and burr zone. The trends of experimental results and FEM simulation results are correctly predicted.

VI. SIMULATION RESULTS AND DISCUSSIONS

A. Crack Initiation and Propagation

Fig.5 shows material deformation, the crack initiation and propagation, and material fracture

separation in the blanking process with clearance of 0.1mm and corner radii of 0.05mm as per the guidelines of Pressmatic Electro Stampings Pvt. Ltd. It can be observed that the distortions of the meshes are restricted to a small area near to the punch–die clearance. It is generally believed that metal material can undergo a specified plastic deformation before fracture. In like manner, there are plastic deformations in the blanking process.

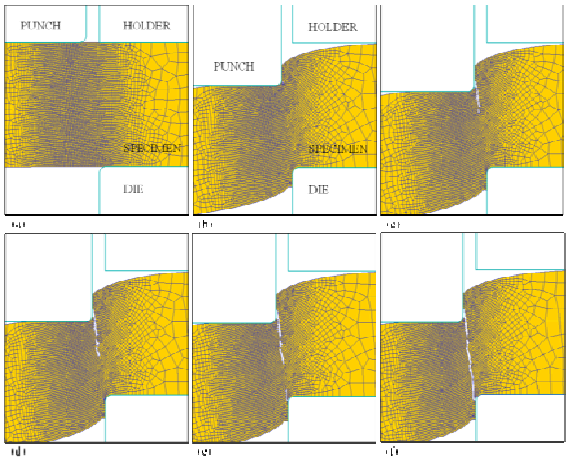

Fig. 5 : Crack initiation and propagation and material fracture separation in the blanking process (S denotes the percentage stroke of punch, t -thickness): S = 0%t; (B) S = 34.5% t; (C) S = 40% t; (D) S = 41% t; (E) S = 41.8% t; (F) S = 42.3% t

The fracture process can be seen in the simulation results. Initial condition is shown in Fig.5 (a). First, under the penetration of the punch and the constraint of the die and holder, plastic deformation occurs in sheet material. This plastic deformation and its speed of deformation decide the rollover zone. When punch penetration reaches 34.5% of sheet thickness, Fig.5 (b) shows first crack initiation is observed near the edge of the punch. The crack propagation is observed as the punch penetrates the sheet, Fig.5 (c) shows the crack propagation at 40% of punch penetration. Fig.5 (d) shows the crack initiation near the edge of the die, when the stroke of the punch approaches 41%. The crack propagation is observed as the punches penetrates the sheet at both punch and die side, Fig.5 (e) shows the crack propagation at 41.8% of punch penetration. As the crack propagation continues with punch penetration, cracks of the top and the bottom propagates and coincides and the workpiece separates as shown in Fig.5 (f) at 42.3% of punch penetration. The complete rupture is observed at approximately 43% of punch penetration. These simulation results about material fracture and separation are in good agreement with published experimental results [3-9].

It is indicated that the crack initiates at the cutting edges of the tools. The crack propagates in the direction of the punch penetration. Fig.6 shows the relative crack propagation (expressed in percent of sheet thickness) vs. the relative punch displacement.

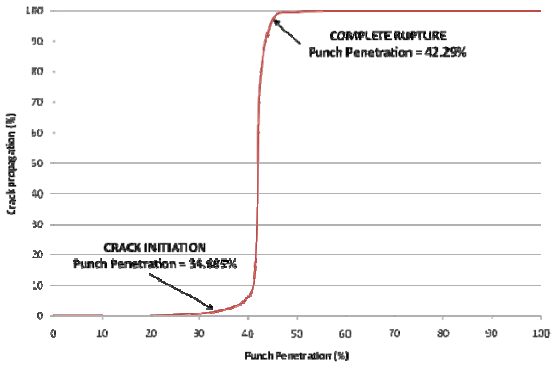

Fig. 6 : Crack propagation vs. punch penetration

B. Shape Defects On the Sheared Surface

The blanking clearance (BCl) can have a great influence upon the shape and dimensional precision of the workpiece. Five blanked profiles corresponding to different punch–die clearances are shown in Fig. 7. Fig.7-e and Fig.7-f show that in the case of a large clearance, the profile of the workpiece boundary causes a bad quality due to the presence of large rollover zone, increased depth of crack penetration and longer burrs. When the clearance is undersize (Fig.7-a, b), a secondary burnished zone will occur. These defects will decrease the precision of the shape and the dimension. A decrease in clearance can contribute to improve the precision of the workpiece.

But as BCl=10% and BCl=15% gives the good results. In Fig.7 it can be observed that the quality of sheared surfaces are good in all zones for BCl=10% (Fig.7-c) and BCl=15% (Fig.7-d).

C. Punch force Predictions

The It is observed that as clearance increases the maximum blanking load at punch also increases. From Fig.8, trend difference is observed at 0% and 15% of clearance. It is because; at the respective clearance the crack initiation is observed at the die edge instead of punch edge. Hence more punch force is required to move the sheet metal. It is observed that as clearance increases the punch penetration value for complete rupture also increases and for lower values of clearance the trends of blanking load curves are similar, however, for higher values of clearance the trend of the curves changes. For all curves, initially there is high increase in blanking load at punch without increase in punch stroke. This is because of elastic deformation of blank sheet. As the punch stoke increases, the blanking load at punch

increases to maximum value and further reduces drastically. This is because of the crack initiation phenomenon at the tool edges. This is analogous to the Stress-Strain curve for steel material.

It is observed that the blanking load at punch reduces without much change in punch stroke; this is due to crack propagation phenomenon.

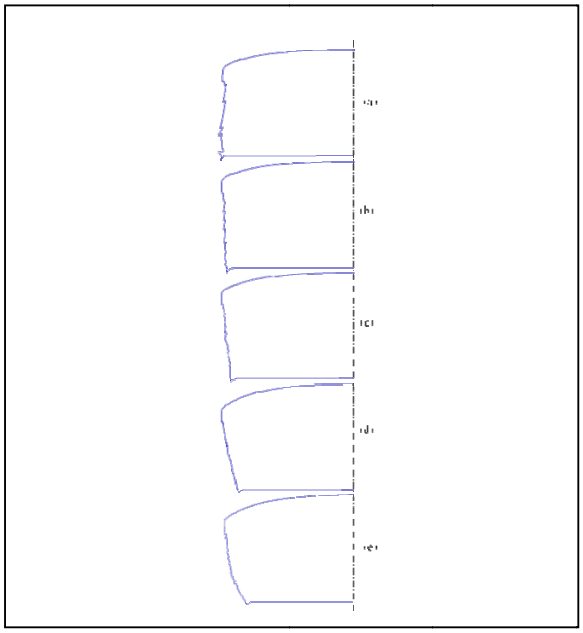

Fig. 7 : The simulated blanked profiles

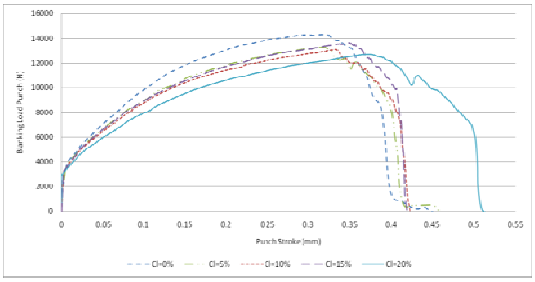

Fig. 8 : Simulated punch stroke–blanking load curves

D. Clearance variation

The It is observed that the clearance is a major process parameter which affects the quality of the blanked component the most.

Fig.9 shows the typical blanked profiles. In Type 1 (Clearance, 17-21%), it is observed that rollover zone, depth of crack penetration and Burr height are maximum. In Type 5 (Clearance, 1-2%), it is observed that rollover zone and depth of crack penetration are minimum. Multiple shear zones and fracture zones are also observed. The depth of crack penetration is negligible in case of Type 5.

In this paper the current industry practice of using 10% clearance as an optimal value for better quality of the blanked product is also confirmed with the FEM results.

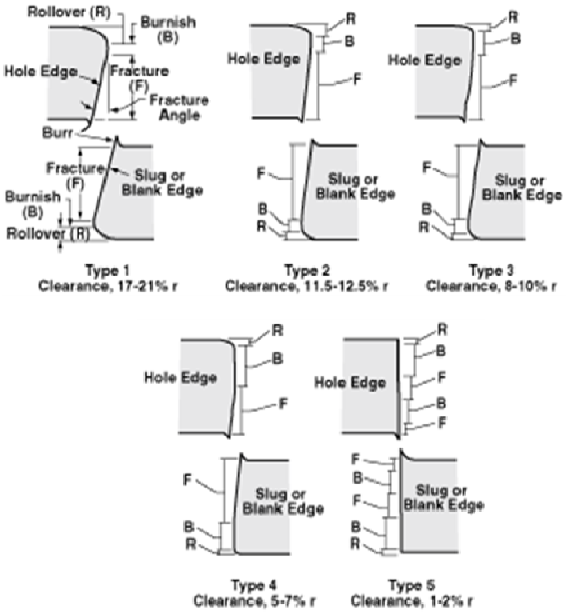

Fig. 9 : Influence of clearance on quality of the blanked component

VII.CONCLUSION

Blanking is one of the main sheet metal forming processes, so attention must be focused on its simulation. It has been shown that an FEM simulation of the process leads to an optimal choice of forming parameters. A large deformation FEM simulation has been conducted to study the blanking process. The Normalized Cockroft–Latham criterion for ductile fracture is a realistic and sufficient damage law used to simulate metal blanking. The crack initiation and propagation can accurately be predicted without computational divergence. From the moment of the crack initiation to the complete rupture of the sheet-part, experimental and numerical results are all in good agreement. It can be concluded that the quality of the blanked component can be controlled by initiating the crack from the die corner than from punch corner. As has been shown, the simulation of sheet blanking by a punch-die arrangement is a difficult problem due to the choice of realistic hypotheses, especially in accounting for damage, and to the complexity of numerical calculations involved in large displacements.

ACKNOWLEDGMENT

The authors would like to gratefully acknowledge the support of the Pressmatic Electro Stampings Pvt. Ltd., Karad.

REFERENCES

[1] D. Brokken, W.A.M. Brekelmans and F.P.T. Baaijens: "Numerical modelling of the metal blanking process", Journal of Materials Processing Technology 83 (1998), pp.192–199.

[2] Gang Fang, Pan Zeng and Lulian Lou: "Finite element simulation of the effect of clearance on the forming quality in the blanking process", Journal of Materials Processing Technology 122 (2002), pp.249–254.

[3] Song Yu, Xiaolong Xie, Jie Zhang and Zhen Zhao: "Ductile fracture modeling of initiation and propagation in sheet-metal blanking processes", Journal of Materials Processing Technology 187–188 (2007), pp. 169–172.

[4] Quang-Cherng Hsu: "Studies on the Punching Characteristics of Rigid Copper Clad Laminates", Journal of National Kaohsiung University of Applied Sciences, Vol. 33 (2004), pp. 31-40.

[5] A. M. Goijaerts, L. E. Govaert and F. P. T. Baaijens: "Prediction of Ductile Fracture in Metal Blanking", Journal of Manufacturing Science and Engineering, Vol. 122, AUGUST 2000.

◈◈◈

Optimization of Process Parameters for Compression Moulding of Glass Reinforced- Resin

Shraddha Deshpande & P. J. Pawar

K.K.W.I.E.E.R, Nashik, India

Abstract - This paper optimizes the compression moulding process for dimensional variations of glass reinforced resin using Taguchi method. Four controllable factors of the manufacturing process were studied at three levels each. The single response optimization of dimensional variation was conducted by Taguchi method. Controllable parameters are melting temperature, compression pressure, holding time and weight of the raw material. The dimensional variations are studied to predict the quality of product with regard to the thickness and centre distance of clamping holes. Results show that the 3000 bar compression pressure and 229 gms weight of the resin are significant variables for improvement in the thickness of the component, while 2500 bar compression pressure and 227 gms weight are significant for getting improved center distance.

Keywords - *compression-moulding; Taguchi method, glass reinforced resin.*

I. INTRODUCTION

Plastic products range from sophisticated products like prosthetic hip and knee joints to disposable food utensils. The tremendous range of properties exhibited by plastics and their easy of processing is one of the reasons for enormous popularity of plastics in wide variety of industrial applications. The compression moulding process is widely used to produce glass fiber reinforced thermoset composite parts. Using matched steel moulds and presses as large as 4,000-tons, processors use Sheet Molding Compound [SMC], Bulk Molding Compound [BMC], granulated compounds, with cure times typically ranging from 30-seconds to several minutes. The moulding of sheet moulding compound (SMC) has been used to produce automotive body panels and structural components. Applications vary across a broad range of industries, but automotive and electronics dominate when measured by volume. In today's global economy, thermoset processors are under constant pressure from shareholders and customers to reduce costs and improve quality. If the manufacturing process is not validated, it makes pile up rejected products. Some time it may happen that the product is very near to the quality norms but the consistency could not be maintained. The compression moulding process requires a dedicated press operator to place the raw material in the mould at a predefined location.

Process parameters such as weight, preheating temperature, melting temperature, breathing time, holding pressure, holding time, curing time and also post curing time and post curing temperature need to be optimized so as to produce a quality product. If weight is less then it will result in short filled component causing bad finish. If temperature of mold top and bottom is not maintained properly, if under heated low heating patches will be observed resulting in bad finish and if over heated bubble formation will start resulting in bad finish. Regarding breathing, gases releasing due to heating of the compound will get entrapped in the moulded component giving porosity, bad finish and lower strength. Every molded component is shaped under pressure. If pressure is less, it results in more height and more pressure may damage the mould. Plastic thermoplastic or thermosets need to be hold at particular pressure at constant temperature for particular time. In holding time, material flows in all directions in the mould. In case of curing or cooling time, compound gets cooled and thus hardens to its final shape. If curing time is not sufficient, warpage would be noticed in the component. If over cured, component will stick to the mould cavity making ejection difficult which causes warpage. Thus optimization of parameters is essential to get quality product at reasonable cost.

II. LITERATURE REVIEW

Moo-Sun Kim et al. [1] presented the study to optimize the precharge conditions such as the precharge location and dimensions that give significant effects on the mechanical performance of composite structures manufactured by the compression moulding process. As preliminary step of optimization, the author developed a manufacturing simulation program to predict the fiber volume fraction and fiber orientation. Coupled with this simulation program , a structural analysis program, a genetic algorithm (GA) is implemented to optimize the precharge conditions. The penalty function method and the repair algorithm are modified for handling constraints. The repair algorithm is applied to a symmetric structure and an arbitrary shape structure to find optimal precharge conditions. Mohd Zulkefli Selamat et al. [2] have presented the research on the

effect of compression molding parameters on conducting polymer composite (CPC) properties such as electrical conductivity and flexural strength. The Taguchi's L9 orthogonal array has been used as design of experiment (DOE) while the electrical conductivity and flexural strength were assumed to be quality characteristic (responses). The electrical conductivity was measured using four point probes and flexural strength was measured using three point tests according to ASTM D638. Author has investigated the significance of each compression molding parameters and finally proposes the optimum compression moulding parameters. But for several responses, the optimum condition for one response is not very likely to the optimum condition for other response. In the paper Chung-Feng et al [3] Taguchi method is applied along with Grey Relational Analysis to examine multiple quality optimization of the moulding of polyether Ether Ketone (PEEK). Taguhi method is applied to cut down on the number of experiments. The quality characteristics of this experiment were the screws' outer diameter, tensile strength and twisting strength. First the process parameters that may affect the injection moulding were determined. They were moulding temperature, re-plasticity amount, injection pressure, injection speed, screw speed, packing pressure, packing time and cooling time. Experiment was performed with a set up of an L18 (21 X 37) orthogonal array. Taguchi method was used for obtaining the optimum processing combination for a single quality characteristic only. For multiple quality characteristics and process parameter author had used Grey relational analysis. It was identified that the mould temperature is the most sensitive processing parameter. Ziegmann et al. [4] designed and fabricated a special mould. Author investigated the developing duration of micro scale weld line during injection moulding, the visualization unit was integrated in the tool. The optimal processing parameters and the significance order of processing parameters influencing weld line were obtained by Taguchi method. By confirmation experiments it was proved that prediction errors in the model were less than 21%. In the paper S.Kamaruddin et al. [5] presented a study in which an attempt is made to improve the quality characteristics of an injection moulding component by optimizing the injection moulding parameters using Taguchi method. The performance of the component is evaluated in terms of its shrinkage behavior. The analysis of the results shows that the optimal combination for low shrinkage are low melting temperature, high injection pressure, low holding pressure, long holding time and long cooling time.

III. METHODOLOGY

Taguchi's philosophy is an efficient tool for the design of high quality manufacturing system. Dr. Genichi Taguchi, a Japanese quality consultant, has developed a method based on orthogonal array experiments, which provide much reduced variance for the experiment with optimum setting of process control parameters. Its main trust is the use of parameter design that focuses on determining the parameter (factor) settings producing the best levels of a quality characteristic (performance measure) with minimum variation. It is a powerful tool for the design of high quality system. It provides a simple, efficient and systematic approach to optimize designs for performance, quality and cost. Taguchi parameter design can optimize the performance characteristics through the settings of design parameters and reduce the sensitivity of the system performance to sources of variation. The Taguchi method attempts to optimize a process or product design based upon three stages. Concept design, parameter design and tolerance design. In concept design, the technical knowledge and experiences are gathered. I parameter design, the best setting of the control factors is determined. The third step is exercised when improvements are required for the optimized design. This phase focuses on the trade off between quality and cost. It provides a powerful and efficient method for designing processes that operate consistently and optimally over variety of conditions. Depending upon the number of factors, interactions and their level, Taguchi method uses a special design of orthogonal arrays. The experimental results are transformed into signal-to-noise (S/N) ratio. Taguchi recommends the use of the S/N ratio to measure the quality characteristics deviating from the desired values. Usually there are three categories of quality characteristics deviating from the desired values. The lower the better, the higher the better and the nominal the better. The S/N ratio for each level of process parameter is computed based on S/N ratio analysis. A greater S/N ratio corresponds to the better quality characteristics.

IV. PARAMETER DESIGN BY TAGUCHI METHOD

Step (1): *Identification of quality characteristics*.

The component under study is transformer housing manufactured in SMC 405 material which is a long fiber glass reinforced resin. This component gets manufactured in two halves. In order to achieve correct dimensions inside the housing, thickness of the housing is important and to house the transformer correctly, clamping holes centre distance has to be perfect. Therefore the quality characteristics identified are thickness and centre distance. Fig 1 shows detailed drawing of the component. Ideal thickness required is 4.00 mm and ideal centre distance is 145.00 mm.

FIG 1: TRANSFORMER HOUSING

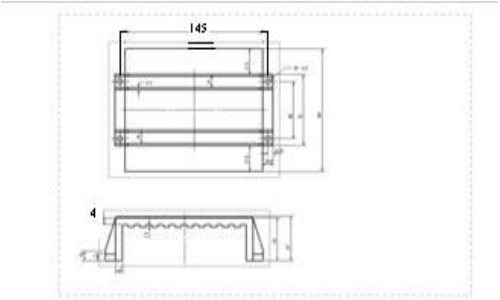

Step (2): *Selection of controllable process parameters and determination of the number of levels for the parameters.*

Four controllable parameters are selected. They are melting temperature, compression pressure, holding time and weight of the raw material. Melting temperature is the temperature which is conducted to the raw material by mould top and bottom. Thus this is temperature of the mould top and bottom. Compression pressure is the pressure which can shape the component. Holding time is the time which is required for the raw material to shape under required temperature and pressure and to get cooled at constant pressure for particular time. Weight defines strength, finish, homogeneity of the component. The feasible space for the moulding parameters was defined by varying the melting temperature in the range 140 to 160 ºC, holding pressure in the range 2000 to 3000 bar, holding time from 3.5 min to 4.5 min and weight from 227 to 229 grams. Most of the ranges were selected from the data available in the machine technical data book and moulding handbook. Three levels each of four factors were selected as shown in Table 1.

TABLE 1:PARAMETER SELECTION AND THEIR LEVELS

Symbol	Factor	Units	Level 1	Level 2	Level 3
A	Melting temperature	ºC	140	150	160
B	Holding pressure	Bar	2000	2500	3000
C	Holding time	Sec	3.5	4.0	4.5
D	Weight	grams	227	228	229

Step (3): *Selection of the appropriate orthogonal array and assignment of design parameters to the orthogonal array.*

The selection of appropriate orthogonal array (OA) depends on the total degree of freedom of the parameters. Degrees of freedom are the number of comparisons between process parameters that need to be made to determine which level is better and specify how much it is. Here since each parameter has three levels and the total degrees of freedom (DOF) for the parameters are equal to 7, computed as follows

DOF = (No. of levels-1) for each factor + (No. of levels -1) X (No. of levels – 1) for each interaction + 1

= (3-1) + (3-1) x (3-1) +1 = 7.

TABLE 2 : ORTHOGONAL ARRAY

Experiment No.	A	B	C	D	N I	N II
1	1	1	1	1	-----	------
2	1	2	2	2	-----	------
3	1	3	3	3	-----	------
4	1	1	2	3	-----	------
5	1	2	3	2	-----	------
6	1	3	1	1	-----	------
7	1	1	3	2	-----	------
8	1	2	1	1	-----	------
9	1	3	2	3	-----	------
10	2	1	1	1	-----	------
11	2	2	2	2	-----	------
12	2	3	3	3	-----	------
13	2	1	2	3	-----	------
14	2	2	3	2	-----	------
15	2	3	1	1	-----	------
16	2	1	3	2	-----	------
17	2	2	1	1	-----	------
18	2	3	2	3	-----	------
19	3	1	1	1	-----	------
20	3	2	2	2	-----	------
21	3	3	3	3	-----	------
22	3	1	2	3	-----	------
23	3	2	3	2	-----	------
24	3	3	1	1	-----	------
25	3	1	3	2	-----	------
26	3	2	1	1	-----	------
27	3	3	2	3	-----	------

Two types of OA can be selected, L9 and L27. For the purpose of conducting exhaustive and satisfactory trials, an Orthogonal array L27(3**4) is selected . The experimental layout for the compression moulding parameters using L27 OA is shown in Table 2. Each row of this table represents an experiment with different combination of parameters and their levels. The last two

columns of the OA are left empty for the error detection of experiment.

Step (4): *Conducting the experiments based on the arrangement of the orthogonal array.*

Transformer housings are produced on BEMCO make NM150/2 compression moulding machine as per the experimental plan shown in Table 2. Factor assignment to A, B, C and D are shown in Table 1. The compression moulding machine is shown in Fig 2. On the front side of the machine two heaters are seen for heating the mould bottom. On rear side there are two more heaters to heat mould top. There locations are predefined to balance the heat flow. Pressure gauge is seen which indicates selected pressure. Holding time is set on the timer and an electronic scale is used to weigh the SMC roll. The roll is placed at the predefined location.

FIG 2: COMPRESSION MOULDING MACHINE.

Immediately after manufacturing of each housing its thickness (dimension in Y-direction) and centre distance (dimension in X-direction) were measured with the help of Mitutoyo digital micrometer and Mitutoyo digital vernier (accuracy ±0.001mm) instrument. Reading is taken for dimensional variation in thickness and centre distance. From the above data the MSD (Mean square Division) can be computed which is the quality loss function. Depending upon the experimental objective, the quality function can be of three types. 1) Lower-the-better (LB), Higher-the-better (HB) and Nominal-the better (NB).

Quality loss values (MSD) is calculated as

$$MSD = 1/n\sum yi^2 \quad (\text{for } i= 1 \text{ to } n),$$

Where y_i is the observed data of quality characteristic at the ith trial and n is the number of repetitions at the same trial.

TABLE 3: EXPERIMENTAL RESULTS FOR THICKNESS AND CENTRE DISTANCE

A	B	C	D	Variation w.r.t. mean thickness	Variation w.r.t. mean centre distance
140	2000	3.5	227	0.0523	0.049
140	2000	3.5	227	0.0012	0.052
140	2000	3.5	227	-0.0.33	0.080
140	2500	4	228	0.1233	0.067
140	2500	4	228	0.0154	0.088
140	2500	4	228	-0.1012	0.058
140	3000	4.5	229	0.0689	0.049
140	3000	4.5	229	0.0499	0.084
140	3000	4.5	229	0.0121	0.100
150	2000	4	229	0.0956	0.062
150	2000	4	229	0.0499	0.075
150	2000	4	229	-0.0111	0.122
150	2500	4.5	227	0.0657	0.090
150	2500	4.5	227	0.0011	0.086
150	2500	4.5	227	-0.0965	0.099
150	3000	3.5	228	0.0822	0.152
150	3000	3.5	228	0.0368	0.121
150	3000	3.5	228	-0.0178	0.081
160	2000	4.5	228	0.0947	0.131
160	2000	4.5	228	0.0387	0.122
160	2000	4.5	228	0.0027	0.148
160	2500	3.5	229	0.1210	0.163
160	2500	3.5	229	0.0068	0.151
160	2500	3.5	229	-0.0011	0.149
160	3000	4	227	0.0510	0.166
160	3000	4	227	0.0011	0.097
160	3000	4	227	-0.0501	0.099

S/N ratio can be computed mathematically as,

$$\eta = -10 \log (MSD)$$

S/N ratio represents the desired part/undesired part. It is the quality characteristic for observed data. Aim of this experiment is to maximize the S/N ratio. From the S/N ratio, effective parameters having influence on process results can be seen and best set of process parameters can be determined. Computation and

prediction of results is done using MINITAB14 software. Table 3 shows the experimental results for thickness and centre distance and its variation with respect to the ideal size. Since the experimental design is orthogonal, it is possible to separate out the effect of each parameter at different levels. The signal to noise (S/N ratio) was used to measure the sensitivity of the quality characteristic being investigated.

Step (5): *Analysis of the experimental results using the S/N ratio.*

TABLE 4: EXPERIMENTAL RESULTS FOR THICKNESS AND CENTRE DISTANCE WITH S/N RATIO

A	B	C	D	SNRA1	SNRA2
140	2000	3.5	227	37.5872	78.5456
140	2000	3.5	227	*	*
140	2000	3.5	227	*	*
140	2500	4	228	31.0624	79.4841
140	2500	4	228	*	*
140	2500	4	228	*	*
140	3000	4.5	229	42.9133	74.9048
140	3000	4.5	229	*	*
140	3000	4.5	229	*	*
150	2000	4	229	37.5656	73.2485
150	2000	4	229	*	*
150	2000	4	229	*	*
150	2500	4.5	227	33.7797	86.7655
150	2500	4.5	227	*	*
150	2500	4.5	227	*	*
150	3000	3.5	228	38.1225	72.2067
150	3000	3.5	228	*	*
150	3000	3.5	228	*	*
160	2000	4.5	228	38.8161	80.8216
160	2000	4.5	228	*	*
160	2000	4.5	228	*	*
160	2500	3.5	229	35.4404	85.6525
160	2500	3.5	229	*	*
160	2500	3.5	229	*	*
160	3000	4	227	37.968	71.3528
160	3000	4	227	*	*
160	3000	4	227	*	*

In Taguchi method, the term signal represents the desirable effect (mean) for the output characteristic and the term noise represents the undesirable effect (signal disturbance S.D.) for the output characteristic which influence the outcome due to external factors namely noise factors.

V. ANALYSIS

Main effects plotted for dimensional variation in thickness are plotted for data means, standard deviation and S/N ratio Vs each factor are as follows.

FIG 3:: PLOT OF MEANS TO EACH PARAMETER

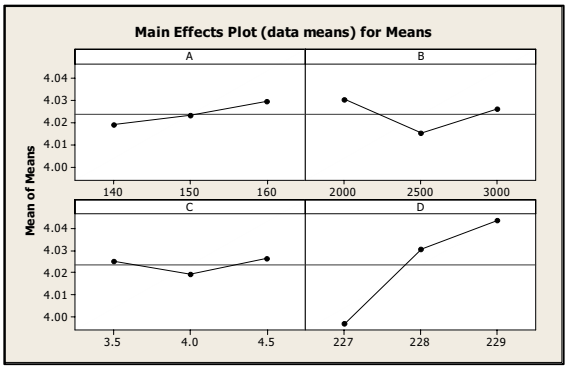

FIG 4: PLOT OF STANDARD DEVIATION

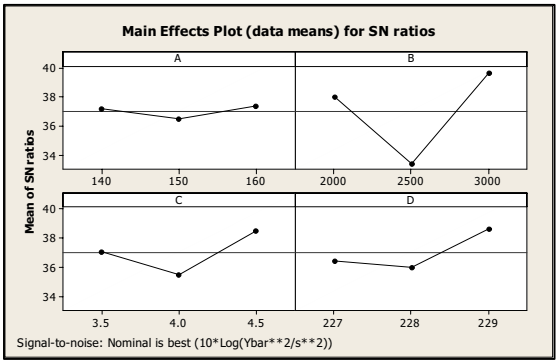

Similarly main effects plotted for dimensional variation in centre distance are plotted for data means, standard deviation and S/N ratio Vs each factor are as follows.

FIG. 6: PLOT OF MEANS TO EACH PARAMETER

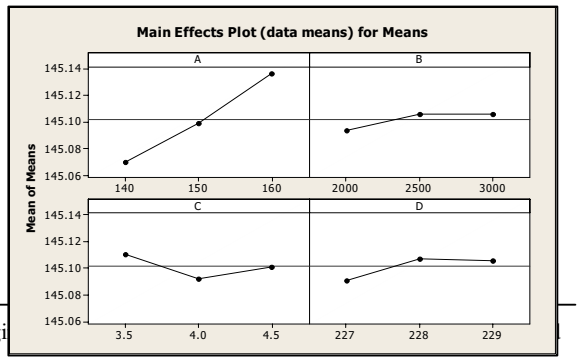

FIG 7: PLOT OF STANDARD DEVIATION

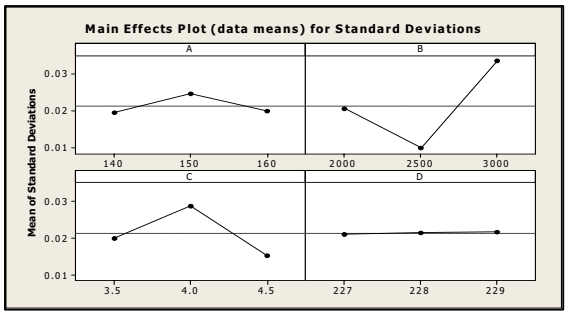

FIG 8: PLOT OF S/N RATIO TO EACH PARAMETER

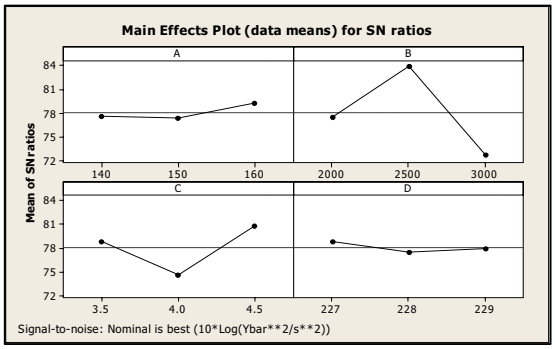

From above the graphs it can be found which parameter significantly affects the quality characteristic. We have mean of means, standard deviation and S/N ratio graphs. Thus it can be stated that the quality characteristic thickness can be best achieved at melting temperature 160ºC, compression pressure of 3000 bar, holding time 4.5 min and weight 229 grams. Thick can be justified practically by confirmation experiment. Thus for considered process variable, the level corresponding to the highest average S/N ratio is selected, irrespective of whether a LB or HB characteristic is involved. Hence best combinations of process variables are as shown in Table: 5 and Table 6. These are the optimal levels of all factors for achieving minimum variation in thickness and centre distance.

Step (6): *Selection of the optimal levels of design parameters*

TABLE 5: OPTIMAL LEVELS FOR THICKNESS

A	B	C	D
160	3000	4.5	229

TABLE 6: OPTIMAL LEVELS FOR CENTRE DISTANCE

A	B	C	D
160	2500	4.5	227

Step (7): *Verification of the optimal design parameters through the confirmation experiment.*

Confirmatory trial is performed with predicted optimal parameters and results are shown in Table 7.

TABLE 7: CONFIRMATORY TRIAL RESULTS.

Thickness	**Centre distance**
4.05	145.01

IV. RESULTS

From the analysis of the results in compression moulding of plastic component produced from SMC 405 20% glass using Taguchi method, results are shown in Table 8.

TABLE 8: RESPONSE TABLE

Response	**Parameters**			
	A	B	C	D
Height	160	3000	4.5	229
CD	A	B	C	D
	160	2500	4.5	227

V. CONCLUSION

From the analysis of the results in compression moulding of glass reinforced resins SMC 405 20% electric black, with respect to the factors which take into account the effects of the melting temperature, holding pressure, holding time and weight, using Taguchi method, the following can be concluded from the present study:

Optimal parameters for dimensional variation of thickness:

- The optimum conditions are A3, B3, C3, D3 i.e. melting temperature 160ºC, Compression pressure 3000 bar, holding time 4.5 min and weight 229 grams.

Optimal parameters for dimensional variation of centre distance:

- The optimum conditions are A3, B2, C3, D1 i.e. melting temperature 160ºC, Compression pressure 2500 bar, holding time 4.5 min and weight 227 grams.

Taguchi method works out to be simple and efficient tool for single objective optimization for compression moulding process.

REFERENCES:

[1] Moo-Sun Kim, Woo Il Lee , Woo-Suck Han , Alain Vautrin, 2011,"Optimization of location and dimension of SMC precharge in compression moulding process", Computers & Structures, 89,1523-1534.

[2] Mohd Zulkefli Selamat , Jaafar Sahari, Norhamidi Muhamad, Andanastuti Muchtar,., 2011, Key Engineering Materials Journal, Composite science and Technology, Volumes 471-472, 361-366.

[3] Chung Feng, Jeffrey Kuo and Te-Li Su., (2006), "Optimization of Multiple Quality Characteristics for Polyether Ether Ketone Injection Moulding Process" Fibres and Polymers Vol 7 404-413.

[4] Lei, Xie, Gehard, Ziegmann., 2009, "Influence of Processing parameters on micro injection moulded weld line mechanical properties of Polypropylene" Microsystems technology.Vol.15, 1427-1435.

[5] S.Kamaruddin,, Zhaid A.Khan and S.H.Foong., 2010, "Application of Taguchi Method in the Optimization of Injection Moulding parameter for Manufacturing products from Plastic Blend", IACSIT International Journal of Engineering and Technology, Vol.2.No.6, 574 – 580.

[6] P.K.Bharti, M.I.Khan., 2010, "Recent Methods for Optimization of Plastic Injection Moulding Process- A retrospective and Literature Review" International Journal of Engg , Science & Tech Vol 2(9),4540-4554.

[7] Avinash Kumar Dubey, Vinod Yadava, 2007, "Multi objective optimization of Nd:YAG laser cutting of nickel based superalloy sheet using orthogonal array with principal component analysis", Science Direct Optics and Laser Engg .Vol 46(20080124-132).

◈◈◈

Multi Objective Optimization of Machining Processes Using Non Dominated Sorting Genetic Algorithm

P.J. Pawar & Dhiraj Rai
Department of Production Engineering, KKWIEE&R, Nashik, India.

Abstract - Determination of machining parameters in any machining process is critical as it significantly affects the production rate, quality of product and cost of component. This paper presents a multi objective optimization technique known as non dominated sorting genetic algorithm (NSGA) and for the purpose of demonstration it is applied to optimize the cutting parameters of wire electro discharge machining process. In the proposed work NSGA is used to obtain non-dominated set and a pareto optimality front graph.

I. INTRODUCTION

The need of optimization of machining processes mainly arises due to the following reasons i.e. to increase the production rate, to increase material removal rate, to improve product quality, to reduce production cost, to reduce tool wear, to reduce operating and maintenance cost etc.

It is been seen that researchers have attempted optimization of process parameters of machining processes but have used single objective optimization technique.

However most of the real world problems involve multiple objectives which are even conflicting in nature the purpose may not be to find solution which better with respect to one objective but needs to compromise with other objective when rest of the objectives are also equally important. Such problems are termed as multiple conflicting objective problem. In case of such problems their may not exist one solution which is best with respect to all objectives.

Most of the machining processes to be optimized consist of multiple objective and it is difficult to find single optimum combination of parameters.

Researchers have also attempted multi objective optimization but by using the priori approach, wherein the process engineer needs to have a thorough knowledge of order of importance of the objectives prior to the optimization. And any change in order of importance requires the process engineer to recalculate the optimum solutions.

As the current market scenario is subjected to frequently changing customer demand the order of importance of objectives also changes frequently. Hence there is a need of optimization technique that is free from the above mentioned drawback. i.e. the posteriori approach.

The present study involves the application of a well known posteriori approach i.e. the non dominated sorting genetic algorithm (NSGA), for optimization of process parameters of non conventional machining process i.e. the Wire Electro Discharge machining for which optimum solutions are already been obtained but by using the priori approach.[1]

II. LITERATURE REVIEW.

Researchers have attempted optimization of various machining processes mostly non convention machining processes using priori as well as posteriori approach.

Rao and Pawar [1] made an attempt to optimize the process parameters of the Wire Electro discharge machining process using the artificial bee colony algorithm (ABC), with an objective to maximize cutting velocity and minimize surface roughness.

Sardinas et el. [2] have employed micro genetic algorithm to optimize process parameters of turning process, considering optimization of two conflicting objectives i.e. tool life and operation time to be optimized simultaneously

Satish Kumar et el [3] have applied non traditional optimization techniques such as ants colony optimization (ACO), simulated annealing (SA), genetic algorithm (GA) with a view to optimize the depth of cut in the multi pass turning operation and the results thus obtained are compared.

Kuraikose et el. [4] have applied NSGA to optimize the parameters of WEDM with an objective to improve cutting performance by maximizing cutting velocity and minimizing surface finish. They have applied a multiple regression model to represent relationship between input and output variables

Abburi et el. [5] proposed real parameter genetic algorithm (RGA) for the optimization of process

parameters of multi pass turning operation, with an objective to minimize production time and then used sequential quadratic programming (SQP) to further improve to obtained solutions.

Somashekhar et el [6] have made an attempt to optimize the process parameters of micro Electro discharge machining process. Artificial neural network were used to develop the parameter optimization model and then GA was applied to determine optimum process parameters.

Rao and Pawar .[7] have optimized process parameters of ultrasonic machining (USM). The objective considered is maximization of material removal rate (MRR) subjected to the constraint of surface roughness. The process variables considered for optimization are amplitude of ultrasonic vibration, frequency of ultrasonic vibration, mean diameter of abrasive particles, volumetric concentration of abrasive particles, and static feed force. The optimization is carried out using three nontraditional optimization algorithms, namely, artificial bee colony (ABC), harmony search (HS), and particle swarm optimization (PSO). The results of the presented algorithms were compared with the previously published results obtained by using genetic algorithm (GA)

III. NON DOMINATED SORTING GENETIC ALGORITHM

Genetic algorithm (GA) possesses advantages that it does not require any gradient information and inherent parallelism in searching the design space, thus making it a robust adaptive optimization technique . For multi-objective optimization methods, some modification to simple GA is necessary. Multi-Objective Genetic Algorithm (MOGA), Vector Evaluated Genetic Algorithm (VEGA) and Non-Dominated Sorting Genetic Algorithm (NSGA) are examples of GA based multi-objective solution methods. In present work NSGA is used to find a set of optimum values of the process parameters of a well known machining process. [8].

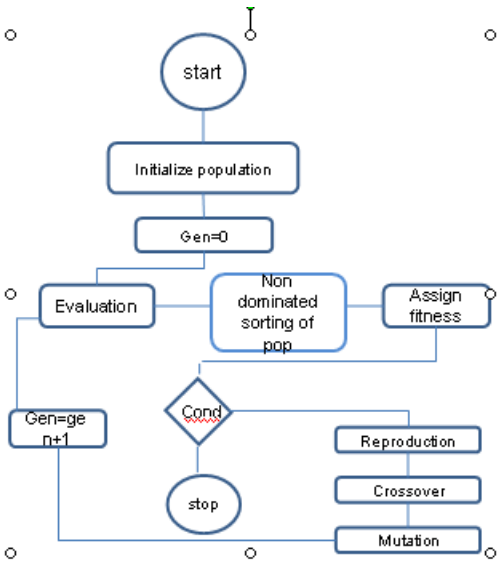

Figure I Steps in NSGA

Fig. 1 shows the details of NSGA. The crossover and mutation operators remain as usual, but selection operator works differently from simple GA. In NSGA, a shared fitness is used for selection. The shared fitness value is calculated based on a non-dominated sorting and ranking procedure that is briefly explained below. In first sorting, each chromosome is selected and checked whether this chromosome satisfies the rules given below with respect to any other chromosome in the population [4]

$$\text{Obj.1}[i] < \text{Obj.1}[j] \text{ and } \text{Obj.2}[i] > \text{obj.2}[j],\ i \neq j \quad (1)$$

If the rules are satisfied for any one of the remaining chromosomes, then the selected chromosome is marked as dominated. Otherwise, the selected chromosome is marked as non-dominated. All the non-dominated chromosomes in the first sorting are ranked 1. From the remaining dominated chromosomes from the first sorting, again chromosomes are sorted and the non dominated chromosomes in second sorting are ranked 2. This procedure is repeated until all the chromosomes are ranked. The subpopulation with rank 1, referred to as first front set, is assigned a dummy fitness value . Then, the normalized Euclidean distance of each chromosome is calculated with respect to all other chromosomes within this first front set using the formula [4]

$$dij = \sqrt{\sum \left(\frac{x_s^i - x_s^j}{x_s^{max} - x_s^{min}} \right)^2} \quad (2)$$

where, x_s the value of sth decision variable and i j are chromosome numbers. Then, the sharing function values (Sh(dij)) of all the first front chromosomes are calculated using following formula[4]

$$Sh(dij) = \begin{cases} 1 - \left(\frac{dij}{\sigma\ share}\right)^2, & \text{if } dij < \sigma\ share \\ 0, & \text{otherwise} \end{cases} \quad (3)$$

where σ share is the maximum distance allowed between any two chromosomes to become members of a niche. The σshare value in this equation is to be chosen appropriate. A niche count (nc_i) that provides an estimate of the extent of crowding near a chromosome is calculated using the equation[4]

$$nc_i = \sum_{i}^{N} sh(dij) \quad (4)$$

where, N is the total population.

The shared fitness values (F) are then calculated by dividing the dummy fitness values by the niche count, which is given by

$$\text{Actual fitness (F)} = \frac{\text{Dummy fitness (f)}}{(nci)} \quad (5)$$

After calculating the shared fitness values for the first front, a smaller value is subtracted from the minimum shared fitness value in this front and resultant value is given as the dummy fitness value (F2) for all the next front (rank 2) chromosomes and the steps are repeated. This procedure is continued till the shared fitness values are calculated for all fronts.

After calculating the shared fitness for all the chromosomes, a new mating pool is selected from among the given population based on the shared fitness using Roulette wheel selection . After selection, a randomly generation two-point crossover is adopted and a bit-wise mutation is performed subsequently.

In order to demonstrate the operation of NSGA multiple objective optimization of process parameter of a non conventional machining process that is W-EDM with an objective to maximize cutting velocity and minimize surface roughness is considered.

IV. APPLICATION PROBLEM.

Wire-electro discharge machining (Wire-EDM or WEDM) has become an important non-traditional machining process, widely used in the aerospace, nuclear and automotive industries, for machining difficult-to-machine materials (like titanium, nimonics, zirconium, etc.) with intricate shapes . The selection of optimum machine setting or cutting parameters in WEDM is an important step. Improperly selected parameters may impose certain limits on the cutting speed and thus reduce productivity. The process parameters considered are X_1 X_2 X_3 X_4 which correspond to pulse on time (P_{on}), Pulse off time (P_{off}), peak current (I_p), Servo feed setting (F) respectively.

A. Objectives

Obj.1 to maximize cutting velocity given by:

$$V_m = 1.555 + 0.1095X_1 - 0.187X_2 + 0.0929X_3 + 0.1279X_4 + 0.0393X_1X_2 - 0.0793X_1X_3 - 0.01188X_1X_4 - 0.01688X_2X_3 - 0.0793X_1X_3 - 0.01188X_1X_4 - 0.01688X_2X_3 - 0.0493X_2X_4 - 0.0606X_3X_4 - 0.03219X_1^2 + 0.02031X_2^2 - 0.0909X_3^2 - 0.06094X_4^2 \quad (6)$$

Obj.2 to minimize surface roughness given by:

$$R_a = 3.6+0.2979\ X_1 - 0.2979X_2 - 0.1479\ X_3 - 0.03542\ X_4 + 0.021875\ X_1X_2 - 0.2031X_1X_3 + 0.04062X_1X_4 + 0.01562\ X_2X_3 - 0.1531\ X_2X_4 - 0.1031\ X_3X_4 - 0.3182\ X_1^2 - 0.4057\ X_3^2 - 0.2682\ X_4^2 \quad (7)$$

The given relation are modeled using response surface methodology[1]

B. Variable bonds

$4 < P_{ON} < 8$

$10 < P_{OFF} < 30$

$90 < I_P < 140$

$30 < F < 50$.

Table 1 shows results of NSGA for the present optimization problem for 1st iteration. The population size must be greater than the chromosome length and in this work, a size of 25 is chosen. Taking first chromosome as an example, all the steps are discussed. To start with, Obj.1 (value of 1.48914) and Obj.2 (value of 2.813762) of first chromosome are compared with the corresponding objective function values of the second chromosome. The value of Obj.1 and Obj.2 of 1st is lesser than that of the 2nd chromosome .Therefore, it can be said that the first chromosome is non-dominating with respect to second one as Obj.1 is to be maximized however Obj.2 is to be minimized . The comparison is continued for all other chromosomes in the population and if the first chromosome is still non dominant, it is said to be non-dominated, all the solutions which are found to be non dominated in 1st sorting are given rank 1. Neglecting these chromosomes, again sorting is done

for the remaining chromosomes. This procedure is repeated till all 25 chromosomes are sorted and ranked. The ranking procedure emphasizes good solutions and increases the chance of selection of such chromosomes for the mating pool. Again taking the first chromosome as example, the distance of the first chromosome from all other chromosomes having rank 1 is calculated using Eq. (2). With these values, the sharing function values are obtained using Eq. (3). This requires an appropriate value of σ share to distribute the solutions over the search space. For this, a σshare value of 1.00 is taken. The sharing function value is 1.00 between the chromosome and itself. The niche count for the first chromosome is obtained as 1.877551. All chromosomes with rank 1 are given a dummy fitness value of 50. Based on Eq. (5), the shared fitness value of each chromosome in the first front (rank 1) is obtained by dividing the dummy fitness value by the niche count. The minimum of these shared fitness values is obtained for the first chromosome as 9.148027 (=17.175889/1.877551). Dummy fitness for the chromosomes in the second front is taken by subtracting a small value, say 0.2, from the minimum shared fitness value of the first front. This ensures that the chromosomes in the second front get shared fitness value less than those in the first front. Again, the procedure is repeated for all the fronts. The expected count *Ai* is obtained by dividing shared fitness value by the average of shared fitness values considering the entire population. Then the probability of selection *Bi* calculated by dividing *Ai* with total population (*N*= 25). Cumulative probability *Ci* is obtained by summing *Bi* and it will be 1 for the *N*th chromosome. For the first chromosome, a random number (*Di*) of 0.95 is generated and the mating chromosome is selected as 24, which has next upper bound cumulative probability of 1. Although all chromosomes of a particular rank have identical dummy fitness, shared fitness emphasizes less represented chromosomes and gives less emphasis for the crowded solutions. In the present work, single-point crossover is followed .This procedure was repeated 10 times to get more number of points in the Pareto-solution set. The non dominated solution set obtained over the entire optimization process is shown in Fig. 2. This shows the formation of the Pareto front leading to the final set of solutions. The corresponding objective function values and its decision variables of this non-dominated solution set are given in Table 2. Since none of the solutions in the non-dominated set is absolutely better than any other, any one of them is an acceptable solution. The choice of one of solution over the other depends on the requirement of the process engineer. If he requires a better surface finish or a higher production rate, a suitable combination of variables can be selected from Table 2.

Sorting and Ranking

Sr no	Chromosome	Obj.1	Obj.2	Rank (k)
0	1 1 0 1 1 0 1 1 0 1 0 0	1.48914	2.813762	2
1	1 0 1 1 0 0 1 0 0 1 1 1	1.62451	3.255904	5
2	1 1 0 1 0 0 0 0 0 1 1 0	1.56222	3.403993	7
3	1 0 0 1 0 1 0 1 0 1 0 1	1.49239	3.367104	7
4	0 0 0 1 0 1 1 0 0 0 0 0	1.17083	2.665674	3
5	0 0 0 1 0 1 0 0 0 1 1 1	1.1825	2.00258	2
6	0 0 0 0 0 0 0 0 0 1 0 1	1.47575	2.505645	1
7	0 1 1 0 0 1 0 0 1 0 0 0	1.28817	3.047653	5
8	1 0 0 0 1 1 0 0 1 0 1 1	1.46349	3.576489	8
9	1 0 0 1 1 1 1 0 1 0 1 0	1.38692	2.864929	3
10	0 0 0 1 0 0 0 1 0 0 0 0	1.07229	2.616844	3
11	1 1 1 0 1 1 1 1 0 1 1 0	1.64478	2.981963	4
12	1 0 0 0 0 1 1 1 0 0 0 1	1.61494	3.169864	5
13	0 0 1 0 1 1 0 1 0 1 1 0	1.49959	3.053862	5
14	1 0 1 0 1 1 1 0 1 0 1 1	1.61424	3.5268	6
15	0 0 1 0 0 1 1 1 0 1 1 1	1.76077	2.74068	1
16	1 1 1 1 1 1 1 1 0 0 1 0	1.43496	2.522114	2
17	1 1 0 0 0 1 1 1 1 0 1 0	1.6466	2.898803	3
18	1 0 1 1 0 0 1 1 0 1 0 0	1.57522	3.225336	6
19	1 0 1 1 0 0 1 1 0 1 0 0	1.41039	2.452391	1
20	0 0 1 1 0 0 1 1 1 1 0 0	1.49486	2.73348	1
21	1 1 0 0 0 0 0 1 0 0 0 1	1.58641	3.336571	6
22	0 0 0 0 0 1 1 1 0 1 0 0	1.68812	2.831311	2
23	1 1 1 0 1 1 0 0 0 0 0 1	1.38463	3.329078	7
24	1 1 0 1 1 1 1 1 1 1 1 0	1.38235	1.98	1

TABLE I SORTING AND RANKING

V. RESULT.

Results obtained after 10 iterations are as follows

Sr no	Vm (mm/min)	Ra (µm)	Pon (µs)	Poff (µs)	Ip (A)	F
1	1.33029	1.811245	5.142858	30	132.8572	50
2	1.35592	1.862695	8	30	140	50
3	1.555047	2.111684	4	18.57143	140	50
4	1.567261	2.251631	4	18.57143	132.8572	47.1
5	1.580627	2.452365	11.22049	18.57143	140	47.1
6	1.592595	2.636257	7.428572	18.57143	140	50
7	1.618747	2.954127	5.142858	18.57143	118.5714	50
8	1.732127	3.318436	4	12.85714	140	50
9	1.811254	3.58124	6.285714	12.85714	104.2857	50

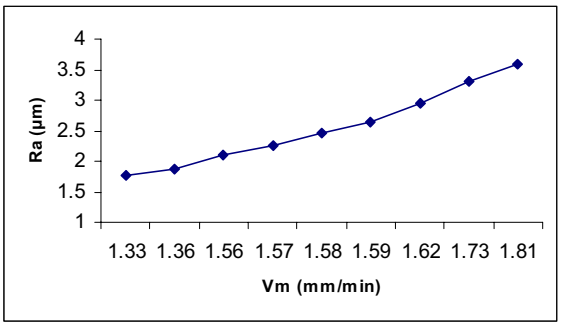

Figure II Non dominated front

Table 2 gives the optimum values of process parameters along with the values of cutting velocity and its corresponding surface roughness.

E.g. If the process Engineer desires to achieve a cutting velocity close to 1.5 then the corresponding values of surface roughness i.e. 2.111684 can be easily determined from table 2 and also the values of the process parameters.

VI CONCLUSION.

Determination of optimum process parameters of machining process greatly influence production rate production cost and quality of the product.

Conventional priori approach if used for multiobjective optimization are not suitable in case of current market scenario which subjected to frequent change in customer demand.

This paper NSGA is applied to the W-EDM process with multiple conflicting objectives i.e. maximizing cutting velocity and minimizing surface roughness.

It can be seen for the results obtained that based on the process plan the process planner can select the optimum combination of process parameters so as to achieve the desired value of surface roughness and cutting speed.

All the points that fall on the curve shown in the fig are regarded as optimum solutions.

The computational experience conducted in this work indicates that the proposed method i.e. non dominated sorting genetic algorithm is effective in optimization of Wire Electro Discharge machining process.

REFERENCES

[1] R V Rao and P J Pawar, Modeling and optimization of WEDM using Artificial Bee colony Algorithm, Proc IMechE, Part B: Journal of Engineering Manufacture November 1, 2009 vol. 223 no. 11 1431-1440

[2] Ramon Quiza Sardinas, Marcelino Rivas Santana, Eleno Alfonso Brindis, 'Genetic algorithm-based multi-objective optimization of cutting parameters in turning processes', Engineering Applications of Artificial Intelligence vol 19 (2006) pg 127–133.

[3] S. Satishkumar · P. Asokan · S. Kumanan, 'Optimization of depth of cut in multi-pass turning using nontraditional optimization techniques' Int J Adv Manuf Technol (2006) vol 29: pg 230–238

[4] Shajan Kuriakose et el, 'Multi objective optimization of W-EDM process by NSGA.' Journal of Materials Processing Technology vol 170 (2005) 133–141

N. R. Abburi . U. S. Dixit, 'Multi-objective optimization of multipass turning processes', Int J Adv Manuf Technol (2007), vol 32: pg 902–910

K. P. Somashekhar, N. Ramachandran, and Jose Mathew, 'Optimization of Material Removal Rate in Micro-EDM Using Artificial Neural Network and Genetic Algorithms', Materials and Manufacturing Processes, 25: 467–475, 2010. Article in a conference proceedings:

[5] R V Rao and P J Pawar,'Parameter Optimization of Ultrasonic Machining Process Using Nontraditional Optimization Algorithms', Materials and Manufacturing Processes Volume 25, Issue 10, 2010, pg 1120-1130.

[6] Kalayanmoy Deb, 'Multi objective optimization using evolutionary algorithms', Wiley India Edition, (2005).

◈◈◈

Heat Transfer Analysis of a Counter Flow Concentric Tube Heat Exchanger with Different Tube Inserts

Pankaj P. Kamaliya, Dattatraya G. Subhedar & Kamlesh V. Chauhan

C.M. Department of Mechanical Engg., Charotar University of Science and Technology, Anand, India

Abstract - In any type of the heat exchanger, the overall heat transfer coefficient (U) play very important role.The value of U depends upon the flow rate; properties of the fluid, material used thermal conductivity (K) and its thickness, heat surface condition and geometic configration of the heat exchanger.I have studied the heat transnfer analysis of concentic tube heat exchanger on the basis of the different flow property and geometric property. In which I have included longitudinal strip inserts with/without holes and twisted-tape inserts with three different twist angles (α=14.67°,25.23° and 33.94°) have been investigated for different inlet frontal velocity of hot fluid 0.3684,3,5,10,15,20,25m/s. Conjugate convective heat transfer in the flow field and heat conduction in the tube inserts are considered. To study the effect of the various inserts and the flow properties on the overall heat transfer I have done the simulation on Fluent (Ansys-12). To validate the simulation result I have performed the experiment on concentric pipe heat exchanger without insert with inlet velocity of hot fluid 0.3684m/s. It is found that the Simulation results are approximately matching with the experimental results. Also it is found that the overall heat transfer coefficient and effectiveness of heat exchanger can be increased by using inserts. We found maximum effectiveness by using twist insert (α =33.94°) than the higher than for all other inserts used.

Keywords - *Heat Transfer, Heat Exchanger, Plane Inserts, Twist Inserts, Overall Heat Transfer Coefficient, Effectiveness.*

I. INTRODUCTION

Effective utilization of available energy becomes need of hour today. This obviously requires effective devising. When it concerns with heat energy the devices are heat exchangers. Heat exchangers are used in variety of applications. Some of the applications of heat exchangers are-in process industries, thermal Power plants, air-conditioning equipments, refrigerators, radiators for space vehicles, automobiles etc. Increase in Heat exchanger performance can lead to more economical design of heat exchanger which can help to make energy, material & cost savings related to a heat exchange process.

The need to increase the thermal performance of heat exchangers, thereby effecting energy, material & cost savings have led to development & use of many techniques termed as Heat transfer Augmentation. Augmentation techniques increase convective heat transfer by reducing the thermal resistance in a heat exchanger. These techniques broadly divided in two groups viz. passive, and active. Active techniques involves some external power input for the enhancement of heat transfer, some examples of active techniques include induced pulsation by cams and reciprocating plungers, the use of a magnetic field to disturb the seeded light particles in a flowing stream, etc Passive techniques generally use surface or geometrical modifications to the flow channel by incorporating inserts or additional devices, for example, use of inserts, use of rough surfaces etc.

II. LITERATURE REVIEW

Ta-Sung Huang, Pai-Hsiang Wang, Yu-Wei Chiu and Jiin-Yuh Jang [1]. Discussed for different kinds of tube inserts, including longitudinal strip inserts with/without holes and twisted-tape inserts with three different twist angles (α=15.3°, 24.4° and 34.3°).The numerical results of heat transfer coefficient for strip inserts without/with holes and twisted-tape inserts agreed with the experimental data within 4.1%, 4.5% and 8.5%, respectively. S. S. Joshi, V.M.Kriplani [2]. In this Study the overall performance of suitably designed concentric tube heat exchanger is analyzed with passive heat transfer augmentation technique.In which different types of twisted tapes with different twist ratios are used. Find the effect of inserts on effectiveness of heat exchanger is analyzed for different Reynold Numbers. Simultaneously the friction factors for both inner and annular flow are analyzed. Anil Singh Yadav[3].Influences of the half length twisted tape insertion on heat transfer and pressure drop characteristics in a U-bend double pipe heat exchanger have been studied experimentally. The heat transfer coefficient is found to increase by 40% with half-length twisted tape inserts when compared with plain heat exchanger. V. N. Kapatkar, Dr. A. S. Padalkar and Sanjay Kasbe [4].An experimental investigation of heat transfer and friction factor of a smooth tube fitted with full length twisted tape inserts for laminar flow have been studied under uniformwall heat flux condition. The tapes have twist ratios from 5.2 to 3.4. The isothermal

frictionfactor for the flow with the twisted tape inserts are 340% to750 % higher as compared with those of smooth tube flow, in the given range of twist ratios. Smith Eiamsa-ard, Chinaruk Thianpong and Pongjet Promvonge [5].In the present study, a twisted-tape was inserted into the inner tube with various free spacingtwisted-tapes: *s = 2P, 3P,* and *4P,* respectively. It is show that the free spacing twisted-tapes, *s = 2P* gives the heat transfer lower than full length twisted tape around 5-15% while it can be decreased the pressure drop around 90%. Watcharin Noothong, Smith Eiamsa-ard and Pongjet Promvonge[6]In the experiments, the swirling flow was introduced by using twisted tape placed inside the inner test tube of the heat exchanger with different twist ratios, y = 5.0 and 7.0. The maximum Nusselt numbers for using the enhancement devices with y = 5.0 and 7.0 are 188% and159%, respectively, higher than that for the plain tube. In addition, the effects of the twisted tape on the heat transfer enhancement efficiency are also investigated.

III. EXPERIMENTAL SETUP

Figure1. Show a schematic view of experimental setup of concentric tube heat exchanger. The apparatus consists of tube in tube type (concentric) heat exchanger with effective heat transfer length of 1.5 m. The hot fluid (hot water) obtained from an electric geyser flows through inner copper tube while the cold fluid (cold water) flows through the annulus between mild steel outer tube and copper inner tube.

The direction of flow of cold water can be altered (Counter/ Co-current flow) using the valves provided. If valve no. 1 and 3 are open while valve no. 2 and 4 are closed the unit operate as counter current flow double pipe heat exchanger and if valve no 2 and 4 are open while valve no. 1 and 3 are closed the unit operates as co-current double pipe heat exchanger.

Inner Tube:

Material of Construction	: Copper
Inner Diameter (d_i)	: 15 mm
Outer Diameter ($d_{o)}$	: 18 mm
Effective Length (L)	: 1500x2 = 3000 mm
Mass Flow Rate	: 0.5 – 5 LPM

Outer Tube:

Material of Construction	: Mild Steel
Inner Diameter (D_i)	: 28 mm
Outer Diameter (D_o)	: 32 mm
Effective Length (L)	: 1500x2 = 3000 mm
Mass Flow Rate	: 0.5 – 5 LPM

The inlet and outlet temperatures of both the cold as well as hot water are measured by mercury in glass thermometers (0-110 °C) and flow rates by rota-meters (1-10 LPM, Fitzer make). Temperature and flow readings are recorded after the steady state is reached. The outer tube is provided with thermal insulation to protect heat transfer to the surroundings.

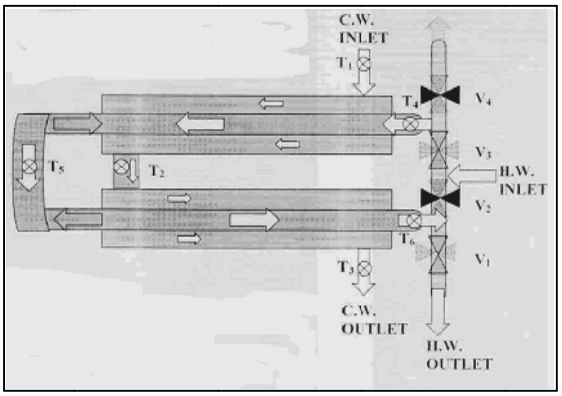

Fig. 1: Concentric Tube Heat Exchanger Setup

IV. EXPERIMENTAL PROCEDURE

Place the thermometers in their respective positions and note down their readings when the equipments is at room temperature and no water is flowing in either side. This is required to correct the temperature measuring error. Start and set the flow of water on hot water side using the rotameter.After ascertaining constant flow of water from the exit end, switch ON the geyser. Start and set the flow of water on cold-water side using the rotameter. By operating the valves 1, 2, 3 and 4 as instructed to make the unit operate as either co-current or counter current heat exchanger. Keeping the flow rates same, wait till the steady state conditions are reached. Record the flow rates and temperatures at all the four places. Repeat the above, with the same value of flow rates and inlet temperature of hot water in another mode (counter/ Co-current flow). Repeat the above experiment with different values of flow rates and temperatures.

We done the experiment on concentric tube heat exchanger with input parameter are mass flow rate both inner tube and outer tube is 4 LPM and the tempratute of inlet water in inner tube is 65.1 °C and the tempratute of inlet water in outer tube is 32.9 °C. Show in table I.we find the following outlet temprature in inner tube and outer tube.

TABLE I. OBSERVATION TABLE

Sr.	Hot Water Side	Cold Water Side

No	*Flow Rate m_h LPM*	*T_{hi} (℃)*	*T_{ho} (℃)*	*Flow Rate M_c LPM*	*T_{ci} (℃)*	*T_{co} (℃)*
1	4	65.1	55.8	4	32.9	41.2

V. MODELS OF INSERTS

To study the effect of flow pattern we are using different inserts in hot fluid tube (inner tube). We have used following inserts for simulation:

1. Flat Plane insert having width (w) 12 mm and thickness (t) 1mm as shown in fig.2
2. Perforated Flat plane insert with width (w) 12 mm and thickness (t) 1mm and pitch of hole (p) 25mm and hole diameter (d) 6mm as shown in fig.3
3. Twist insert with width (w) 12 mm and thickness (t) 1mm and angle of the twist (α) 14.67° and pitch of twist (p) 90 mm as shown in fig.4
4. Twist insert with width (w) 12 mm and thickness (t) 1mm and angle of the twist (α) 25.23° and pitch of twist (p) 50 mm as shown in fig.5
5. Twist insert with width (w) 12 mm and thickness (t) 1mm and angle of the twist (α) 33.94° and pitch of twist (p) 35 mm as shown in fig.6

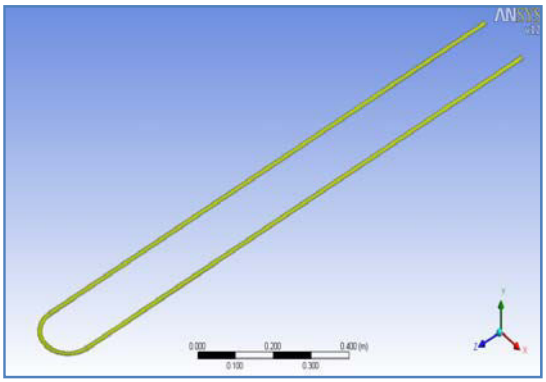

Fig. 2 : Model of Flat Plane Insert

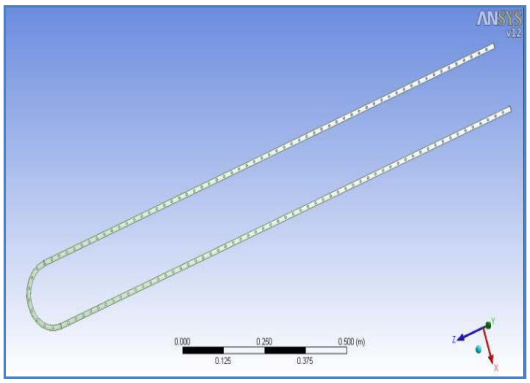

Fig. 3 : Model of Flat Plane Insert With Hole

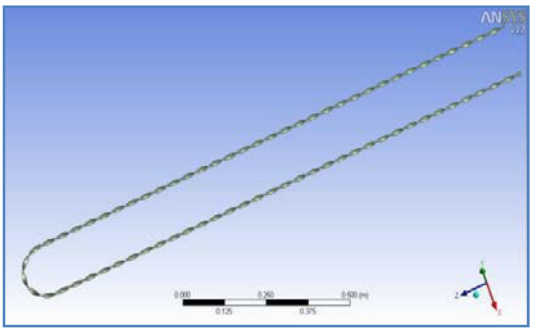

Fig. 4 : Model of Twist Insert (α = 14.67°)

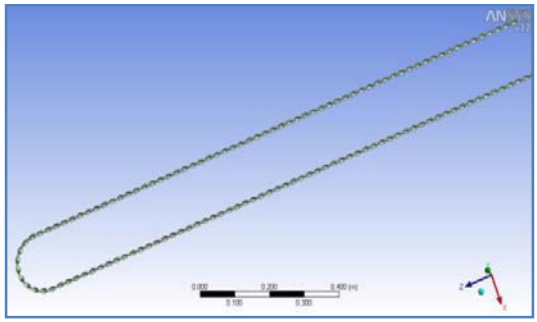

Fig. 5 : Model of Twist Insert (α = 25.23°)

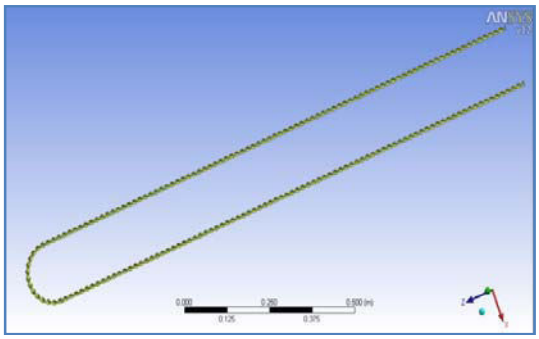

Fig. 6 : Model of Twist Insert (α = 33.94°)

VI. DATA REDUCTION EQUATION

The data reduction of the measured result is summarized in the following procedures.

For fluid flows in a concentric tube heat exchanger, the heat transfer rate of the hot fluid (water) in the inner tube can be expressed as:

Q_h = Rate of Heat Transfer from Hot Water

$$= m_h * C_{ph} * (T_{hi} - T_{ho}) \quad (1)$$

Where m_h is the mass flow rate of hot water, C_{ph} is the specific heat of hot water, T_{hi} and T_{ho} are the inlet and outlet hot water temperatures, respectively.

While the heat transfer rate of the cold fluid (water) in the annulus is

Q_c = Rate of Heat Transfer from Cold Water

$$= m_c * C_{pc} * (T_{co} - T_{ci}) \quad (2)$$

Where m_c is the mass flow rate of cold water, C_{pc} is the specific heat of cold water, T_{ci} and T_{co} are the inlet and outlet cold water temperatures, respectively.

Logarithm Means Temperature Difference for counter flow heat exchanger as

$$LMTD = \frac{\Delta T1 - \Delta T2}{\ln \frac{\Delta T1}{\Delta T2}} \quad (3)$$

$$\Delta T_1 = (T_{hi} - T_{co}) \quad \Delta T_2 = (T_{ho} - T_{ci}) \quad (4)$$

The overall heat transfer coefficient can be calculated using,

A. Practical

For Inner tube side

$$U_{overall} = Q/(Ai * LMTD) \quad (5)$$

For Outer tube side

$$U_{overall} = Q/ (Ao * LMTD) \quad (6)$$

B. Theoretical

For Inner tube side

$$Uoverall = \frac{1}{\frac{1}{hi} + \frac{di}{2k} In\left(\frac{do}{di}\right) + \left(\frac{di}{do}\right)\frac{1}{ho}} \quad (7)$$

For Outer tube side

$$Uoverall = \frac{1}{\frac{1}{ho} + \frac{do}{2k} In\left(\frac{do}{di}\right) + \left(\frac{do}{di}\right)\frac{1}{hi}} \quad (8)$$

Where, h_i Heat transfer coefficient for inner tube flow,

h_o Heat transfer coefficient for outer tube flow,

k Thermal Conductivity of inner tube material,

Heat transfer coefficient on hot water side (h_i) can be calculated from

$$(N_u)_{di} = 0.027* (Re)^{0.8} (Pr)^{0.333}*(\mu_m/\mu_w)^{0.14} [7] \quad (9)$$

$$h_i = (N_u)_{di} *k / d_i \quad (10)$$

Where, Nu Nusselt number

Re Reynold number

Pr Predalt number

μ_m Dynamic viscosity at mean temprature T_m

μ_w Dynamic viscosity at wall tempratureT$_w$

Heat transfer coefficient on cold fluid (water) side (h_o) can be calculated from

$$(N_u)_{De} = 0.027* (Re)^{0.8} (Pr)^{0.333}*(\mu_m/\mu_w)^{0.14} \quad (11)$$

$$h_o = (N_u)_{De} *k / De \quad (12)$$

Where, D_e = Equivalent diameter of Annulus = (Di – do).

The Effectiveness of heat exchanger can be calculated using NTU method.

$$\epsilon = \frac{\text{Actual heat transfer}}{\text{Maximum possible heat transfer}}$$

$$\epsilon = \frac{1 - (e)^{-NTU\,(1-R)}}{1 + R(e)^{-NTU\,(1-R)}}, \quad R < 1 \quad (13)$$

Number of Transfer Unit = NTU = UA/ C_{min} (14)

Where, U= Overall heat transfer coefficient,

A= heat transfer surface area,

R= C_{min} / C_{max}

VII.RESULT AND DISCUSSION

To study the effect of the various inserts and the flow properties on the overall heat transfer and Effectivness of heat exchanger. I have done the simulation on ANSYS-12 Fluent. To validate the simulation result I have performed the experiment on concentric pipe heat exchanger without insert with inlet velocity of hot fluid 0.3684m/s.

A. Validation of simulation of Heat analysis of concentric tube Heat exchanger

TABLE II : OBSERVATION TABLE FROM EXPERIMENT AND SIMULATION FOR WITHOUT INSERT

	T_{hi} °C	T_{ho} °C	T_{ci} °C	T_{co} °C	T_{ha} °C	T_{ca} °C
Experimental result without insert	65.1	55.8	32.9	41.2	60.4	37.0
Simulation result without insert	65.1	54.3	32.9	42.8	59.7	37.8

TABLE III: CALCULATIONS FOR WITHOUT INSERT

Inner Side Overall Heat Transfer coefficient

	Pr	Re	Nu	h_i W/m^2 °C	U_h W/m^2 °C
Experimental Result	3.0	11637.9	57.7	2503.94	967.12
Simulation Result	3.0	11585.7	57.5	2506.39	968.27

Outer Side Overall Heat Transfer coefficient

	Pr	Re	Nu	ho W/m^2 °C	Uc W/m^2 °C
Experimental Result	4.5	2621.7	21.1	1320.49	805.93
Simulation Result	4.5	2606.6	21.0	1322.27	806.89

TABLE IV : EXPERIMENTAL AND SIMULATION RESULT

Property	Experimental result	Simulation result	% Deviation
hi W/m^2°C	2503.942	2506.394	0.0979
ho W/m^2°C	1320.498	1322.272	0.1343
Uh W/m^2°C	967.1207	968.2793	0.1197
Uc W/m^2°C	805.9339	806.8995	0.1198
Effectivness	0.380263	0.380543	0.0736

From table IV we can say that Simulation results are approximately matching with the experimental results. The deviation may be due to the truncation and round off error.

B. Effect of flow pattern on heat transfer in concentric tube Heat exchanger

We have done simulation of concentric tube counter flow heat exchanger for all five inserts. We set the input parameter for simulation as:

Inlet Hot fluid Flow velocity: 0.3684 m/s

Inlet cold fluid Flow velocity: 0.1782 m/s

Hot water temprature inlet T_{hi} : 65.1 ^{0}C

Cold water temprature inlet T_{ci} : 32.9 ^{0}C

The simulation results are as shown in fig 7 to 12 for different inserts.

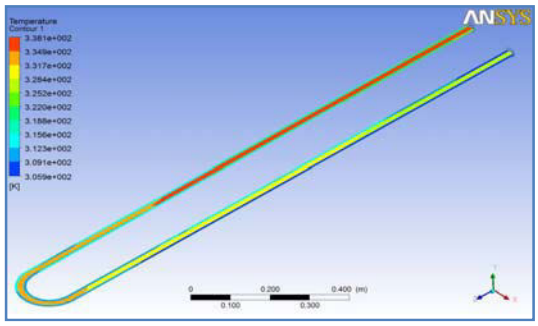

Fig.7 : Temperature Distributions inside the Tube

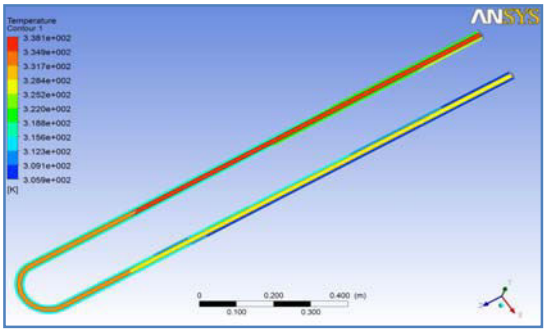

Fig. 8 : Temperature Distributions inside Tube with Plane Insert

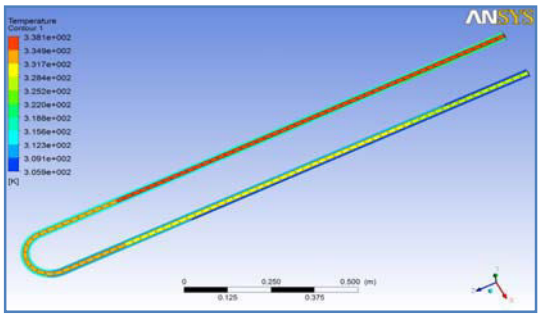

Fig. 9 : Temperature Distributions inside Tube with Plane Insert with Hole

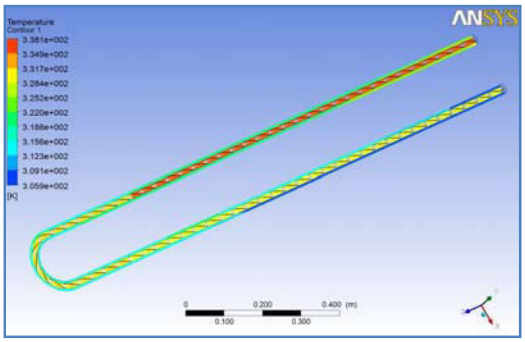

Fig. 10 : Temperature Distributions Inside Tube with Twisted Tap Insert (α = 14.67°)

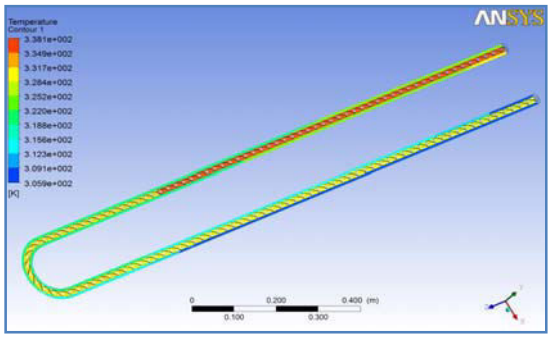

Fig. 11. Temperature Distributions Inside Tube with Twisted Tap Insert (α = 25.23°)

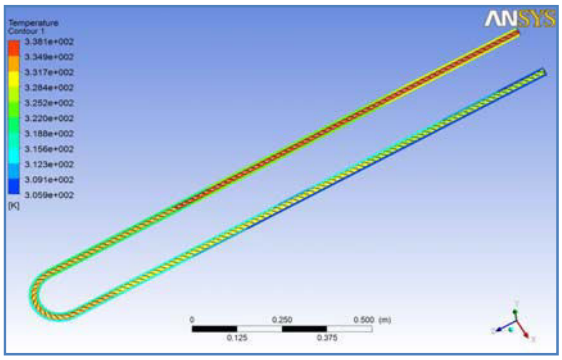

Fig. 12. Temperature Distributions Inside Tube with Twisted Tap Insert (α = 33.94°)

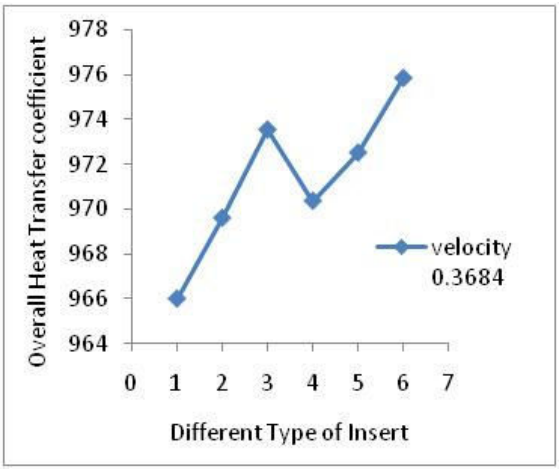

Fig. 13 : Overall heat transfer coefficient Vs different type of inserts

We can see from the simulation temperature contours and fig.13 shown above that by using various inserts in hot fluid flow we can increase the heat transfer rate.

C. Effect of Flow velocity on heat transfer rate in concentric tube Heat exchanger

We also want to study the effect of flow velocity on the effectiveness of the counter flow concentric tube heat exchanger. For that we had done the simulation by considering hot fluid flow velocity as 0.3684m/s, 3m/s, 5m/s, 10m/s, 15m/s, 20m/s and 25m/s with all inserts in hot fluid tube.

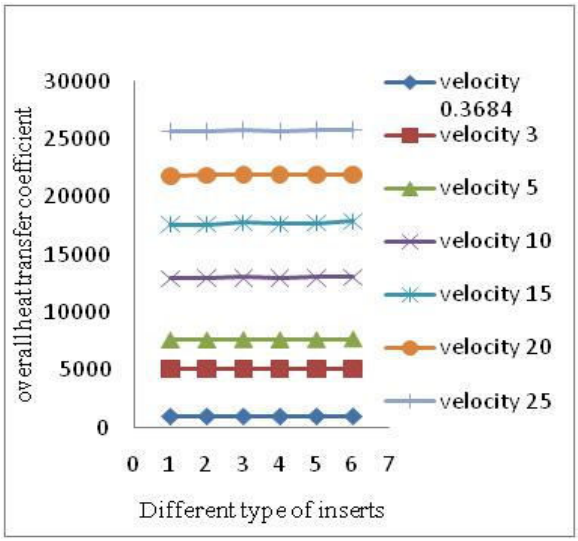

Fig.14 : Overall heat transfer coefficient Vs different type of inserts for different flow velocity.

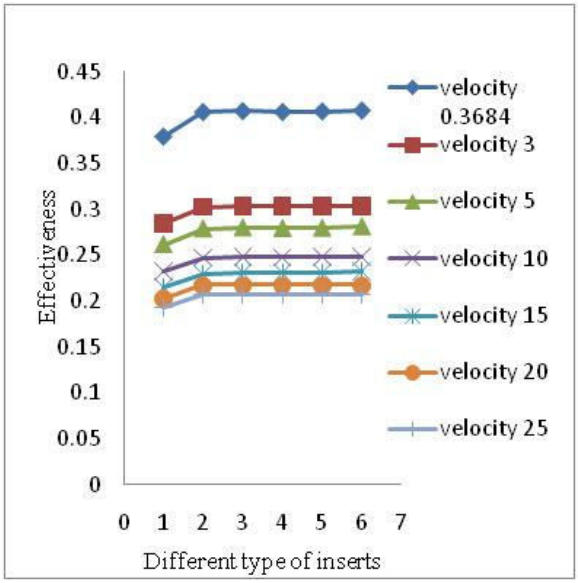

Fig. 15 : Effectiveness Vs different type of inserts for different flow velocity.

Show in fig.13,14 & 15 In which without insert (1), plane insert (2), plane insert with hole (3), twist insert(α=14.67°) (4), twist insert (α = 25.23°) (5), twist insert(α = 33.94°) (6).

Show in fig.14 &15. Effect of different flow velocity on overall heat transfer coefficient and effectiveness on different type of inserts.overall heat transfer coefficient is directly proportional to fluid flow velocity, while effectiveness is inversely proportional to fluid flow velocity

VIII. CONCLUSION

We had studied the heat transfer analysis of the counter flow concentric tube heat exchanger with and without any insert by simulation in Ansys Fluent. We find by using the twist insert (α =33.94°) we can increase the effectiveness by 7.06%.

We also conclude from the simulation analysis that if we increase the inlet flow velocity of the hot fluid the effectiveness of heat exchanger will decrease and overall heat transfer coefficient is increase.

ACKNOWLEDGMENT

The authors would like to gratefully acknowledge the Principle of C.S.P.I.T Changa, HOD of C. M. Department of Mechanical Engg.for giving the permission for using the HMT Lab and Software Lab for this work.

REFERENCES

[1] Ta-Sung Huang, Pai-Hsiang Wang, Yu-Wei Chiu and Jiin-Yuh Jang.2008. Heat and Fluid Flow Analysis over Different Tube Inserts of Recuperator. China Steel Technical Report, No. 21, Page 67－76. China.

[2] S. S. Joshi, V.M.Kriplani. 2011. Experimental study of heat transfer in concentric tube heat exchanger with inner twisted tape and annular insert. International Journal Of Advanced Engineering Sciences And Technologies Vol No. 10, Issue No. 2, Page 334 – 340

[3] Anil Singh Yadav.2009.Effect of half length twisted-tape turbulators on heat transfer and pressure drop characteristics inside a double pipe U-bend heat exchanger. Jordan Journal of Mechanical and Industrial Engineering, Volume 3, Number 1, Page 17- 22.

[4] V.N.Kapatkar, Dr.A.S.Padalkar and Sanjay Kasbe. 2010. Experimental investigation on heat transfer Enhancement in laminar flow in circular tube equipped with different inserts. Proc. of. Int. Conf. on Advances in Mechanical Engineering 2010, Pune,India.

[5] Smith Eiamsa-ard, Chinaruk Thianpong and Pongjet Promvonge.2004. Experimental Investigations of Heat Transfer and Pressure Drop Characteristics of Flow through Circular Tube Fitted with Regularly-spaced Twisted Tape. King Mongkut's Institute of Technology Ladkrabang, Thailand

[6] Watcharin Noothong, Smith Eiamsa-ard and Pongjet Promvonge, 2006. Effect of Twisted-tape Inserts on Heat Transfer in a Tube. The 2nd Joint International Conference on Sustainable Energy and Environment .Bangkok, Thailand.

[7] C.P.Kothandaraman, S.Subramanyan.2010.Heat and Mass transfer data book. New Age International Publishers, Seventh Edition, Chapter 4, Page 126.

◈◈◈

Reduction of Vibration Response of a Hermetic Compressor Suspension System Using Dynamic Balancing and Vibration Analysis

Dattatray S. More[1] & S. G. Joshi[2] & Sanjay S. Gosavi[3]

[1&3]Product Engineering Department, Emerson Climate Technologies India Limited, Karad, India, 415 410
[2]Dept. of Mechanical Engineering, Rajarambapu Institute of Technology, Sakhrale, Islampur, India, 415 414

Abstract - Single cylinder hermetic compressor uses the reciprocating mechanism for its operation. The shaking forces which are associated with acceleration of the connecting rod and piston assembly cause the forces along the line and perpendicular to stroke. These shaking forces act on the compressor body resulting in vibration. These vibrations are transmitted from compressor body to shell through compressor suspension system resulting in the fatigue failure of the suspension springs. Hence, it is necessary to minimize the vibration transmission from compressor body to shell. As such in this paper, the equations for shaking forces have been developed in the approach of Gatecliff. The shaking forces have been minimized by optimizing balance weight for its mass and location in a typical hermetic compressor. The vibration analysis of such a hermetic compressor suspension system for the post-balanced shaking forces has been presented. The effect of the spring-wire diameter on the vibration characteristics and stress analysis of the suspension system have been investigated. Based on these results, suspension system with better isolation and strength criteria has been presented. Also, an experimental investigation for compressor vibration with modified design of the suspension system has been presented.

Keywords - *hermetic compressor, suspension system, shaking forces, balancing, vibration, stress analysis*

I. INTRODUCTION

The reciprocating hermetic compressor is the most widely used type, being employed in all fields of refrigeration and air-conditioning. It is especially adaptable for use with refrigerants requiring relatively small displacement and high discharge pressure. The refrigerants such as R22, R134a, R404a, R500 etc., are used as working fluid in a refrigeration compressor. The hermetic compressor utilizes the slider crank mechanism for its operation. The slider crank mechanism consists of a piston, a connecting rod and a crankshaft. For the application of this mechanism, crankshaft is mounted in vertical direction and is driven by the electric motor. The compressor mechanism along with the motor is fixed on compressor body by bolting and is suspended on the springs. Compressor assembly is installed inside a welded shell as shown in Fig.1.

The shaking forces are generated in the compressor due to motion of the reciprocating mechanism. These shaking forces act on the compressor body resulting in vibration. These vibrations are transmitted from compressor body to shell. It is necessary to keep the vibration transmission to minimum.

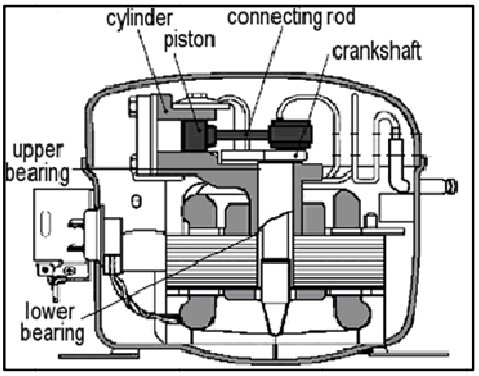

Fig. 1 : Schematic of Hermetic Compressor [2]

Gatecliff [1] has formulated a mathematical model for dynamic response of hermetic compressor. Pressure force, inertia force, unbalance forces due to crankshaft and counterweight, and restoring forces exerted by mounting springs have been considered in the mathematical model. Similarly, Edger et al. [2] have simulated a multi-body dynamic model of the main mechanical components of a hermetic reciprocating compressor. The dynamics of the mechanical components is described with the help of multi-body systems (i.e. rigid components) and finite element method (i.e. flexible components). While, Dufour et al. [3] have studied the single cylinder reciprocating compressor during the start and stops conditions which are sources of significant mechanical problems. The

study is mainly concerned with equations, computer code, and experimental investigations. Gupta [4] has applied the modal analysis procedure to model suspended compressors and their excitation forces. The modal method evaluates the dynamic spring forces and forcing function to determine the effects of a change in suspension configuration on transmitted spring forces.

Thus from the literature review, it is observed that only few investigations have been reported on the design and optimization of the balance weight and suspension system to minimize the vibration transmission from compressor body to housing. Hence, in this paper, first of all, equations for shaking forces have been developed in the approach of Gatecliff. The shaking forces have been minimized by optimizing balance weight for its mass and location in a typical hermetic compressor. The vibration characteristics analysis of hermetic compressor suspension system for its post-balanced shaking forces has been presented. The effect of spring-wire diameter on the vibration characteristics of the suspension system has been investigated. In addition to this, stress analysis of suspension system has been discussed. Based on this, suspension system with better isolation and strength criteria has been presented. Also, an experimental investigation for compressor vibration with modified design of the suspension system has been presented.

II. KINEMATIC MODEL OF HERMETIC COMPRESSOR MECHANISM

The Hermetic reciprocating compressor uses the slider crank mechanism in its operation as shown in Fig.1. For the application of this mechanism crankshaft is mounted in vertical direction and is driven by the electric motor. In order to simplify the kinematic modeling the 2D layout of the mechanism is considered as shown in Fig. 2.

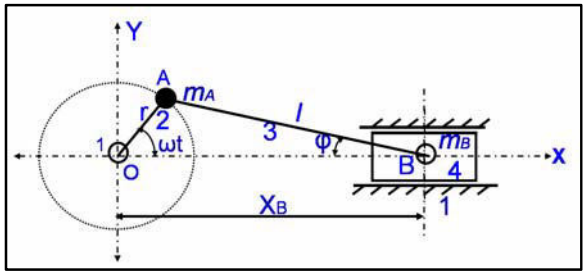

Fig. 2: 2D Layout of Hermetic Compressor Mechanism [5]

It consists of the link 1 as the compressor and it is fixed, link 2 is crankshaft, link 3 is the connecting rod and link 4 as the piston. Masses of the crankshaft eccentric and piston are represented as m_2 and m_4 respectively. During running piston moves along the X direction and its instantaneous displacement and acceleration with reference to O_1 are given as, [5]

$$X_B = r\times\cos\omega t + l\times\sqrt{1-(r/l)^2\sin^2\omega t} \quad (1)$$

$$A_B = -r\times\omega^2[\cos\omega t + (r/l)\cos 2\omega t] \quad (2)$$

Similarly, the crankshaft is rotating with constant angular velocity ω about Z-axis then its displacement and acceleration at point A are given by,

$$R_A = (r\times\cos\omega t)\hat{i} + (r\times\sin\omega t)\hat{j} \quad (3)$$

$$A_A = -r\omega^2(\cos\omega t\hat{i} + \sin\omega t\hat{j}) \quad (4)$$

Equations (2) and (4) have been used to find shaking forces acting on the compressor mechanism.

III. SHAKING FORCES AND RESULTING VIBRATION

Reciprocating and rotating inertia forces act on the compressor during its operation. The reciprocating inertia forces are because of the mass of the piston, piston pin and equivalent reciprocating mass of the connecting rod. While rotating inertia forces are due to rotating masses, which include the crankshaft eccentric mass and equivalent rotating mass of the connecting rod. Fig. 3 shows the free body diagram of a compressor mechanism for its inertia forces.

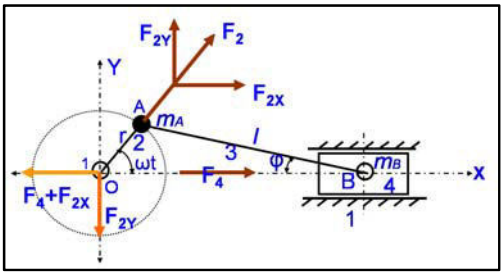

Fig.3 : Inertia Forces Acting on Compressor Mechanism [5]

In Fig. 3, F_4 is the reciprocating inertia force vector acting on the piston and its magnitude is $F_4 = -m_B A_B$ and is in X direction. The rotating inertia force vector F_2 is directed in the radial outward direction of the crank length and its magnitude is $F_2 = -m_A A_A$. The rotating inertia force has the two components. First component is in the direction of the piston and is $F_{2X} = -m_A A_{AX}$. While the second component is perpendicular to first component and is $F_{2Y} = -m_A A_{AY}$. The summation of inertia forces F_4 and F_2 at bearing will generate a resultant dynamic inertia force termed as shaking force F_S [5]. The resultant of these shaking forces from the compressor mechanism causes compressor body to oscillate and results in vibration. These vibrations are

transmitted from body to the shell. It is necessary to minimize the vibration due to shaking forces in compressor. In this paper, this has been achieved by, (i) optimizing the balance weight for its mass and location (ii) suspension system design for better vibration isolation and strength.

IV. SHAKING FORCE MINIMIZATION BY OPTIMIZING THE BALANCE WEIGHT

Typical hermetic compressor mechanism parameters under study have been listed in Table I. These parameters have been used to calculate the shaking forces at the shaft bearing as shown in Fig. 3.

TABLE I : COMPRESSOR MECHANISM PARAMETERS

Parameters	Value	Parameters	Value
Compressor Speed-ω	3000 rpm	Connecting Rod Mass – m_3	0.0348 Kg
Eccentricity- r	7.62 mm	Connecting rod rotating mass- m_{3A}	0.0240 Kg
Piston Diameter- D	22.852m m	Total rotating mass- m_A	0.0427 Kg
Connecting Rod Length- l	41.12 mm	Connecting rod reciprocating mass- m_{3B}	0.0108 Kg
Connecting Rod CG from Eccentricity Centre	12.75 mm	Mass of the piston- m_4	0.0387 Kg
Mass of the Eccentric- m_2	0.0188 Kg	Total reciprocating mass – m_B	0.0495 Kg

From Fig. 4, the X direction shaking force has been observed maximum at 0° and 360°crank-angle position when the piston is at TDC and minimum at 90° and 270°crank-angle position when the piston is at BDC.

Similarly, the Y direction shaking force has been observed maximum at 90° and 270° crank-angle and minimum at 0° and 360° crank-angle. The resultant of X and Y shaking forces as shown in Fig. 4 implies that there are alternating shaking forces acting in X and Y directions on the compressor body during its operation.

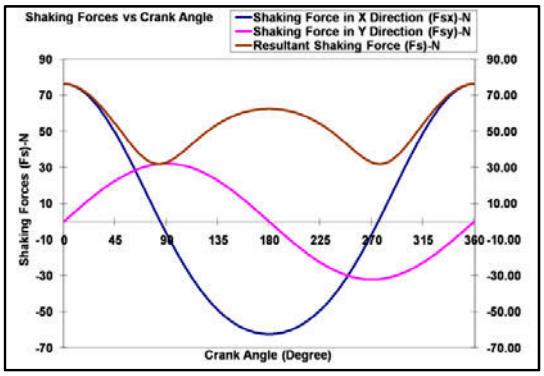

Fig. 4 : Shaking Forces vs Crank Angle

The alternating shaking forces cause the compressor body to oscillate in X and Y direction resulting in vibration. These shaking forces can be minimized by balancing. Hence, balancing simulation has been carried by adding balance mass on the crankshaft using the condition $M_C R_C = m_A r + P m_B r$, where M_C is balance mass and R_C is balance mass radius. The polar plot for shaking forces in X and Y direction with different reciprocating balance mass has been shown in Fig. 5. From Fig. 5, the shaking forces in X and Y directions are of 76.27 N and 32.15 N in magnitude respectively for mechanism without balance mass. If balance mass equal to rotating mass of mechanism attached opposite to the eccentric mass (i.e. γ=180º) then, shaking forces in Y direction became zero and X direction forces has reduced to 44.21 N. Further, by increasing the balance mass by adding the reciprocating mass in steps of 20%, shaking forces in X direction goes on reducing and in Y direction goes on increasing. This reveals that, by creating imbalance in Y direction single cylinder mechanism has been balanced for the reciprocating mass.

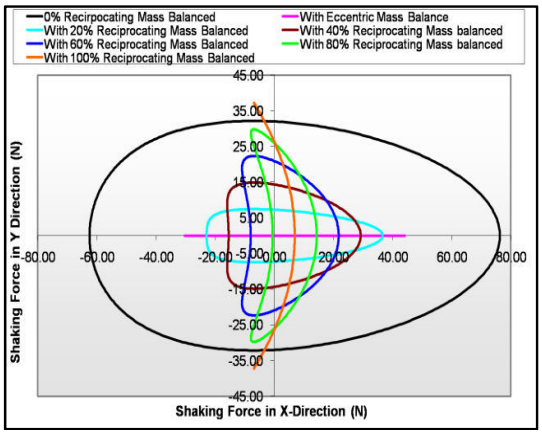

Fig. 5 : Polar plot of Shaking Forces

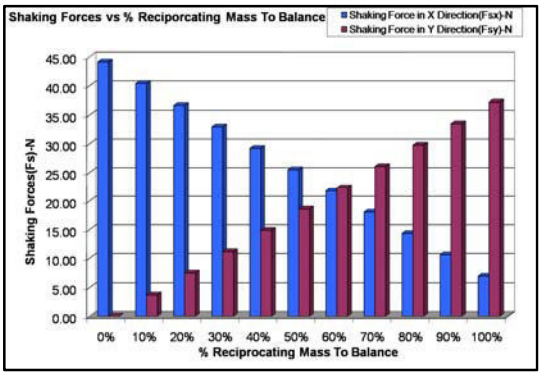

Fig. 6 : Shaking Forces vs % Reciprocating Mass

From Fig. 6, it is observed that, increase in reciprocating mass beyond 60% increases the shaking forces in *Y* direction and reduces it in *X* direction resulting in the increase of shaking forces. Hence, the minimum resultant shaking forces are observed at the condition of 60% reciprocating mass.

Figure 7 is the plot shaking forces against the balance mass position from eccentric for 60% reciprocating mass. It is observed that, the shaking forces in *X* and *Y* direction are minimum for 180° position of balance mass from eccentric mass.

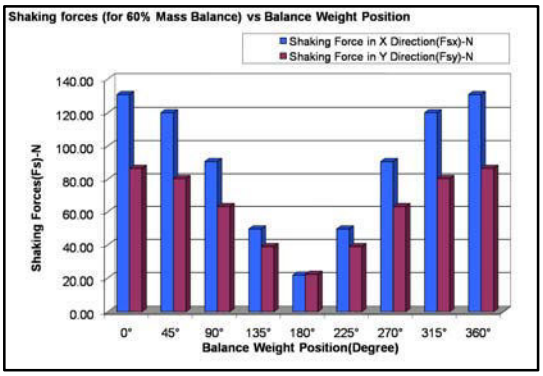

Fig. 7 : Shaking Forces vs Balance Weight Position

Hence, from above minimum shaking forces for typical hermetic compressor has been observed for 60% reciprocating mass with 180° position. The total balance weight mass of rotating mass plus 60% reciprocating mass need to add on the shaft at opposite to eccentric.

V. SUSPENSION SYSTEM DESIGN TO MINIMIZE SHAKING FORCE TRANSMISSION

As seen in Fig. 6, even after balancing there are shaking forces of magnitude 21.79 N and 22.33 N respectively in *X* and *Y* direction. The transmission of these shaking forces to shell has been minimized by designing the hermetic compressor suspension system for better vibration isolation and strength criteria.

As seen in Fig. 1, compressor suspension system consists of the helical compression springs and compressor body. The compressor body comprises the slider crank mechanism and motor assembly. The compressor suspension system holds the compressor body and isolates the body vibration to shell. The dimensional layout of hermetic compressor suspension system which is under study is as shown in Fig. 8.

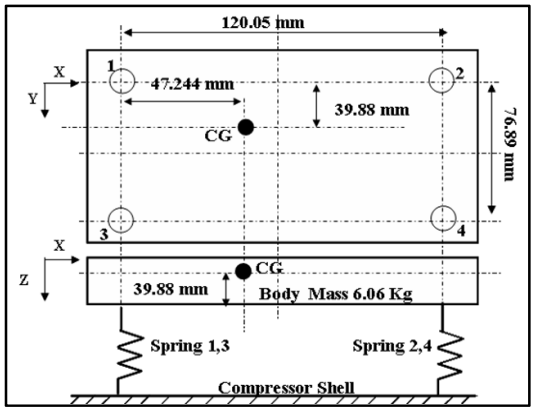

Fig. 8 : Typical Hermetic Suspension System

A. Vibration and Stress Analysis using FEA

For vibration and stress analysis, the compressor body has been modeled with Mass21 element of 1D type from Ansys, at the CG location of the compressor body. Mass21 element type has six degrees of freedom with the consideration of mass attributes. Similarly, the springs have been meshed with BEAM188 element of 2D type. BEAM188 element has six degrees of freedom. The rigid coupling elements have been used to couple the MASS21 element with BEAM188 element as shown in Fig. 9. The rigid coupling elements are with infinite stiffness capability. Hence, rigid elements will not deform. They will couple the displacement of MASS21 element directly with that of BEAM188 element.

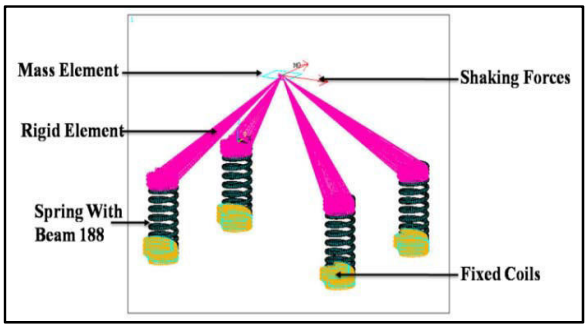

Fig. 9 : Suspension System FEA model and Load Condition Typical

The number of elements used in this analysis is about 2200 of BEAM188 and 1of MASS21 element. For analysis, the bottom dead coils of the springs have been constrained to zero and the shaking forces as calculated earlier were applied at mass element as shown in Fig. 9. With these constraints and load conditions, the harmonic analysis of the suspension system has carried out for different spring-wire diameters. The vibration response of the suspension system carried out at 50 Hz, which is the excitation frequency for compressor. Similarly, stress analysis of the suspension system has been carried out. The vibration response and stress values have been plotted against the spring-wire diameter in Fig. 10.

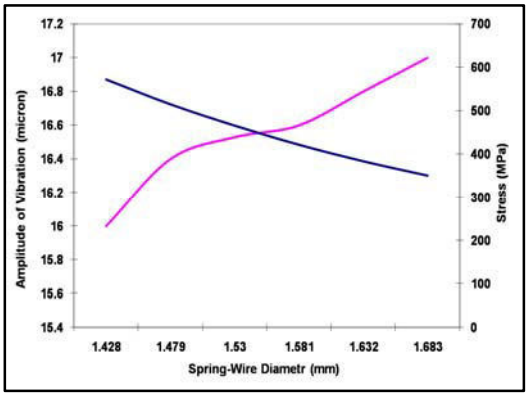

Fig. 10 : Vibration and Stress vs Spring-Wire Diameter

From Fig. 10, it is observed that, the amplitude of vibration increases with increase in spring-wire diameter. Increasing wire diameter causes the decreases in deflection of the suspension system. This means, the stiffness of the suspension system increases. For better vibration isolation, the excitation energy should get absorbed in the form of deflection of the suspension system. Hence, it is said that, smaller the wire diameter better will be the isolation. Similarly, the stresses decrease with increasing diameter. This is due to increase in the resisting area to the load. The amplitude of vibration and stress values cross at a point between spring-wire diameters of 1.53 mm and 1.581 mm. Considering, the factor of safety of 2 with 950 MPa as a limit stress, the stress value in the spring should be 475 MPa. Since, the springs with diameter 1.53 mm and 1.581 mm has the stress value lower than 475 MPa. However, decreasing the wire diameter below 1.53 mm increases the stress value and increasing wire diameter above 1.53 mm increases the vibration. Hence, the spring diameter with 1.53 mm is considered as an optimal value for vibration as well as stress point of view. Now with this spring-wire diameter of 1.53 mm, the stiffness of the suspension system has been calculated by modal analysis. The few natural frequencies and their mode shapes are listed in Table II.

TABLE II: NATURAL FREQUENCIES OF SUSPENSION SYSTEM

Mode 1 (Frequency=3.58 Hz)
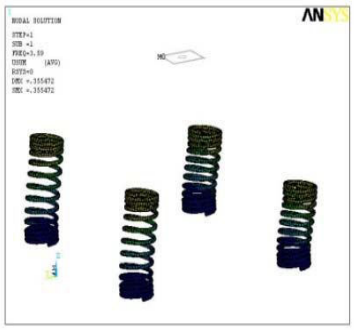
Mode 2 (Frequency=4.21 Hz)
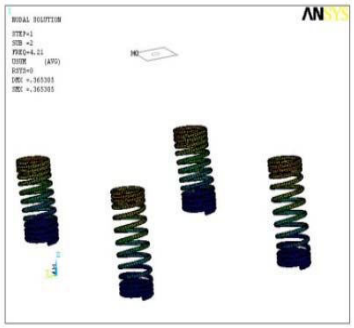
Mode 3 (Frequency=7.46 Hz)
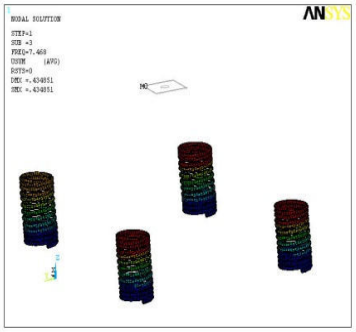

VI. EXPERIMENTAL VIBRATION MEASUREMENT

The hermetic compressor vibration measurement with existing and modified design for balance weight and spring wire diameter has been carried out. The experimental setup used for the vibration measurement in hermetic compressor comprises of the refrigerant gas load stand, assembled compressor, electrical accessories and vibration accelerometer. The schematic layout of the same is as shown in Fig. 11.

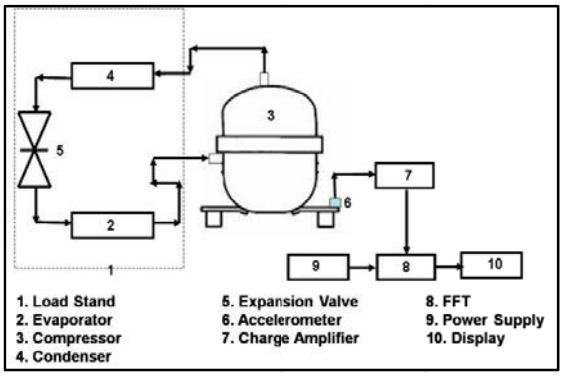

Fig. 11 : Schematic of Experimental Setup Layout

The load stand consists of all the components from refrigeration system such as condenser, evaporator, expansion valve etc. The compressor to test is connected to the gas charging load stand through suction and discharge pipe. The electrical accessories required to start the compressor have been connected to the compressor as shown in Fig. 12.

Fig. 12 : Experimental Setup of Vibration Measurement

Then compressor was charged with the refrigerant gas. Moreover, it was run to attend the test condition at the required temperatures and pressure conditions as per AHRI standard 530-2011. Once the test condition is attained, vibration measurement has been carried out with Datamite made piezoelectric type accelerometer and FFT. Vibration measurement has been carried out at the standard mounting locations as per the AHRI 520-2011 standard. The vibration has been measured in displacement mode and results are given in Table III.

TABLE III : EXPERIMENTAL RESULTS

Test Number	Vibration (micron)	
	Existing Suspension Design	***Modified Suspension Design***
1	40	23
2		25
3		25

VII. CONCLUSIONS

Reciprocating and rotating inertia forces act on the compressor during its operation. The reciprocating inertia forces are because of the mass of the piston, piston pin and equivalent reciprocating mass of the connecting rod. While rotating inertia forces are due to rotating masses and include the crankshaft eccentric-mass and equivalent rotating mass of the connecting rod. These inertia forces are termed as shaking forces and are directed along and perpendicular the piston axis and acts at the main bearing of the shaft, causing compressor body vibration.

To minimize the compressor vibration a partial balancing method can be used. From polar diagram (Fig. 5) of vertical shaking force(F_{sy}) vs horizontal shaking force (F_{sx}), it can be seen that as the value of F_{sx} decreases as value of F_{sy} increases (with 0 to 100 % reciprocating balance mass). From Fig. 6, it is seen that the optimal value of % reciprocating balance mass is 60 %. With small change in value of % reciprocating balance mass about the value of 60% there is a considerable change in value of F_{sx} and F_{sy}.

Even after balancing, there are shaking forces in the mechanism. These remaining shaking forces cause the compressor body to oscillate. The transmission of these shaking forces to shell can be further reduced by an appropriate design of a suspension system using a set of helical compression springs. To reduce the force transmissibility of the suspension between compressor body and its housing, a suspension with low stiffness should be used. Low spring stiffness calls for small spring-wire diameter for a given set of spring parameters. This condition results in higher stresses in the spring leading to a fatigue failure during its service life. Therefore, the design of suspension spring should be a balance between strength and stiffness criteria.

REFERENCES

[1] Gatecliff George W., "Analytical Analysis of the forced vibration of the spring mass of a reciprocating hermetic compressor including comparison with experiment", International Compressor Engineering Conference at Purdue, Purdue University, pp.221-229, 1974.

[2] Estupina Edgar A. and Santos Ilmar F., "Dynamic modeling of hermetic reciprocating compressors, combining multi-body dynamics, finite element method and fluid film lubrication", International Journal of Mechanics, Vol. 1, no.4, 2007, pp. 36-43.

[3] Dufour R., Hagopian Der J. and Lalanne M., "Transient and steady state dynamics behaviour of single cylinder compressors: prediction and

experiments", Journal of Sound and Vibration, Vol. 181, no. 1, pp. 23-41, 1995.

[4] Gupta Nishi, "Design of compressor suspension systems using modal analysis", International Compressor Engineering Conference at Purdue, Purdue University, pp.154-161, 1984.

[5] Shigley Joseph E. and Uicker John J.," Theory of Machine and Mechanism", 3rd Edition, Oxford University Press, New York, 2009

◈◈◈

Design and Development of A System For Rapid Prototyping using Conventional Materials

Shah Samir B. & Doshi H.P.

Mechanical Engineering Dept., L.D.College of Engineering, Ahmedabad, India

Abstract **-** The Components which are prepared in FDM machine and from the ABS (acrylonitrile butadiene styrene) material are very costly because of the material cost is too high so we try to replace wax and conventional plastics which is cheap compare to the ABS material. We used Nozzle, valve and other accessories and setup on VMC machine. The XY-movement is program in VMC machine and the nozzle which is fixed on the Z-axis.

Keywords**:** *Rapid Prototyping, Fused Deposition modelling.*

I. INTRODUCTION

Reduction of product development cycle time is major concern in industries to remain competitive in the marketplace and hence focus on shifted from traditional product development methodology to rapid fabrication techniques like Rapid prototyping (RP).The RP process is capable of building parts of any complicated geometry in least possible time without incurring extra cost due to absence of tooling. Another advantage of RP is to produce functional assemblies by consolidating sub assemblies into single unit at the computer aided design (CAD) stage and thus reduce part counts, handling time and storage requirement and avoids mating and fit problems.

Kochan et al. [3] indicate that RP is a new forming process and principle which is one of the important breakthroughs of the recent technology progress in manufacturing industry. Pham et al. [5] conclude that Rapid prototyping is enabling technology for concurrent engineering. Its goal is to reduce the product development and manufacturing costs and lead times, thereby increasing compititiveness.Sunet al. [6] conclude that bond formation among extruded acrylonitrile butadiene styrene (ABS) filament in the FDM process. Gibson Ian have conclude that RP is a technology that can be used for many different applications both manufacturing and non manufacturing based.Bellumeur et al. [1] conclude that the bonding quality among the polymer filament in the FDM process is determines the integrity and Mechanicalproperties of resultant prototypes. Lee et al.[4]been conclude that the CAD model developed by the RE

Process can be converted to the physical prototype using an RP technique. There are many Processes in RP.

The basic uses the following steps to make prototypes.

1. Create a CAD model of the design.
2. Convert the CAD model to STL file format.
3. Slice the STL file into 2D cross-sectional layers.
4. Grow the prototype.
5. Post processing. [8]

All Basic five steps are shown in Figure

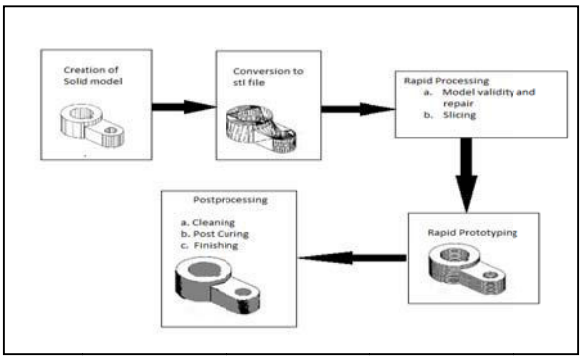

Figure1. Basic five steps of RP Process [8]

II. Fused deposition modelling (FDM)

There are many processes in RP from them we are concentrating on FDM process. The technology was developed by S. Scott Crump in the late 1980s and was commercialized in 1990. The FDM technology is marketed commercially by Stratasys, which also holds a trademark on the term. Like most other additive fabrication processes (such as 3D printing and stereo lithography) FDM works on an "additive" principle by laying down material in layers. A plastic filament or metal wire is unwound from a coil and supplies material

to an extrusion nozzle which can turn on and off the flow. The nozzle is heated to melt the material and can be moved in both horizontal and vertical directions by a numerically controlled mechanism, directly controlled by a computer-aided manufacturing (CAM) software package. The model or part is produced by extruding small.

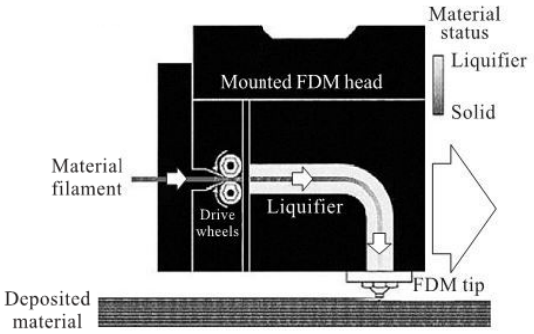

Figure2. Schematic diagram of FDM process

Beads of thermoplastic material to form layers as the material harden immediately after extrusion from the nozzle. Several materials are available with different trade-offs between strength and temperature properties. As well as acrylonitrile butadiene styrene (ABS) polymer, the FDM technology can also be used with polycarbonates, polycaprolactone; polyphenylsulfones. A "water-soluble" material can be used for making temporary supports while manufacturing is in progress. Marketed under the name Waterworks by Stratasys, this soluble support material is quickly dissolved with specialized mechanical agitation equipment utilizing a precisely heated sodium hydroxide solution.

To understand the complete software function of the FDM machine we can experiment on FDM machine using an irregular shape.

Here we produce one irregular component in Pro-e software. According to the RP processes follow all the steps and analyse how FDM machine working.

Figure3. FDM machine manufacture by StratasysCompany [9]

1. Create a CAD component in Pro-e software and convert it in to STL format

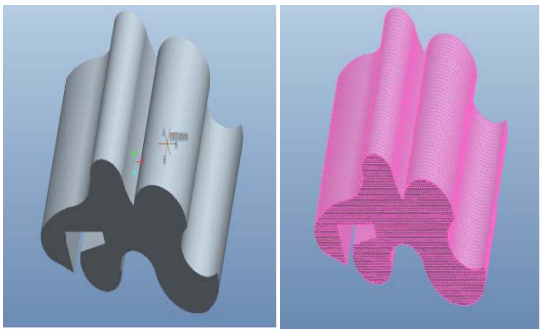

Figure4. CAD model and STL formation of irregular shape

2. Login, down load and Warm-up FDM

-Login to FDM computer

Login to the appropriate computer using your SUNetID and password. The FDM computers are located to the right of the FDM machines: FDM fortus360mc computer on left, computer on right.

-Move Your Files to the FDM.for.all Folder

Once logged in, create your own sub-folder in the "FDM.for.all" folder on the desktop. You will use this folder to hold the FDM files you generate. Do not attempt to run files off of a removable media (e.g. USB memory stick) or off of a network drive. Removable drives and network drives time-out in Windows XP, and FDM parts can take days to build. Therefore, run files only from the FDM.for.all folder on the desktop. That said the FDM.for.all folder is not permanent storage and could be removed by PRL staff. Store your files

permanently on either your AFS space or on a removable media. If you are doing your FDM license, you should use the FDM_key_license.STL file on the desktop. Please do not move the FDM_key_license.STL file.

-Warm up FDM

Set the temperatures on your intended machine's temperature controllers to the correct values as described below. The FDM should already be on, and its front door should be closed and latched. If this is not the case, please talk to the TA on duty. The temperature controllers are located at the top front of the machines. The green number is the current temperature of the item (model, support, or envelope) in degrees Celsius. The red number is the temperature that the machine is currently set to maintain. Change the set temperature by using the increase-decrease buttons on each controller. Note that it is important to use the correct temperatures or the material will not behave properly.
Standard **ABS** Material Temperatures Model: 270 Support: 265 Envelope: 70

Investment Casting **Wax** (ICW) Material Temperatures Model: 71 Support: 73 Envelope: 43

4) Preparing Files in the FDM Software

Start the insight software: Insight is the program we use to process an STL file and send it to the FDM machine. It is only available on the two computers next to the FDM machines. Insight is the program we use to process an STL file and send it to the FDM machine. It is only available on the two computers next to the FDM machines. Insight is the program we use to process an STL file and send it to the FDM machine. It is only available on the two computers next to the FDM machines. Click the "Insight" link on the computer's desktop, or click "Start", "Programs", "InsightV21", and "Insight" to start the program.

Menus and Toolbar There is a great deal of flexibility to what Insight can do, but we have found that the standard settings and procedures work best. Most of the commands we use appear both in the top text menu and in the main toolbar.

Figure5. Main Toolbar of the Insight software

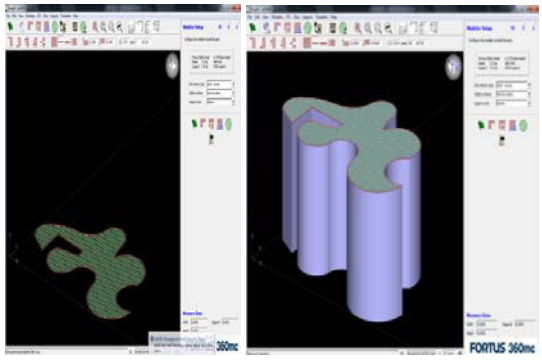

Figure6. First slice and complete process in insight software

After completion of working of whole insight software the last procedure is to save the file, We have finished processing our STL, and ready to save the job and start working with the FDM machine. In the File menu, click "Save as", "Job", and then navigate to your sub-folder of the FDM.for.all folder and click "Save".

This action will cause Insight to create a folder called ssys_filename (e.g. ssys_fdm_key_license) in your folder. It will save the processing that you just finished as a batch of different files inside this new folder. The file that encapsulates this job is the .sml.gz, which you can re-use later if you want to remake the same part on the same machine.

Now after completion the whole process on FDM machine using ABS material same component are prepare on VMC machine using Wax. For it there are too much changing in the set-up on VMC machine. The schematic diagram of set up on VMC machine shown in below figure.

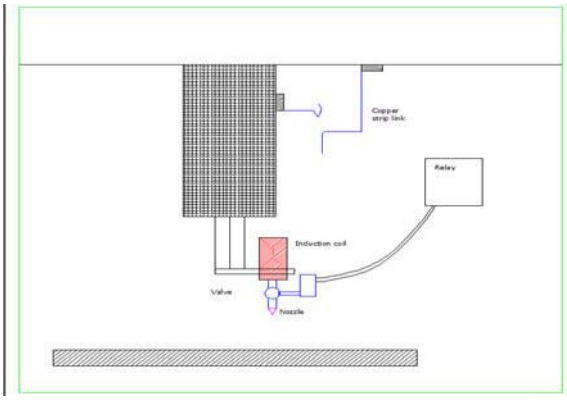

Figure7. Set up on VMC machine

For it the main components are Nozzle, Controller, Valve, Relay and the Wax are the main components and set on a VMC machine.

III. DESIGN OF NOZZLE AND CONTROLLER

Here we used tip type nozzle and its diameter is 0.30 mm the schematic diagram is shown in below figure. Here the melt wax is come in the Nozzle and according the on/Off of the solenoid valve the wax is flow as a drop type. To control the pressure and temperature the controller are needed whose specification are as under.

- Device - Controller

  Name - AC&R Controller

  Type - RWR470.10

  Datasheet No. -CB1Q3900en

- Device –temperature sensor

  Type- QAZ21.682/101 with a sensing element LG Ni 1000 Ω, Silicon cable 200cm, with -50º C…+80º C measurement range

  Datasheet no.-Q1848

- Device-Pressure sensor

  Type- QBE2001-P10U, -1…+9 bars / QBE2001-P25U, -1…+24 bars / QBE2001-P60U, -1…+59 bars. With DC 0…10 V output signal

  Datasheet no-N1907

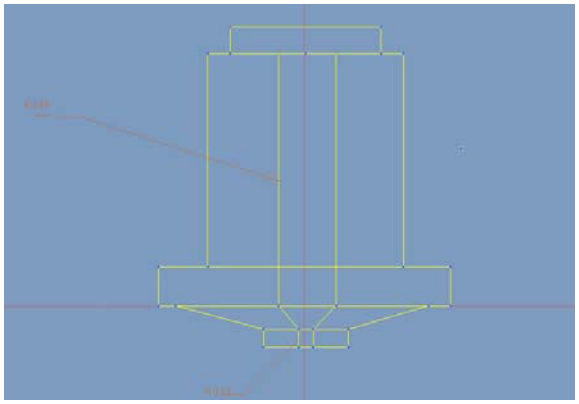

Figure8. Schematic diagram of Nozzle

IV. SELECTION OF VALVE

As per our requirement in nozzle from the various types of valves here we select Solenoid valve.

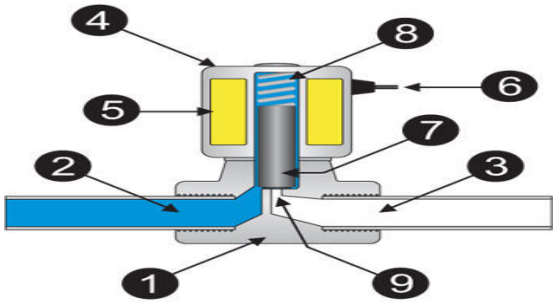

Figure 9.cross section of the Solenoid valve [10]

1. Inlet port 4.Coil/Solenoid 7.Plunger
1. 2.Outlet port 5.Col winding 7.Spring
3. Valve body 6.Lead wires 9.Orifice

For open closed the nozzle here need a valve. As per experiment and situation we select a solenoid valve. The illustration bellow depicts the basic concept of Solenoid valve. The valve shown in the figure is normally closed, direct-acting valve. The media controlled by the solenoid valve enters the valve through the inlet port (part 2 in the illustration above).the media must flow through the orifice (9) before continuing into the outlet port (3).The orifice is open and closed by the plunger (7).The valve is a normally-closed solenoid valve. Normally closed valve used a spring (8) which presses the plunger tip against the opening of the orifice. The sealing materials at the tip of the plunger keep the media from entering the orifice, until the plunger is lifted up by an electromagnetic field created by the coil.

V. PUT RELAY ON CONTROLLER

A relay is an electromechanical switch. More importantly, relays are used in virtually every type of electronic device to switch voltages and electronic signals.

Inductor (wire coil) one contact is connected to (-) ground and the other is connected to a wire which only turns (+) positive when triggered Inductor coils are neutral in electric terms. Either end can be (+) positive or (-) negative. But neither end can be both at the same time or the relay will not operate.

Swing Arm of Switch When the relay is off, the arm is at rest against the “normally closed contact”. When the relay is in the “off” position; the swing arm is in contact with the normally closed contact. This means that when the relay is in the “off” position, the normally closed contact is also conducting to the main contact. When the relay is activated, the magnetic field created by the

inductor coil pulls the swing arm until it makes contact with the normally open contact connecting the circuit connected to the normally open contact to the circuit connected to the main contact. This is what makes relays so powerful, they can be used to switch between circuits or turn a circuit on and off.

VI. SELECTION OF WAX

There are many types of wax in the nature. Like Animal Waxes, Vegetable Waxes, Petroleum Waxes, Mineral Waxes and Synthetic Waxes. From these Synthetic Waxes are better for my work. From Synthetic Waxes Paraffin Wax's Properties are Suitable for my work.

Properties of Paraffin WAX

Paraffin WAX is mostly found as a white, odourless, tasteless, waxy solid, with a typical melting point between about 46 and 68 °C (115 and 154 °F) and having a density of around 0.9 g/cm^3 .It is insoluble in water, but soluble in ether, benzene, and certain esters. Pure paraffin wax is an excellent electrical insulator, with an electrical resistivity of between 10^{13} and 10^{17} ohm meter. This is better than nearly all other materials except some plastics (notably Teflon). It is an effective neutron moderator . Paraffin wax ($C_{25}H_{52}$) is an excellent material to store heat, having a specific heat capacity of 2.14–2.9 J g^{-1} K^{-1} (joule per gram Kelvin) and a heat of fusion of 200–220 J g^{-1}. This property is exploited in modified drywall for home building material.

VII.CONCLUSION

The RP process is capable of building parts of any complicated geometry in least possible time without incurring extra cost due of absence of tooling. The Parts which are prepared in FDM machine and from the ABS (acrylonitrile butadiene styrene) material are so costly because of the material cost is too high. So if we want to use RP as a general purpose we must optimize the cost to replace the material. To fulfil this function we can use a conventional cheap material like wax and Plastics. We arranged all setup on VMC machine. If we replace only material the component cost is automatic optimize up to 75%.

REFERENCES

[1] Bellehumeur celine, Li Longmei, Sun Qian, Gu Peihua,"Modeling of bond formation between polymer filament in the fused deposition modelling process", journal of manufacturing process,2004, vol.6/No.2.

[2] Gibson Ian "Rapid prototyping: A tool for product development", computer aided design & applications, 2006, vol.2, no 6, pp 785-793.

[3] Kochan detlef, Kai chua chee, Zhaohui, "Rapid prototyping issues in the 21st century", computers in industry 39, 1999, pp3-10

[4] Lee Kwan H., Woo H., "Direct integration of reverse engineering and rapid prototyping", Computers and industrial engineering 38, 2000, pp 21-38.

[5] Pham D.T., Gault R.S., "A comparisons of rapid prototyping technologies", International journal of machine tools & manufacture 38,1998,pp 1257-1287.

[6] Sun Q., Rzvi G.M., Bellehumeur C.T, GU P.,"Experimental study of the cooling characteristics of polymer filaments in FDM and Impact on the mesostuctures and properties of prototypes",2003.

[7] Yonginian Yan,shengjie li,Renji Zhang,Feg lin,Rendog Wu,Qingping Lu,Zhuo Xiong, Xiohong Wang, "Rapid prototyping and manufacturing technology: Principle, Representative technics, Applications, and development Trends", Tsinghua Science and technology, June 2009, pp 1-12 volume 14 , Number s1.

[8] Noorani Rafiq "Rapid Prototyping Principal and Applications, 2005"

[9] www.stratasys.com

[10] www.wikipedia.com

[11] www.sciencedirect.com

Vibration Condition Monitoring Technique For Identifying Fault In Motor Pump Assembly

Nagrani Seema Rajkumar & S S Pathan & I H Bhoraniya
Mech Engg. Dept, L D Engg. College, Ahmedabad, Gujarat, India.

Abstract **-** The major problem with the mechanical system is, they run smoothly for a long time and the suddenly develop a defect. The defect may slowly increase and deteriorate the condition of the machine. The maintenance engineer is required to detect the fault in the mechanical system. With the industrial growth, it has become necessary to monitor the condition of the machine/system. The vibration analysis is the most common method to identifying the defects in the mechanical system. Vibration-based monitoring techniques have been widely used for detection and diagnosis of defects for several decades. These methods have traditionally been applied, separately in time and frequency domains. The present work is based on the one of the technique of condition monitoring is signature analysis. The signatures are collected through the experimental work on the motor pump assembly for diagnosis the spectrums and the fault can be identified.

I. INTRODUCTION

Condition-based maintenance (CBM) programs are now widely used in industry in order to reduce unscheduled downtime and production losses. The condition monitoring system is required to provide condition information that is accurate. However, most condition monitoring techniques are implemented under a certain specified operating conditions. Therefore, consideration of possible operating and/or environmental fluctuations into a condition monitoring system is usually neglected in conventional condition monitoring techniques. The currently intensively exploited non-parametric time–frequency techniques (wavelets, short time Fourier transforms) are subject to operational and environmental variables and represent the signal dynamics in time–frequency domain caused by both the object of interest and other irrelevant external sources [1]. The objective of condition monitoring of a machine is to predict a fault well in advance of its occurrence. Therefore, a measurement of the overall vibration level will not provide successful prediction because the highest vibration component within the overall frequency range will dominate the measurement [2]. In signal analysis, we determine the response of a system under a known excitation and present it in a convenient form. Often, the time response of a system will not give much useful information. However, the frequency response will show one or more discrete frequencies around which the energy is concentrated. Since the dynamic characteristics of individual components of the system are usually known, we can relate the distinct frequency components (of the frequency response) to specific components [3]Vibration analysis has provided quick and reliable information on the condition of the bearings. Integration of this condition monitoring technique with another condition technique resulted in a comprehensive diagnosis of the machinery condition [4]. The characteristics of a machine vibration can be used to identify specific problems. There are numerous causes of vibration in machines, but about 90% of all problems are due to unbalance or misalignment. Some of the other Sources of vibration are mechanical looseness, bad drive belts or chains, bad bearings (antifriction type), hydraulic forces, bent shafts, electromagnetic forces, aerodynamic forces, resonance, worn, damaged or eccentric gears and rubbing [5]. In general, the vibration will exist in the radial direction, axial direction, or both. The radial direction is usually broken up into the vertical and horizontal planes to better describe the characteristics of the vibration. The understanding of this allows the determination of ideal sensor positions likely to record a maximum of information in the best Conditions [6]. Misalignment is common cause of machinery malfunction. A poorly aligned machine can cost a factory 20% to 30%. In machine down time, replacement parts, inventory, and energy consumption. A large payback is often seen by regularly aligning machinery. Operating life is extended and process conditions are optimized [7]. Shaft misalignment occurs when the centerlines of rotation of two or more machinery shafts are not in line with each other. There are two types of misalignments: parallel misalignment occurs when the shaft centerlines of the two machines are parallel, but offset to each other, and angular misalignment occurs when the shaft centerlines are not parallel, but inclined to each other. Misalignment in shafts produces high radial loads in one or more

bearings [8]. The present work is based on the signature analysis of the motor pump assembly with the help of the FFT analyzer to determine the fault in the system.

Fig. 1 Motor Pump Assembly.

II. EXPERIMENTAL SETUP

The vibration analysis is important for the detecting the fault in the mechanical system. The PL-31 FFT analyzer is used to collect the spectrums of vibration for the signal analysis. The experimental system is taken which consists the motor and pump assembly for diagnosis. The Fig. 1 represents the motor pump assembly. In this system the motor and pump are connected through the coupling. In the Fig. 2 the lock diagram is shown which gives the idea where the vibration values are measured.

The Table 1 represents the detail of the motor pump assembly.

Table 1. Detail of motor pump assembly.

Plant	:	Godrej industries,Mumbai
Motor Power	:	15KW
Motor RPM	:	1500
Rotor RPM	:	1500

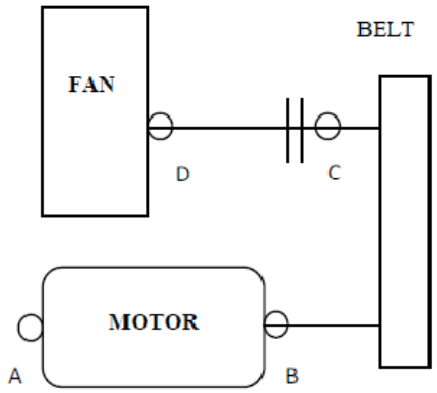

Fig. 2 Block diagram of motor pump assembly.

The vibration is measured at the point A NDE of motor, Point DE of motor, point C DE of fan and point D NDE of fan.

III SELECTION OF AMPLITUDE FOR ANALYSIS

In the signature analysis, the spectrums are studied. The fault machinery spectrums are compared with the ideal machine and fault is determined. The spectrums are nothing but the amplitude graph versus frequency. There are three vibration amplitude used to measure the vibration viz, displacement, velocity and acceleration. On the basis of the speed of the system amplitude is selected. For the given system the speed is in medium region so the velocity amplitude is measured. The FFT analyzer can convert the acceleration value into the velocity.

IV. PROCEDURE OF CONDUCTING EXPERIMENT

1. Change the setting of the FFT analyzer as per the requirement of collecting amplitude. For displacement measurement maximum frequency range should be 200HZ and 1600 spectrum lines and for velocity measurement maximum frequency range should be 1000HZ and 800 spectrum lines. For all types of settings use utility or menu option in FFT analyzer.
2. Connect acceleration sensor with the FFT.
3. Mount the sensor on the particular point of the system vertically, horizontally and axially and get the data and spectrum on the FFT screen.
4. To investigate the spectrum uploads the spectrums from FFT to computer.

The data are collected from the point A, B, C and D as shown in Fig.2, in radial as well as axial direction.

V. RESULTS AND DISCUSSION

In this assembly the motor is running at the 1500 RPM so the velocity should be measured. The input power is 15 KW therefore it is under the class – I as per the ISO -10816. The maximum permissible velocity is 4.5 mm/s. For analysis of the system spectrums are collected through the PL- 31 FFT analyzer. The values in vertical, horizontal and in axial direction are measured.

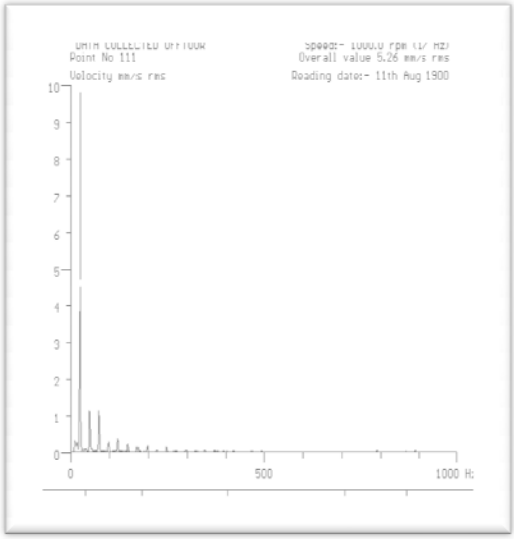

Fig. 3 Motor NDE Vertical.

In the Fig. 3 the rms value is 5.26mm/s at the 25 Hz, Which is more than the acceptance.

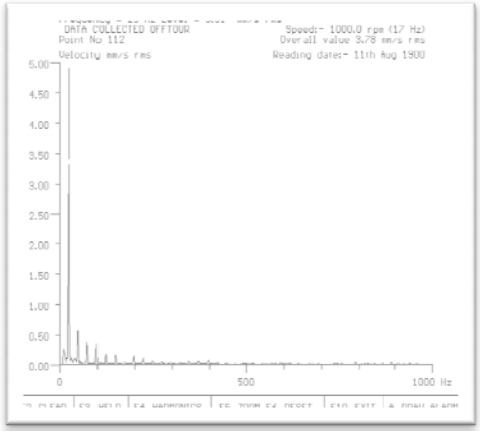

Fig. 4 Motor DE Horizontal.

The value of rms in Fig. 4 is not beyond the ISO- 10816, so it is not indicate any problem.

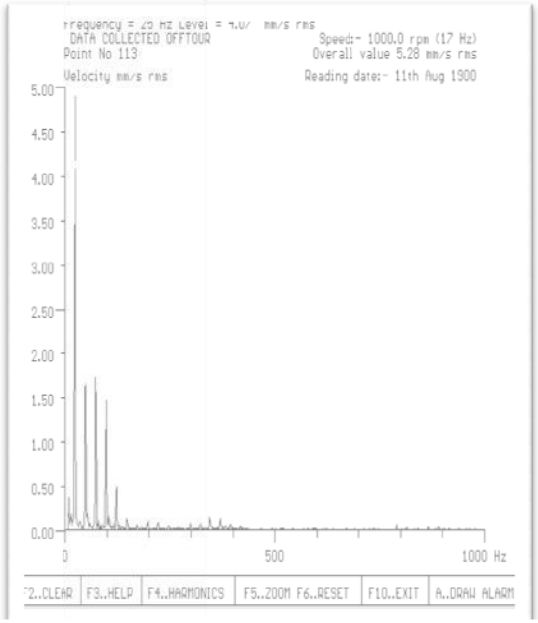

Fig. 5 Motor NDE Axial.

The overall rms value is 5.29mm/s, which is more than the permissible limit, so there is problem which is highlighted in the axial direction also.

In this way the spectrums are collected for the point B in all direction from Fig. 6 to Fig. 8.

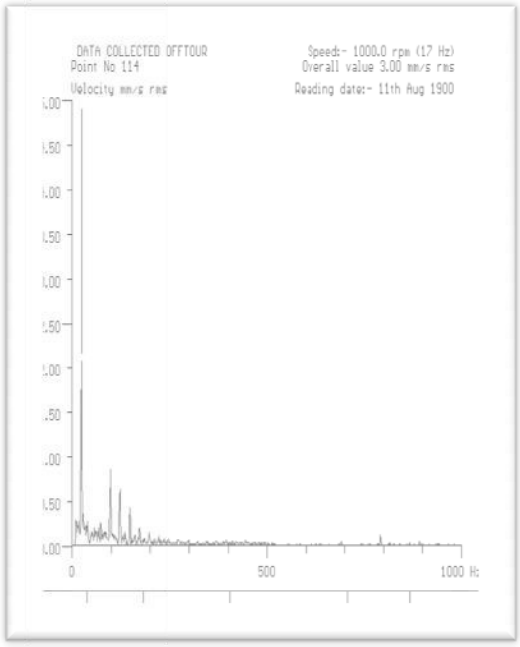

Fig.6 Pump DE Vertical.

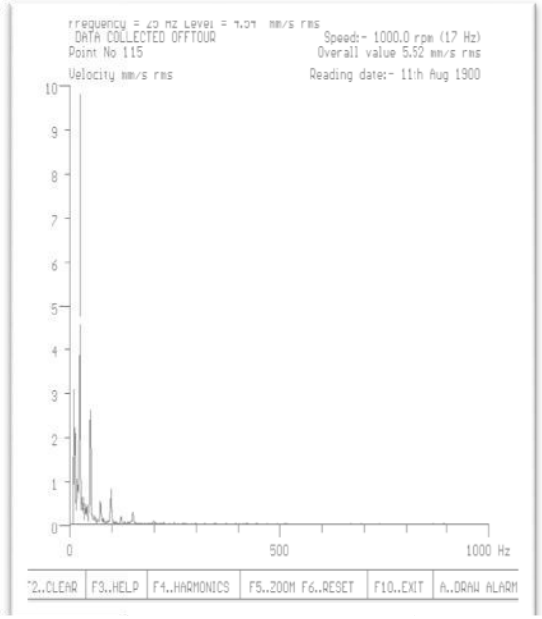

Fig. 7 Pump DE Horizontal.

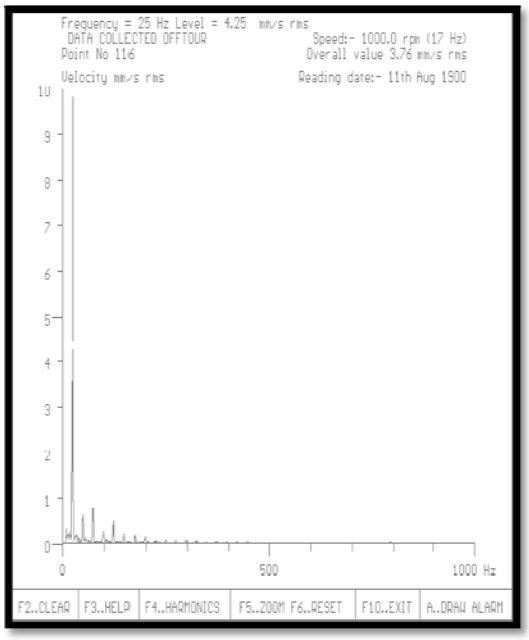

Fig. 8 Pump DE Axial.

The velocity values are not more in the vertical and in axial direction but the values more in the horizontal direction; therefore it is difficult to conclude which kind of defect is there. The advance investigation is required to find the defect which is present or may be will create in future. Table 2 represents the vibration values at the peak frequency which are collected from the spectrum at each point.

Table 2 : Overall values Motor pump assembly

Motor NDE vertical		**Motor NDE horizontal**		**Motor NDE axial**	
Freq	Vel. mm/s	Freq	Vel. mm/s	Freq	Vel. mm/s
25	4.51	25	3.31	25	4.07
50	1.09	50	0.53	50	1.65
75	0.88	75	0.26	75	1.40
Motor DE vertical		**Motor DE horizontal**		**Motor DE axial**	
Freq	Vel. mm/s	Freq	Vel. mm/s	Freq	Vel. mm/s
25	2.07	25	4.54	25	4.25
50	0.13	50	2.59	50	0.62
75	0.24	75	0.49	75	0.76
Pump DE vertical		**Pump DE horizontal**		**Pump DE axial**	
Freq	Vel. mm/s	Freq	Vel. mm/s	Freq	Vel. mm/s
25	1.9	25	2.68	25	1.92
50	0.06	50	0.37	50	0.2
75	0.28	75	0.60	75	0.31

Pump NDE vertical		**Pump NDE horizontal**		**Pump NDE axial**	
Freq	Vel. mm/s	Freq	Vel. mm/s	Freq	Vel. mm/s
25	1.07	25	1.87	25	1.87
50	0.14	50	0.26	50	0.26
75	0.21	75	0.19	75	0.17

From the Table 2, it is clear that the peak occurs at the 1x, 2x and 3x at all points and in all direction. The

values are more at the motor NDE and motor DE side, so from this it is proved that there is the misalignment between the motor and the coupling, but there is no fault in the pump or even the alignment of the pump and coupling.

VI. CONCLUSION

1. The peak occurs at the 1x, 2x and 3x rpm represents the misalignment problem.
2. Most probably the maximum peak occurs in the vertical and axial direction, but the load is transferred to the other points also so the unexpected result will also occur.
3. Vibration amplitude should be measured at all points in all the phases for finding the correct result.
4. The maximum peak occurs in the 1x direction, if it is angular misalignment.

REFERENCES

[1] Yimin Shao et.at "Gearbox vibration monitoring using extended Kalman filters and hypothesis test",journal of Sound and Vibration 325 (2009) 629–648.

[2] Mitchell, J. S.: "An Introduction to Machinery Analysis and Monitoring," Penwell Publishing Company,Tulsa, Okla., 1981.

[3] Singiresu S. Rao, " Mechanical Vibrations", chap 10, vibration measurement and application, Pearson publication, 2004.

[4] Tejas H. Patel et al., "Vibration response of misaligned rotors", Journal of Sound and Vibration 325 (2009) 609–628.

[5] Robert B. McMillan, "Rotating machinery: practical solutions to unbalance and misalignment" New York, Marcel Dekker, 2004.

[6] Sadettin Orhan , Nizami Akturk , Veli Celik, " Vibration monitoring for defectdiagnosis of rolling element bearings as a predictive maintenance tool: Comprehensivecase studies", Elsevier , NDT&E International 39 (2006), 293–298

[7] S. Ganeriwala, et at, "The truth behind misalignment vibration spectra of rotating machinery", Richmond, 2009.

[8] P. John, "Shaft Alignment Handbook", CRC Press; Taylor & Francis Group LLC, New York, NY, USA, 3rd edition, 2007.

◈◈◈

Analysis of Self Aligning Bearing System Having A Local Defect Through Vibration Signals

Shukla Rajkamal Santoshbhai & U.A.Patel

B.E. Mechanical, M.E. CAD/CAM, L.D. College of Engineering, Ahmedabad, India

Abstract **-** Modern trend of Dynamic analysis is useful in early prediction; simulation of rotor bearing system as manufacturing of prototype is time consuming, costly, and required further analysis for fatigue failure. The rolling bearings dynamical behaviour analysis is a critical condition to determine the machine vibration response. The rolling bearing, with outer ring fixed, is a multi body mechanical system with rolling elements that transmit motion and load from the inner raceway to the outer raceway. In this paper various experiment result are mentioned for study of the vibration characteristics of the bearing rotor system. Some literature study has been done before carry out this work. Dynamic analysis has become a very powerful tool for the betterment of the actual performance of the system. The methodology for prediction and validation of dynamic characteristics of bearing rotor system vibration is studied. Bearing rotor system theoretical formulation is described in this paper. The goal of this study is to prevent the system from the breakdown by continuous monitoring of vibration values.

Keywords **:** *Ballpassfrequency, rolling element,vibration monitering*

I. INTRODUCTION

A common ball bearing consists of a number of rolling elements and two rings- the inner and the outer ring with cage which is used to support the ball during motion of the bearing. Harris [13] and Gargiulo developed a non-linear stiffness coefficient matrix. This derivation is based on force displacement relations, which are commonly used by designers to design rolling element bearings. Hoon-Voon Liew, Teik C. Lim [3] in 2005 done Analysis of bearing for time varying characteristics in rolling element. Tatjana Lazovic [8] described a Mathematical Model of Load Distribution in Rolling Bearing in which External load of rolling bearing is transferred from one ring to the other one through the rolling elements. S.P.Harsha [1] in 2006 done a non linear dynamic analysis of an unbalanced rotor supported by rolling bearing, the non-linearity in the rotor bearing system is due to Hertzian contact, unbalanced rotor effect and radial internal clearance.

To reduce the friction and wear in the rolling contacts, bearings are lubricated with oil. The part of the surrounding structure that is connected to the bearing is usually referred to as the housing. The bearings and the housings have to provide sufficient static support for the shaft. The purpose of a ball bearing is to reduce rotational friction and support radial and axial loads. It achieves this by using at least two races to contain the balls and transmit the loads through the balls. Usually one of the races is held fixed. As one of the bearing races rotates it causes the balls to rotate as well. Because the balls are rolling they have a much lower coefficient of friction than if two flat surfaces were rotating on each other. Ball bearings tend to have lower load capacity for their size than other kinds of rolling-element bearings due to the smaller contact area between the balls and races.

In this paper Self-aligning ball bearings is considered whose bearing number is 1205k; it is constructed with the inner ring and ball assembly contained within an outer ring that has a spherical raceway. This construction allows the bearing to tolerate a small angular misalignment resulting from deflection or improper mounting. Experimental modal analysis, structural dynamics modification and finite element analysis were used to analyze the dynamic properties of a test structure. Most noise, vibration or failure problems in mechanical structures and systems are caused by excessive dynamic behavior. In recent years, however, the implementation of the Fast Fourier Transform (FFT) in low cost computer-based signal analyzers has provided the environmental testing laboratory with a fast and more powerful tool for acquisition and analysis of vibration data.

The FFT spectrum analyzer samples the input signal, computes the magnitude of its sine and cosine components, and displays the spectrum of these measured frequency components. The FFT is simply a clever set of operations which implements Fourier's theorem. The resulting spectrum shows the frequency components of the input signal.

The big advantage of this technique is its speed. Because FFT spectrum analyzers measure all frequency

components at the same time, the technique offers the possibility of being hundreds of times faster than traditional analogue spectrum analyzers. To measure the signal with higher resolution, the time record is increased. But again, all frequencies are examined simultaneously providing an enormous speed advantage.

II. MODELING OF THE SYSTEM

As a first step in investigating the vibrations characteristics of ball bearings, a model of a rotor bearing assembly can be considered as a spring-mass system, where the rotor acts as a mass and the raceways and balls act as mass less nonlinear contact springs. In the model, the outer race of the bearing is fixed in a rigid support and the inner race is fixed rigidly with the rotor. A constant radial vertical force acts on the bearing. Therefore, the system undergoes nonlinear vibrations under dynamic conditions. Elastic deformation between the race and ball gives a non-linear force deformation relation, which is obtained by using the Hertzian theory. Other sources of stiffness variation are the positive internal radial clearance, the finite number of balls whose position changes periodically and waviness at the inner and outer race. They cause periodic changes in stiffness of the bearing assembly. When the shaft is rotating, applied loads are supported by a few balls restricted to a narrow load region and the radial position of the inner race with respect to the outer race depends on the elastic deflections at the ball to raceways contacts. Balls are deformed as they enter the loaded zone where the mutual convergence of the bearing races takes place and the balls rebound as they move to the unloaded region.

As the time needed for a complete rotation of the cage is $2\pi/\omega_c$ the shaft will be excited at the frequency of (Nb * ω_c known as the ball passage frequency. Here ω_c is the speed of the cage. Since outer is assumed to be constant, the ball passage frequency is

$$\omega_c = \frac{\omega inner}{2}\left(1-\frac{db}{dm}\right)+\frac{\omega outer}{2}\left(1+\frac{db}{dm}\right) \quad (1)$$

$$\omega_{bp}=\frac{1}{2}N_b\frac{\omega inner}{2}\left(1-\frac{db}{dm}\right)+\frac{1}{2}Nb\frac{\omega outer}{2}\left(1+\frac{db}{dm}\right) \quad (2)$$

$$\omega_{bp}=\frac{1}{2}N_b\frac{\omega inner}{2}\left(1-\frac{db}{dm}\right) \quad (3)$$

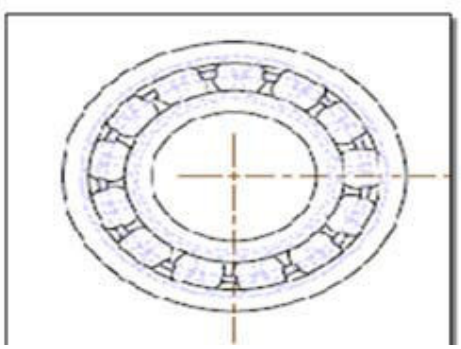

The load distribution on a rolling element bearing is given by

$$Q(\psi) = qmax[1-\frac{1}{2\xi}(1-\cos(\psi))]^n \quad (4)$$

Where q_{max}-Maximum load

Y-limiting angle

e - Load distribution factor

n= 3/2 for roller bearings

n=10/9 for ball bearings

In a bearing with nominal diametral clearance, qmax can be approximated as,

$$Qmax=\frac{5Fr}{zcosa} \quad (5)$$

Table1: Parameters for the self aligning bearing

self aligning bearing 1205k	Values
Outer diameter	52mm
Inner diameter	25mm
Thickness	15mm
Mean diameter	38.5mm
Ball diameter	8.1mm
Number of balls	26

III. EXPEMENTAL SETUP

An experimental test rig built to predict defects in self aligning bearings is shown in Figure2. The test rig consists of a shaft with central rotor, which is supported on two bearings. A motor coupled by a flexible coupling drives the shaft.

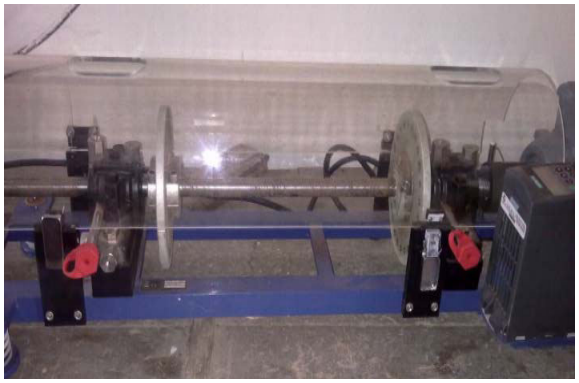

Figure 2: Experimental setup for bearing testing

Self aligning double row ball bearing is mounted at driver end and other defective bearing is mounted at free end.

V. RESULT AND DISCUSSION:

Vibration characteristics are very important in the study of diagnostics for the system. In the experiment setup two bearing are considered in which one bearing was without defect and other bearing was with defect, both the bearing was attached to the system one by one for carry out the result. The dimension of the bearing are given in the Table 1. After taking the result it was seen that the values of amplitudes was more for the bearing with defect compare to bearing which has no defect. The natural frequency of the system was around the 34hz,it was seen at the time of processing the data that for the defect bearing the values of amplitude was increasing when frequency of the was nearby natural frequency of the system. The various values of accerlation, velocity for the study of the vibration characteristics were taken and these are shown in the figure respectively.

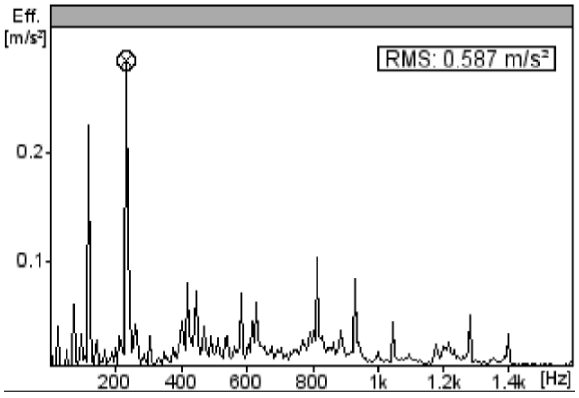

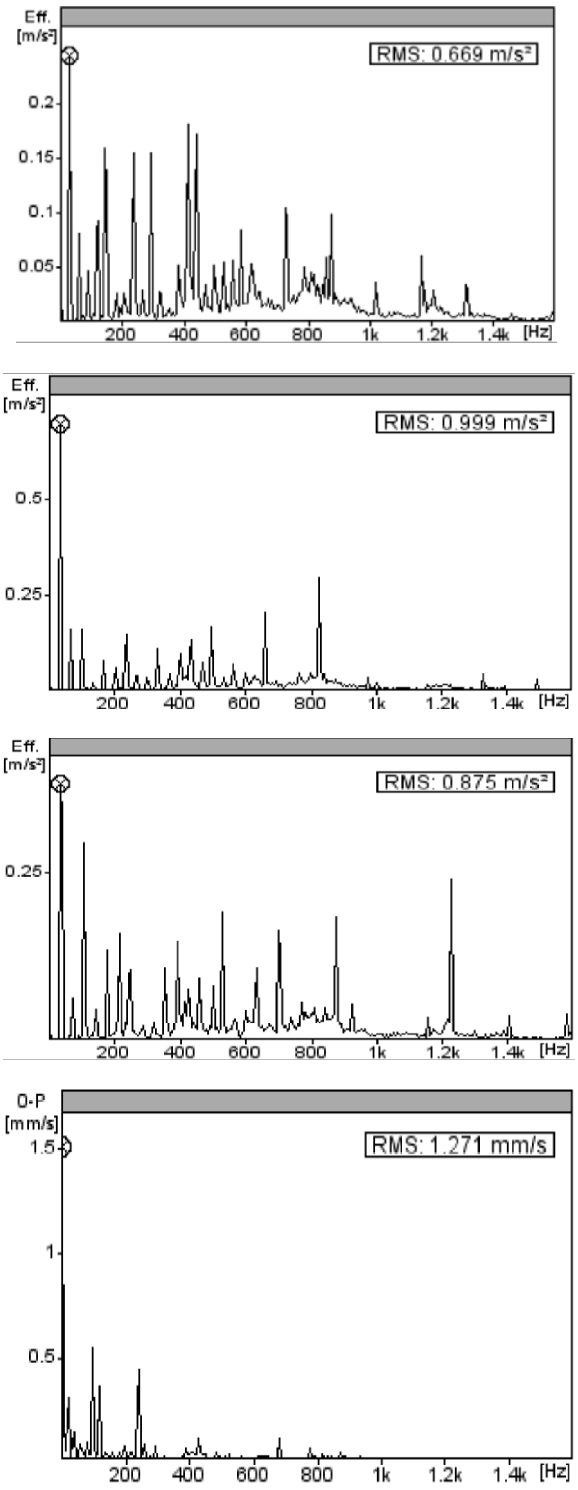

Figure3 (A, B, C, D, and E): amplitude values in terms of Accerlation at different shaft speed

Figure 3A is showing the result of amplitudes in terms of accerlation which has value 0.269m/s^2 at 240Hz, at this time the shaft speed was 1200rpm.Similarly figure 3B has accerlation value 0.287m/s^2 at 233Hz for shaft speed 1440rpm.Figure 3(C, D, E) showing the values of amplitude in terms of accerlation which are 0.669m/s^2,0.384m/s^2,0.746m/s^2 which is obtained at 33.50Hz, 35.50Hz, and 239.00Hz at corresponding 2040rpm, 2160rpm and 2400rpm.By comparing this accerlation amplitude values with bearing system which has no defect in the bearing it was seen that both frequency and amplitude values were varying in the same fashion which is in the bearing system with defect. Also the amplitude values for defect bearing system were much higher than the bearing system which was without defect. The frequency values at which peak was obtaining was continuously decreasing before the natural frequency was achieved but it was continuously increasing when it goes above the natural frequency.

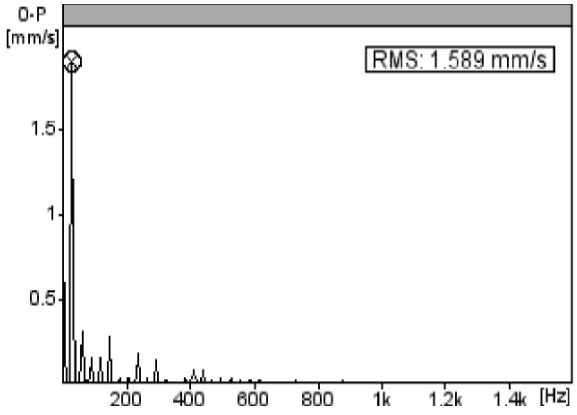

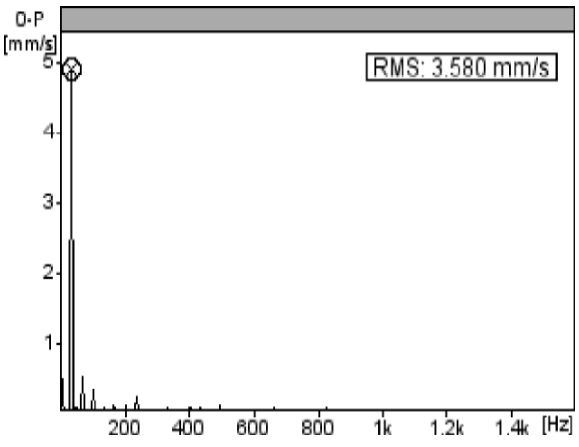

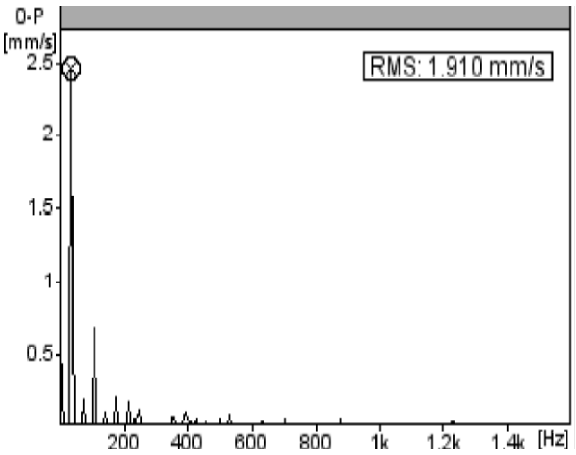

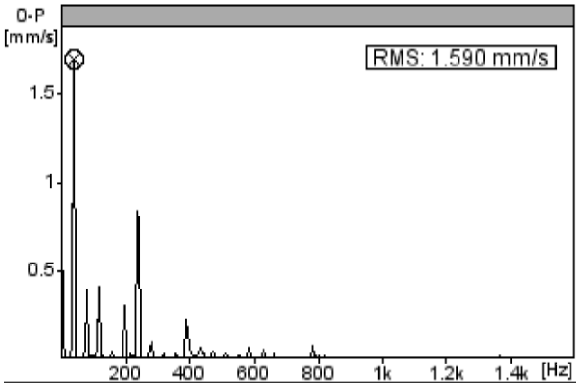

Figure4 (A.B, C, and D): Amplitude values in terms of velocities for different shaft speed

In the experiment setup two bearing was considered in which one of the bearing the defect has in the outer ring of 0.2mm^3 volume. This defect volume was eight in number and was placed along the outer ring in two rows. Figure 4A is showing the amplitude values in terms of velocity which nearby 1.520mm/second for shaft speed 1200rpm. Similarly Figure 4(B, C, and D) is showing the amplitude values for vibration characteristics in terms of velocity as 3.580mm/second,1.920 mm/second,1.590mm/second. In this the same result as in accerlation terms was obtained when it was compare with the bearing system which has no defect.

V. CONCLUSION:

It has been shown that experiment modelling can be effectively used to differentiate between vibration signatures of two bearing system in which one is running without defect and other is running with the local defective bearing. The vibration characteristics has been studied through this experiment and conclusion

have been made that the amplitude values was more for defect system compare to the system which was running without defect. The natural frequency of the system was around 34Hz because for both the system the amplitude that was obtained during the study of the experimental result was maximum than any other values. Assumptions have been made for the variation of forces exerted by the rolling element on the outer ring in the vicinity of the defect. Though the values for the forces employed in this analysis are not exact, the aim has been to understand the trend of vibration signatures. Two systems have been studied with and without defect the vibration accerlation and velocity plots were generated with the help of FFT analyser. An objective method to compare the defect size was proposed and its application to the two cases was demonstrated. A more detailed analysis based on this project could point to a way for comparing the defect sizes based on the vibration signatures.

VI. FUTURE WORK:

It is important to be able to precisely understand the variation of forces due to the rolling element passing over a defect in a bearing. A detailed analysis using FEA on a bearing structure should be performed. The finite element model can then be iteratively adjusted so as to conform to the vibration signature that is arrived at by experimentation. Such an exercise would improve the accuracy of the finite element modelling results.

ACKNOWLEDGEMENT:

I owe a great many thanks to a many people who helped and supported me during mine dissertation work, from bottom of my heart I want to thank my guide prof.U.A.patel who correct me and guided me throughout my dissertation work. I want to extent my thanks to D.N.Shah sir who is the assistance of dynamic laboratory of L.D.College of Engineering.

REFERENCES:

1. S.P. Harsha, “Nonlinear dynamic analysis of an un balanced rotor supported by roller bearing” World Academy of science, Engineering and technology(76),2004
2. Jang, G.H., & Jeong, S. W, “Vibration Analysis of a rotating System Due to the Effect of Ball Bearing Waviness”, Journal of Sound and Vibration (269) 2004, 709-726.
3. Hoon Voon Liew,“Analysis of time varying rolling element bearing characteristics, “ Jounral of sound and vibration 283,1163- 1179
4. Roger boustang,“ A subspace method for the blind extraction of a Cyclostationary sources: application to rolling element bearing diagnostics, mechanical system and signal processing (19) 2005,1245-1259
5. R.K.Purohit, “Dynamic analysis of ball bearing with effect of preload and number of ball,” International journal of applied mechanics and engineering,vol.11 2006, pp 77-91
6. Qiuhua Du,“Application of the EMD method in the vibration analysis of the ball bearing,” mechanical system and signal processing (21) 2007, 2634-2644
7. H.Mohammadi, “Prediction of defect using vibration signal analysis,” World applied science journal 4(1): 150-154
8. Tatjana Lazovic,“ Mathematical model of load distribution on rolling bearing: Faculty of mechanical engineering 2008 (36),189-196
9. Abhay Utpat, R.B. Ingle and M.R.Nandgaonkar, “A model for study of the defects in rolling element bearings at higher speed by vibration signature analysis,” World Academy of science, Engineering and technology 2009 (56)
10. M.S Patil, Jose Mathew & P.K. Rajendrakumar, “A theoretical model to predict the effect of localized defect on vibrations associated with ball bearing,” International journal of mechanical science(52) 2010, 1193-1201
11. Radoslav tomavic, “Calculation of the boundary values of rolling bearing deflection in relation to the number of active rolling elements,” Mechanism and machine theory (21) 2011,364-368.
12. Chen Wenham, “Quasi static analysis of thrust – loaded angular contact bearing Part 1: theoretical

◈◈◈

Effect of Number of Spots On The Shear Strength of spot Welded Lap Shear Specimen

Prasad P Kulkarni & M. L. Kulkarni

Mechanical Dept SVERI's College of Engineering, Pandharpur

Abstract **-** The effect of number of spots, distance between two spots, squeezing force, welding current and sheet thickness on the shear strength of two similar galvanized steel sheets are investigated through experiments using Taguchi method. Similar sheets of galvanized steel sheets are made by resistance spot welding at different processing conditions and these joint populations were tested under lap-shear loading conditions. Fixture is used to load the lap shear specimen in the universal testing machine Regression analysis is done to obtain relationship between shear strength and selected parameters. The experimental results indicate that the failure loads of spot welds in lap-shear specimens increase when number of spot squeezing force, welding current and sheet thickness increase for the given ranges.

Keywords-*Number of spots, Shear Strength, Process parameters*

I. INTRODUCTION

Resistance spot welding (RSW) is a process of joining metal components through the fusion of discrete spots at the interface of the work pieces . It is one of the most useful and practical methods for the manufacture of sheet metal assemblies. This process is common for welding sheets of aluminum, stainless steel, titanium alloys etc. A typical automobile consists of more than 5000 spots [1].This study gives relationship among process parameters and strength of spot weld. Galvanized sheets are spot welded at permissible level of parameters so as to visualize interfacial mode of failure after tensile shear test [2]. Author considered processing time as parameter. It was observed that shear strength of spot weld increases with increasing processing time [3]. This study consists of application of Taguchi method to study effect of process parameters on strength of spot weld [4]. This study consists of relationship between pre-straining and shear strength of spot weld [5]. Lap shear specimen is used and its fatigue strength is obtained through experimentation .Effect of nugget diameter on fatigue strength of spot weld is studied [6]. Effect of fusion zone size on the shear strength is studied [7]. Experiments were planned on the basis of response surface methodology (RSM) [8].Strength of spot weld defines the quality of integrated structure of automobile and improves the reliability of assembled sheets. Structural stability of multi spot welded structure depends upon number of spots, their locations and variable loads acting on it. So, investigation on the relations between the strength of spot weld and number of spots is the key to solve problem in the design of multi-spot welded structure. Effect of different parameters can be seen on cause effect diagram.

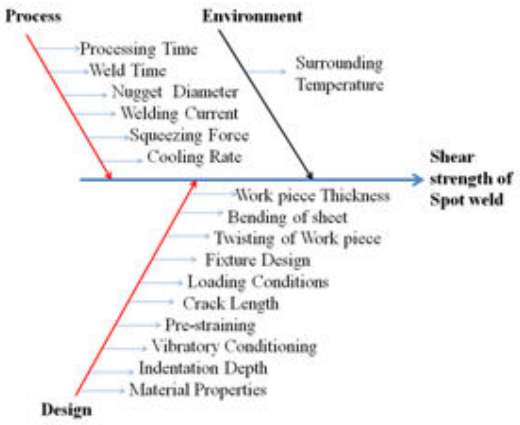

Fig.1. Cause-effect diagram

The diameter of the spot weld nugget, d, is chosen based on an empirical formula recommended by the American Welding Society (AWS), diameter of nugget is considered as follows.

$$d \geq 4\sqrt{t} \qquad (1)$$

However, several author claim that this equation is not safe for thickness beyond 1.5 mm. Though the effect of the process parameters on the mechanical behavior of resistance spot welds on steels is well documented, study of failure modes of spot weld.

Table I .Chemical Composition of Galvanized steel sheet

T.S	Y.S	Alloying elements (wt%)					
MPa							
		c	Mn	Si	S	p	Cr
350	240	0.16	0.30	0.25	0.030	0.03	0.004

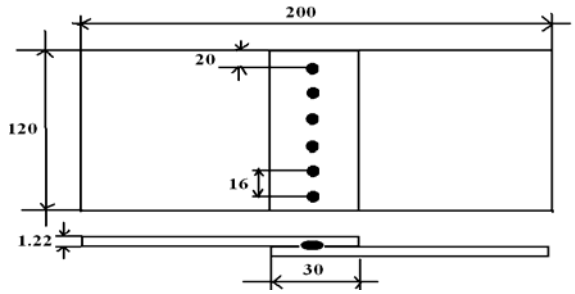

Fig.2. Dimensions of tensile-shear test specimens (not to scale, dimensions in mm).

The welds were done using a RSW electric resistance spot welding machine, with a nominal welding power of 10 kVA.

II. EXPERIMENTAL PROCEDURE

Mechanical properties of galvanized steels are given in Table 1. Resistance spot welding lap joints were done on specimens of 120 mm× 200 mm×1.22mm in size.Figure2 shows the geometry and dimensions of the welded specimens. Sheet surfaces were randomly abraded with silicon carbide paper P220 grade

Fig.3 Local display of experimental set up

Table II Ranges of parameters

Sr	Parameters	Ranges		
No.	**and Designations**	Low	Middle	High
1	Force (F)	700	800	900
2	Number of spots(n)	2	4	6
3	Distance between two spots(X)	12	14	16
4	Thickness(t)	0.71	0.91	1.22
5	Current(I)	7	8	9

Table III Resistance spot welding parameters and corresponding strength (Taguchi's L_{27} Array)

F (N)	n	X (mm)	t (mm)	I (KA)	P(N)
700	2	12	0.71	7	3000.23
700	2	14	0.91	8	5002.63
700	2	16	1.22	9	7997.59
800	4	12	0.71	7	5870.96
800	4	14	0.91	8	7205.01
800	4	16	1.22	9	8201.75
900	6	12	0.71	7	4991.97
900	6	14	0.91	8	6857.89
900	6	16	1.22	9	8596.89
800	6	12	0.91	9	5089.6
800	6	14	1.22	7	7956.87
800	6	16	0.71	8	5895.5
900	2	12	0.91	9	3574.26
900	2	14	1.22	7	7958.544
900	2	16	0.71	8	6578.68
700	4	12	0.91	9	7856.56
700	4	14	1.22	7	5904.6
700	4	16	0.71	8	5917.6
900	4	12	1.22	8	6897.5
900	4	14	0.71	9	4058.56
900	4	16	0.91	7	5123.68
700	6	12	1.22	8	7158.56
700	6	14	0.71	9	5891.56
700	6	16	0.91	7	7589.51
800	2	12	1.22	8	5478.54
800	2	14	0.71	9	4789.54
800	2	16	0.91	7	5017.45

The shear strength testing was done in a servo hydraulic Universal Testing machine at a constant cross-head speed of 1.31mm/min up to the final failure of the joint. Specimen failed Partially by pull out faiure mode

under constant loading velocity. Eqaution 2 is regression equation

$$P = -3707 + 147\,I + 4210t + 306\,X + 295n - 0.93f \quad (2)$$

Where,

P=Shear Strength in N.

I=Current in Kamp.

T=Thickness in mm

X=Distance between two spots

n= Number of spots

f=Electrode force in N

III RESULT AND DISCUSSION

According to the results of experimentations and regression analysis, effect of number of spot, distance between two spot, electrode force, weld current and specimen thickness is obtained. Scattered plots are drawn according to the design matrix L_{27} of Taguchi. All spots are failed at once due to axially applied load and it is uniformly distributed over sheet surface.

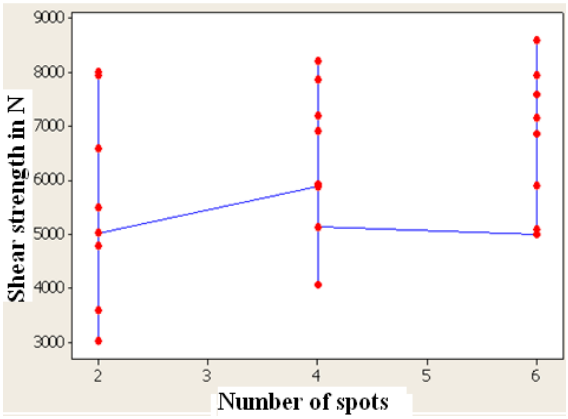

Fig. 4 Relationship between strength and number of spots

It is observed that there is significant increase in shear strength of spot weld when number of spot increase .Figure 4.shows relationship between number of spot and shear strength of spot weld. Specimens having six number of spot but made at lower values of other parameters , got the strength in between the range 3000N-5000N.Spot welds made at lower level are failed in interfacial failure mode while spot welds made at higher level are failed at pullout failure mode.

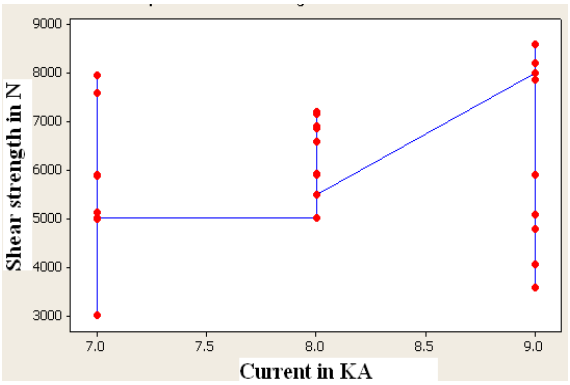

Fig .5 Relationship between shear strength and current

It is observed that there is significant increase in shear strength of spot weld when spot welding current increases .Figure 5 shows relationship between spot welding current and shear strength of spot weld. Spot welds made at 9 Kamp current and having six number of spots, got the strength in between the range 7500N-8500N.Spot welds made at 9 Kamp current but having lower value of thickness and number of spot, got the strength in between the range 3000N-4500N.

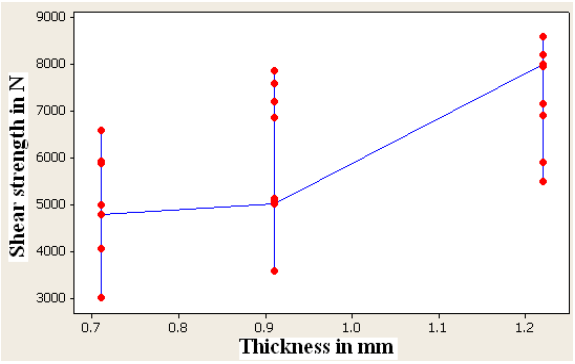

Fig 6 Relationship between Specimen thickness and shear strength of spot weld

It is observed that there is significant increase in shear strength of spot weld when specimen thickness increases. Figure 6 shows relationship between Specimen thickness and shear strength of spot weld. Spot welds made 1.22 mm thickness and having six numbers of spots, got the strength in between the range 7500N-8500N. It is observed that compromising with number of spots and increasing specimen thickness shear strength can be improved. Spot welds made 1.22mm thickness but having lower value of current and number of spot, got the strength in between the range 3050N-4500N.

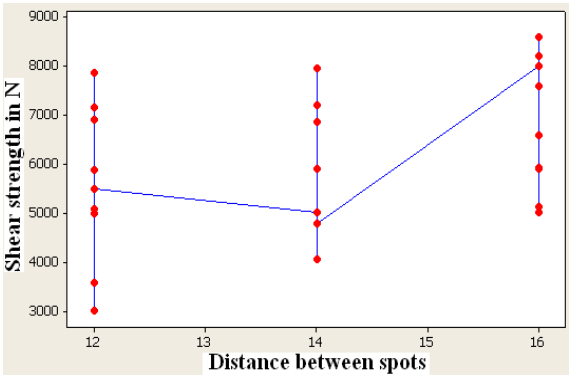

Fig 7 Relationship between distance between spots and shear strength of spot weld.

It is observed that there is significant decrease in shear strength of spot weld when distance between two spot decreases in between range 10mm-13mm.This is the least range at which there was no overlapping of two spots. Figure 7 shows relationship between distance between two spot and shear strength of spot weld. Spot welds made at distance 16 mm and having six numbers of spots, got the strength in between the range 7500N-8500N. It is observed that up to certain range of distance between two spots, shear strength increases and after that strength decreases. Spot welds made 1.22mm thickness but having lower value of current and number of spot, got the strength in between the range 3050N-4500N.

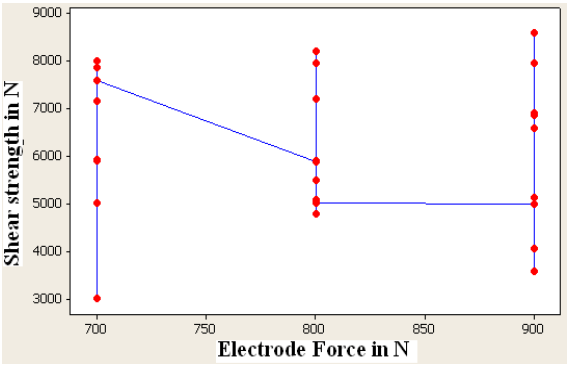

Fig.8 Relationship between electrode force and shear strength of spot weld..

It is observed that there is significant increase in shear strength of spot weld when electrode force increases .Figure 8 shows relationship between electrode force and shear strength of spot weld. Spot welds made at 900N force and having six number of spots, got the strength in between the range 7500N-8500N.Spot welds made at 900N force but having lower value of thickness and number of spot, got the strength in between the range 3000N-4500N

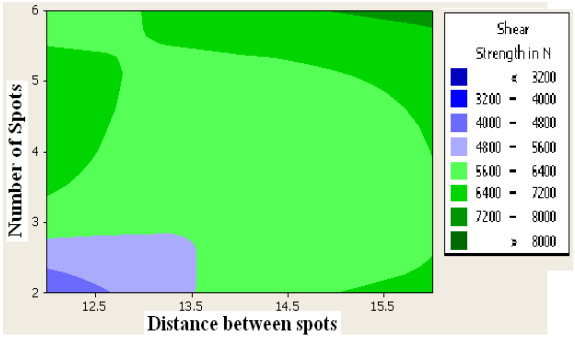

Fig. 9 Shear Strength Vs Number of spots and distance between two spot

Figure 9 shows contour plot of Shear Strength Vs Number of spots and distance between two spot. Specimens which are having number of spot four and five at the same time, specimens having distance between two spots 11.5mm to 12.5 failed in the green colored region. It has shear strength in the region 6400-7200N. Specimens which are having number of spot six and at the same time, specimens having distance between two spots 14.75mm to 16 in the region 6400-7200N.

Table IV Result of Confirmation test (P in N)

Sr.No	Regression model	Experimental
1	4801.1	4806.78
2	3330.1	3319.13

IV. CONCLUSION

The conclusions obtained are summarised as follow

1 The Taguchi's L27 array is used to evaluate the effects of selected spot welding process and design parameters. It is an effective method used in the experimental design and the investigation for regression models between spot welding process and RSW quality of galvanized steel sheet.

2 The effect of selected welding process parameters and design parameters on the tensile–shear strength can be analyzed on the basis of mathematical regression models of galvanized steel sheet and it can provide profitable reference to welding process devising as an assistant means.

3 The effect of number of spots on the shear strength of spot weld is analyzed. There is significant increase in the strength of spot weld as number of spots increase. Moreover, effect of distance

between two spot on the strength is analyzed. This study helps to find optimum number of spots and optimum distance between two spot.

REFERENCES

[1]. V.X. Trana, J. Pana,, T. Panb, "Effects of Processing Time on Strengths and Failure Modes of Dissimilar Spot Friction Welds Between Aluminum 5754-O and 7075-T6 Sheets" J materials processing technology 209(2009)3724–3739.

[2]. Luo Yi a,b,, Liu Jinhe , Xu Huibin , Xiong Chengzhi , Liu Lin , "Regression Modeling And Process Analysis Of Resistance Spot Welding On Galvanized Steel Sheet". Materials and Design 30 (2009) 2547–2555

[3]. A.M. Pereira, J.M. Ferreira . A. Loureiro, J.D.M. Costa , P.J. Bártolo, "Effect of Process Parameters on The Strength of Resistance Spot Welds In 6082-T6 Aluminium Alloy". Materials and Design31(2010)2454–2463

[4]. A.G Thakur and V.M Nandedakar, "Application of Taguchi Method to Determine Resistance Spot Welding Conditions. of Austenitic Stainless Steel AISI304",Journal of scientific research Vol No.69 ,Septmber 2010 pp.680-683.

[5]. G. Mukhopadhyay .S. Bhattacharya b, K.K. Ray a, "Effect of Pre-Strain on The Strength of Spot-Welds". Materials and Design 30 (2009) 2345–2354.

[6]. M. Vural , A. Akkus,, B. Eryurek, "Effect of Welding Nugget Diameter on The Fatigue Strength of The Resistance Spot Welded Joints of Different Steel Sheets". J Materials Processing Technology 176 (2006) 127–132.

[7]. M. Pouranvari , S.M. Mousavizadeh , S.P.H. Marashi , M. Goodarzi , M. Ghorbani , "Influence of Fusion Zone Size And Failure Mode on Mechanical Performance of Dissimilar Resistance Spot Welds of AISI 1008 Low Carbon Steel And DP600 Advanced High Strength Steel".J Materials and Design xxx (2010) xxx–xxx.

[8]. S.M. Darwish*, S.D. Al-Dekhial, "Statistical Models For Spot Welding Of Commercial Aluminium Sheets", International Journal of Machine Tools & Manufacture 39 (1999) 1589–1610.

◈◈◈

Hydrogen Production from Ethanol for PEM Fuel Cell Using Auto-Thermal Reformer

Pritesh K Jaradi & C Somayaji

Dept. Mechanical Engineering, Indian Institute of Technology Guwahati, Guwahati, India - 781039

Abstract - This paper presents the results of a study for a PEM fuel cell system. The major system components are an auto-thermal reformer, high and low temperature shift reactors, a preferential oxidation reactor, a PEM fuel cell. The process simulation package 'ASPEN-HYSYS 2006.5' has been used along with conventional calculations. The operation conditions of the auto-thermal reformer have been studied in detail to determine the values, which lead to the production of a hydrogen rich gas mixture with CO concentration at ppm level. The operation parameters of the other reactors have been determined considering the limitations implied by the catalysts involved. Hydrocarbon fuel ethanol has been studied as the source for hydrogen production. The chemical composition of the hydrocarbon fuel affects the favorable operation conditions of auto-thermal reforming and the following fuel purification steps.

Keywords - *auto-thermal reforming; ethanol; hydrogen; fuel cell*

I. INTRODUCTION

In recent years, increasing environmental concerns over vehicle-generated pollution and increasing demand for energy sources have generated interest in alternative fuels and energy sources. The high efficiency and near-zero emissions of fuel cells make it a potential alternative energy source for both automotive and stationary power applications. Fuel cell energy is anticipated to replace traditional power sources in the future. One of the most critical challenges facing the world is the development of clean, reliable, and efficient energy conversion processes. As the demand for energy will inevitably increase, at the same time, it is widely accepted that this increasing demand for energy must not compromise the environment (i.e. pollution, CO emission, greenhouse effect & global warming).

Advanced technologies designed to meet this challenge include processes as wind, solar, hydroelectric, photovoltaic, and others. Among the most promising technologies are those based on fuel cells, which convert chemical energy into electrical energy with higher efficiencies and far fewer environmental effects than other options.

Since most fuel cells are powered by hydrogen, the most likely solution to generate hydrogen is by extracting it from hydrocarbon fuels such as natural gas, methanol, gasoline or ethanol. There are mainly three types of reforming technologies available, namely steam reforming (SR), partial oxidation reforming (POX) and auto-thermal reforming (ATR). Auto-thermal reforming is the combination of steam-reforming (SR) and partial-oxidation (POX), in order to achieve a minimum energy input necessary to maintain the required reformer temperature.

II. PROBLEM STATEMENT

It is desired to construct a simulation of an ethanol fuel processor to identify potential design issues and obtain a preliminary estimate of the variation of species concentration and temperature. Significant variation in output can be identified and their effect on the overall system performance can be evaluated.

A. Objective of Study

The objective of this study is to develop and study a steady state model of hydrogen production for fuel cell applications from ethanol.

Scopes for this study are:

1) *To develop steady state base case study model using simulation tool Aspen HYSYS 2006.5.*
2) *Heta integration between three material streams i.e. ethanol, air and water*
3) *To perform clean-up process to reduce carbon monoxide (CO) concentration.*

III. MODELLING

A. Assumption

1) *In the modelling of fuel processing unit, it is assumed that there are no piping losses and frictional losses.*
2) *Reformer is modelled under steady state condition, i.e. hydrogen rich gas is generated at steady state.*
3) *All the reactors are assumed to be homogeneous*
4) *Ethanol is assumed to be fully converted in the reformer reactor.*
5) *PEM fuel cell modelling is carried out for dynamic conditions taking the practical fuel cell operation into consideration*
6) *Effect of Nitrogen is not considered.*

B. Fuel Processing Unit

ASPEN Hysys® has been chosen as the process simulator for this research, since it interactively interprets commands as they are entered one at a time and the information propagates both in forward and reverse directions, performing back-calculation in a non-sequential manner.

a) Process Description

The fuel processing unit can be divided into auto-thermal reactor (ATR), water-gas-shift (WGS) reactor and preferential Oxidation (PROX) reactor [7]. The outlet stream from ATR will enter the WGS reactor. There are three reactors in WGS section; high temperature shift (HTS), medium temperature shift (MTS) and low temperature shift (LTS). Finally, the product gases from the WGS enter the PROX reactor and the product will be thus ready to enter the fuel cell [6].

b) Conversion Process

Mixture of ethanol, air and water are fed into a single auto-thermal reactor (ATR) in vapour phase. The reaction that occurs inside the ATR is as follows [1].

$$7CH_3CH_2OH + 5.5O_2 + 2H_2O \rightarrow 6CO_2 + 8CO + 23H_2 \quad (1)$$

Ethanol (boiling point 78.4 ^{0}C) and water (boiling point 100 ^{0}C) are heated to 100 ^{0}C to convert them into gas phase. Air was heated up to 100 ^{0}C to increase the rate of reaction. Pressure for the system is maintained at 1 atm.

c) Water Gas Shift (WGS) reactor

The CO is produced as a by-product in ATR along with H2. Water gas shift reaction (WGS) and Preferential oxidation (PROX) reactions are used for reducing the percentage of CO in the output stream of ATR.The output from the ATR is cooled down to a suitable temperature in the cooler and then supplied to the HTS. In the HTS, CO reacts with H2O to form hydrogen and CO2. The outlet from the HTS is passed through a cooler before entering the MTS. In the MTS, some amount of CO reacted with water and the process repeat until LTS reactor.

$$CO + H_2O \rightarrow CO_2 + H_2 \quad (2)$$

d) Preferential Oxidation (PROX) Reactor

The PROX is attached after the WGS unit. It is required in order to reduce the CO concentration to permissible levels. The PROX reactor was modelled as a conversion reactor based on two reactions to oxidize CO.

$$CO + \frac{1}{2}O_2 \rightarrow CO_2 \quad (3)$$

$$H_2 + \frac{1}{2}O_2 \rightarrow H_2O \quad (4)$$

C. PEM Fuel Cell

The modelling and analysis of fuel cell is carried out by dividing the entire fuel cell into three control volumes viz cathode channel, anode channel and membrane electrode assembly [2]. The electrons are passed through the external load as current to the cathode and the H+ ion goes through the membrane. In the cathode, the electron, H+ ion and oxygen are combined to form water and some amount of heat is also generated.

$$H_2 \rightarrow 2H^+ + 2\bar{e} \quad \text{(Anode)} \quad (5)$$

$$2H^+ + \frac{1}{2}O_2 \rightarrow H_2O \quad \text{(Cathode)} \quad (6)$$

a) *General governing equations*

For analyzing the control volume we use continuity and energy equation to each of the three control volumes. The physical properties associated with the control volumes are assumed to be uniform. The continuity equation in integral form is given as

$$\frac{\partial}{\partial t}\iiint_{CV} \rho dV + \iint_{CS} \rho(\vec{V}.\vec{n})\, dA = 0 \quad (7)$$

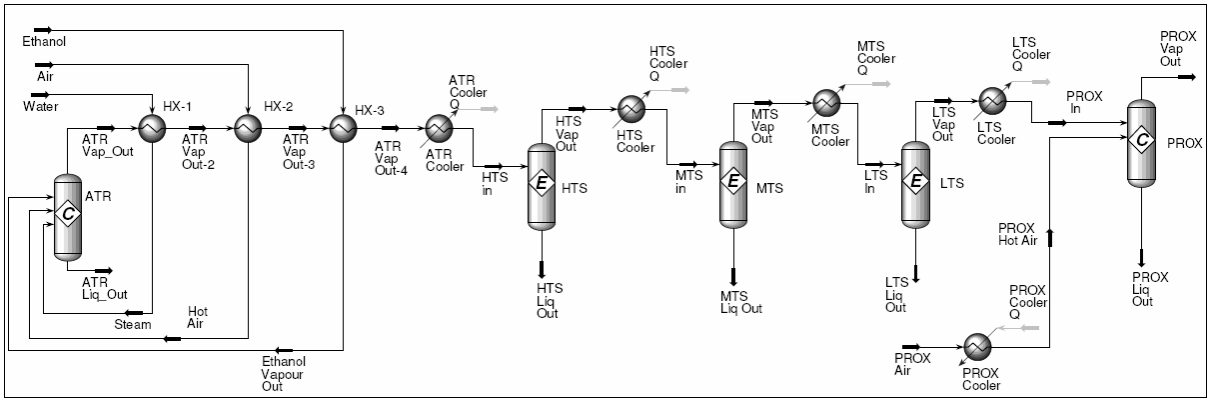

Figure 1 : Fuel Processing Unit in Hysys 2006.5

.

$$\frac{\partial}{\partial t}\iiint_{CV}\rho dV+\iint_{CS}\rho(\vec{V}.\vec{n})\,dA=0$$

Energy equation is given as,

$$\frac{\partial}{\partial t}\iiint_{CV}\rho e_t dV+\iint_{CS}\rho h(\vec{V}.\vec{n})\,dA=\frac{dQ}{dt}+\frac{dW}{dt} \quad (8)$$

$\vec{V}$ is velocity vector of flow fluid, $\vec{n}$ the unit vector normal to the control surface toward the outside, e_t the specific internal energy, Q the heat added to the control volume, and W the work done on the control volume .

b) Anode and Cathode channel Dynamics

For anode and cathode channel, the first term in the continuity equation represents the rate of change of masses in the control volumes and second term is mass flow rate through the surface of the control volumes. The different flows are, mass entering to the channel, mass consumed for the reaction and mass leaving the channel.

Hydrogen mass flow rate through the control surface of Anode [8].

The rate of change of mass of hydrogen in the anode channel,

$$\frac{\partial}{\partial t}\iiint_{CV}\rho_{H_2}dV=\frac{dm_{H_2}}{dt} \quad (9)$$

Hydrogen mass flow rate through the control surface,

$$-\iint_{CS}\rho h_{H_2}(\vec{V}.\vec{n})\,dA=k_{up,an}\left(P_{s,an}-P_{an}\right)-k_{down,an}\left(P_{an}-P_{atm}\right)-N\frac{i}{2F}M_{H_2} \quad (10)$$

$k_{up,an}$ and $k_{down,an}$ are input and output anode mass flow rate coefficient. $P_{s,an}$, P_{an} and P_{atm} are source, anode and atmospheric pressure respectively. N number of cells in stack. i is the cell current and M_{H_2} molecular weight of hydrogen. F is Faraday constant.

Rate of change of energy in the anode channel control volume,

$$\frac{\partial}{\partial t}\iiint_{CV}\rho_{H_2}e_t dV=\frac{d\left(m_{H_2}c_{v,H_2}T_{an}\right)}{dt} \quad (11)$$

Where c_{v,H_2} is specific is heat of hydrogen at constant volume and T_{an} is the anode temperature.

The heat transfer to the anode channel control volume through the hydrogen mass transfer through the anode channel control surface,

$$-\iint_{cs}\rho_{H_2}h_{H_2}(\vec{V}.\vec{n}dA)=k_{up,an}(P_{s,an}-P_{an})c_{P_{H_2}}(T_{an,in}-T_0)-k_{down,an}(P_{an}-P_{atm})c_{P_{H_2}}(T_{an}-T_0)-N\frac{i}{2F}M_{H_2}c_{P_{H_2}}(T_{an}-T_0) \quad (12)$$

The convection heat transfer between cell body and anode channel is

$$\frac{dQ}{dt} = k_{conv,an}(T_{body} - T_{an}) \quad (13)$$

Where, $k_{conv,an}$ is the total heat convection coefficient and T_{body} is temperature of the cell body.

The work done by the hydrogen mass flow to the system is negligible i.e. $\frac{dW}{dt}$=0. By combining equations (9) and (10) we can calculate hydrogen mass changes and by the equations (11), (12) and (13) anode temperature.

The rate of change of mass of oxygen in the cathode channel,

$$\frac{\partial}{\partial t}\iiint_{cv} \rho_{O_2} dV = \frac{dm_{O_2}}{dt} \quad (14)$$

Oxygen mass flow rate through the cathode control surface,

$$-\iint_{cs} \rho_{O_2}(\vec{V}.\vec{n}\,dA) = k_{up,ca}(P_{s,ca} - P_{ca}) - k_{down,ca}(P_{ca} - P_{atm}) - N\frac{i}{4F}M_{O_2} \quad (15)$$

$k_{up,ca}$, $k_{down,ca}$ are inlet and outlet cathode mass flow rate coefficient. $P_{s,ca}$ and P_{ca} are the supply cathode pressure and cathode pressure respectively.

Rate of change of energy in the cathode channel control volume,

$$\frac{\partial}{\partial t}\iiint_{CV} \rho_{O_2} e_t dV = \frac{d(m_{O_2} C_{v_{O_2}} T_{an})}{dt} \quad (16)$$

The heat transfer to the cathode channel control volume through the oxygen mass transfer through the anode channel control surface,

$$-\iint_{cs} \rho_{O_2} h_{O_2}(\vec{V}.\vec{n}\,dA) = k_{up,ca}(P_{s,ca} - P_{ca})c_{P_{O_2}}(T_{ca,in} - T_0) - k_{down,ca}(P_{ca} - P_{atm})c_{P_{O_2}}(T_{ca} - T_0) - N\frac{i}{4F}M_{O_2}c_{P_{O_2}}(T_{ca} - T_0) \quad (17)$$

The convection heat transfer between cell body and cathode channel is,

$$\frac{dQ}{dt} = k_{conv,cath}(T_{body} - T_{cath}) \quad (18)$$

By combining equations (14) and (15) we can calculate oxygen mass changes and by the equations (16), (17) and (18) cathode temperature.

c) Cell Body Dynamic equations

In the cell body the rate of change of mass is nearly equal to zero. The mass of water generated in the cell body is very less compared to the cell body mass so we can say as,

$$\frac{\partial}{\partial t}\iiint_{cv} \rho_{body} dV = 0 \quad (19)$$

Mass flow rate through the cell body control surface,

$$-\iint_{cs} \rho_{body}(\vec{V}.\vec{n}\,dA) = N\frac{i}{2F}M_{H_2} + N\frac{i}{4F}M_{O_2} - m_{H_2O} \quad (20)$$

Rate of change of energy in the cell body control volume,

$$\frac{\partial}{\partial t}\iiint_{cv} \rho_{body} e_t dV = \frac{d(m_{body} C_{p_{body}} T_{body})}{dt} \quad (21)$$

In the cell body we can say that both heat and work output will get therefore the energy equation to the fuel cell body can be written as follows,

$$\frac{dQ}{dt} + \frac{dW}{dt} = k_{conv,an}(T_{an} - T_{body}) + k_{conv,ca}(T_{ca} - T_{body}) + k_{conv,amb}(T_{amb} - T_{body}) - \Delta H_{R,T} N\frac{i}{2F}M_{H_2} - NV_{cell}i \quad (22)$$

d) Electro-chemical equations

The fuel cell output voltage is always less than the theoretical voltage this is because of losses. Meanly there are two types of losses in it ohmic voltage loss and activation.

voltage loss. The actual output voltage of the fuel cell is reducing these voltage losses from the Ernest voltage [5].

Nernst voltage,

$$E_{Nernst} = 1.229 - (8.5e-4)(T_{body} - 298.15) + (4.308e-5)T_{body}[\ln(P_{H_2}) + 0.5\ln(P_{O_2})] \quad (23)$$

Where P_{H_2} and P_{O_2} are the partial pressure of hydrogen and oxygen respectively,

Activation voltage,

$$\eta_{act} = \zeta_1 + \zeta_2 T_{body} + \zeta_3 T_{body} ln(i) + \zeta_4 T_{body} ln(C_{O_2}) \quad (24)$$

Where ζ_1, ζ_2, ζ_3 and ζ_4 are empirical constants and C_{O_2} is the concentration of oxygen

$$C_{O_2} = \frac{P_{O_2}}{508e6\,exp\left(\frac{-498}{T}\right)} \quad (25)$$

Ohmic voltage loss,

$$\eta_{Ohmic} = i\left(\zeta_5 + \zeta_6 T_{body} + \zeta_7 i\right) \quad (26)$$

Due to the collection of charges on the electrode and electrolyte there is a effect of capacitance will occur for incorporating this dynamic effect the activation voltage will change as follows , [6]

$$\frac{dv_{act}}{dt} = \frac{i}{C} - \frac{v_{act}}{R_a C} \quad (27)$$

Therefore the output voltage of the fuel cell can be written as,

$$V = E_{Nernst} + \eta_{Ohmic} + V_{act} \quad (28)$$

IV. RESULTS AND DISCUSSION

A. Auto-thermal Reformer

1) Conversion process

In the ATR, ethanol will react with water and air to form hydrogen along with some amount of CO and CO2. In the ATR reactor, ethanol is completely converted and this results in some amount of Hydrogen. Molar flow of hydrogen is 3.2857 Kgmole/hr. Some amount of water molecule is also formed during the process and is used for water gas shift reaction in the next stage.

2) Water Gas Shift reactor

The molar flow of CO in the feed to the WGS is 1.1429 Kgmole/hr. In the first reactor (HTS) of WGS section, molar flow is 0.5837 Kgmole/hr due to water gas shift reaction and this process is repeated up to LTS. Finally, the molar flow of CO will reduce to 0.4304 Kgmole/hr, correspondingly mole fraction of water will also reduce and hydrogen production will increase due to this reaction.

TABLE I. OUTPUT FROM DIFFERENT REACTOR (KGMOLE/HR)

Comp	ATR	HTS	MTS	LTS	PROX
H_2O	0.7143	0.1552	0.0056	0.0019	0.0021
CO	1.1429	0.5837	0.4342	0.4304	0.009
H_2	3.2857	3.3448	3.9944	3.9981	3.657
CO_2	0.8571	1.4163	1.5658	1.5696	1.991

3) Preferential Oxidation (PROX) reactor

Due to the oxidization reaction CO mole fraction is reduced from 0.4304 Kgmole/hr to 0.0009 Kgmole/hr. The H_2 is reduced from to 3.657 Kgmole/hr and water mole fraction increases to 0.0021 Kgmole/hr.

4) Temperature profile of Fuel Processor system

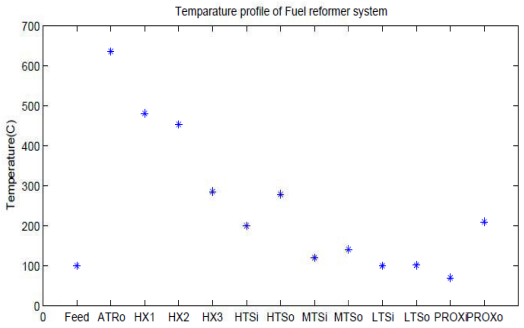

Figure 2. Temperature Variation in Fuel Processing Unit

The temperature profile for the whole process, starting from temperature of raw materials feed into the reactor to the temperature of PROX vapor is as shown in the Figure 2. Feed temperature is 100 °C. In the reformer temperature rise up to 635.8 °C. This heat can be used for the heating purpose of the raw materials by heat integration. The feed stream then cooled down to 200 °C in the HX. Then it is passed through various reactors and coolers.

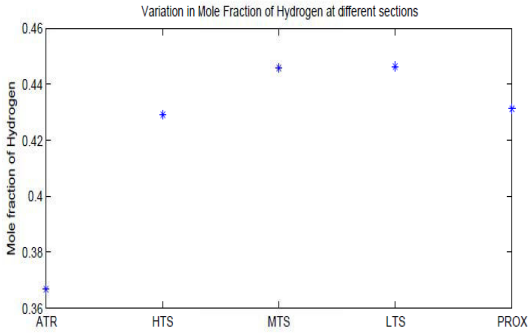

Figure 3. Variation of Hydrogen

5). Hydrogen Mole fraction Variation

The output from the ATR was supplied to WGS system for reducing the percentage of CO in the

mixture. In WGS reactor CO reacts with H_2O to form hydrogen and CO_2 thus mole fraction of hydrogen is increasing in the WGS system. But in the PROX reactor some amount of hydrogen oxidized with water and thus mole fraction of hydrogen is reduced.

B. Fuel Cell

1. Output Voltage change

Up to 30000 sec, the voltage and current are constant. After 30000 sec as the current is increased to 50 A, the voltage will reduce. The varying voltage is the due to the capacitance, temperature and partial pressures

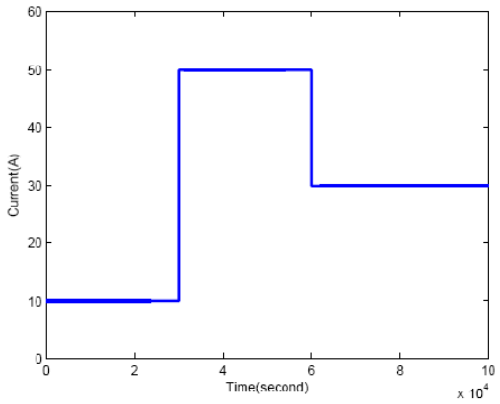

Figure 4. Input Current

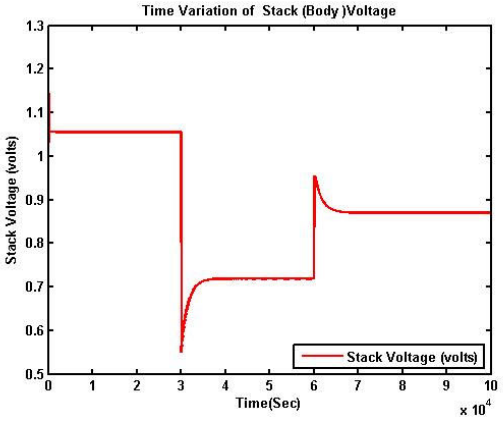

Output Voltage

2) Temperature Change

Up to 30000 sec, temperature profiles corresponding to all three CVs are similar. After 30000 sec, as the current is increased, heat released during the chemical reaction, will make the temperature profile to deviate from each other. After 60000 sec, there will be a temperature drop due to decrease in load current.

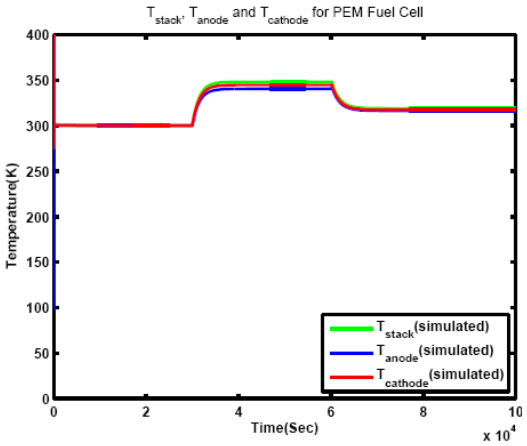

Temperature Variation in Fuel cell system

V. CONCLUSION

Analysis of a fuel processor for PEMFC systems is performed, considering ethanol as fuel in the ATR. Simulation results presented above clearly indicate the transients expected in a PEMFC. The results have shown that the model is capable of predicting transient behavior in voltage and temperature. From the simulation results it seems that maximum hydrogen efficiency and low carbon monoxide content is possible for reforming operation.

REFERENCE :

[1] Akande, A., R. Idem and A. Dalai, Synthesis, "characterization and performance evaluation of Ni/Al2O3 catalysts for reforming of crude ethanol for hydrogen production", Applied Catalysis, 287, 159-175,2005.J. Clerk Maxwell, A Treatise on Electricity and Magnetism, 3rd ed., vol. 2. Oxford: Clarendon, 1892, pp.68–73.

[2] Al-Dabbagh A. W., L. Lu, and A. Mazza, "Modelling, simulation and control of a proton exchange membrane fuel cell (PEMFC) power system", International Journal of Hydrogen Energy, 35, 5061–5069, 2010.K. Elissa, "Title of paper if known," unpublished.

[3] Ali D.M.,"A simplified dynamic simulation model (prototype) for a stand-alone Polymer Electrolyte Membrane (PEM) fuel cell stacks", MEPCON, 12th Int. Middle-East Power Systems Conference, 480–485,2008..

[4] Comas L.M., J. and N. Amadeo ," Thermodynamic analysis of hydrogen production from ethanol using CaO as a CO_2 sorbent, Journal of Power Sources, 61-67, 2004..

[5] Pathapati P.R., X. Xue, and J. Tang," New dynamic model for predicting transient phenomena in a PEM fuel cell system", Renewable Energy, 30, 1–22, 2005.

[6] Rabenstein G. and V. Hacker, "Hydrogen for fuel cells from ethanol by steam-reforming, partial-oxidation and combined auto-thermal reforming: A thermodynamic analysis", Journal of Power Sources, 185, 1293–1304, 2008.

[7] Shekhawat D., J. J. Spivey, D. A. Berry, "Fuel Cells: Technologies for fuel processing", Elsevier, 2-4, 2010.

[8] Xue X., Tang, A. Smirnova, R. England, and N. Sammes, "System level lumped parameter dynamic modelling of PEM fuel cell", Journal of Power Sources, 133,188–204, 2004.

[9] Zamora I.,J.I. San Martin, J.J. San Martín ,V. Aperribay, P. Eguia , "Performance Analysis of a PEM Fuel Cell", International Conference on Renewable Energies and Power Quality,1-6, 2010

[10] Vaidya, P.D. and Rodrigues, A.E. "Insight into steam reforming of ethanol to produce hydrogen for fuel cells". Chemical Engineering Journal. 117. 39–49, 2005.

[11] Fierro, V., Akdim, O., Provendier, H. and Mirodatos, C. "Ethanol oxidative steam reforming over Ni-based catalysts". Journal of Power Sources. **145.** 659–666, 2005

◈◈◈